# NATIONAL ADVISORY COMMITTEE FOR AERONAUTICS

TECHNICAL NOTE

No. 987

## NONDESTRUCTIVE MEASUREMENT OF RESIDUAL AND ENFORCED STRESSES BY MEANS OF X-RAY DIFFRACTION

## II - SOME APPLICATIONS TO AIRCRAFT PROBLEMS

By George Sachs, Charles S. Smith, Jack D. Lubahn,
Gordon E. Davis, and Lynn J. Ebert
Case School of Applied Science

Washington
November 1945

NATIONAL ADVISORY COMMITTEE FOR AERONAUTICS

TECHNICAL NOTE NO. 987

# NONDESTRUCTIVE MEASUREMENT OF RESIDUAL AND ENFORCED STRESSES BY MEANS OF X-RAY DIFFRACTION

## II - SOME APPLICATIONS TO AIRCRAFT PROBLEMS

By George Sachs, Charles S. Smith, Jack D. Lubahn, Gordon E. Davis, and Lynn J. Ebert

## SUMMARY

Tests on the use of X-ray diffraction methods for determining surface stress distributions in notched tensile bars and in the vicinity of a welded joint in aircraft steel tubing are described. Data on the effects of stress and degree of notching on the principal stresses and stress-concentration factors for flat notched tensile-test specimens were obtained. For the greater part the results confirm previous analytical and photoelastic determinations of these quantities. It was found that X-ray techniques were of limited value for determining the direction and magnitude of residual stresses in weldments since the condition of the metal was such as to prevent an accurate determination of the lattice parameters.

## INTRODUCTION

Among the problems interesting to the aircraft industry which might be subject to a commercial application of X-ray stress measurements are (a) the distribution of stresses under load in structures of changing section, or "notched" sections, and (b) the distribution of residual stresses in

---

Note.- A complete and detailed report on this investigation containing information on the effects of variables in the metal condition and experimental technique on the X-ray measurement of stress may be obtained on loan from the Office of Aeronautical Intelligence of the National Advisory Committee for Aeronautics, Washington 25, D. C.

welded structures. While some investigations in these directions have been carried out previously, as discussed in reference 1, they are not sufficiently extensive to reveal the general applicability of the X-ray diffraction method to such problems.

Consequently, of these two groups of problems, one special problem in each group was selected. The investigation was particularly concerned with the reliability and accuracy of the stress measurements and their general usefulness.

This investigation, conducted at the Case School of Applied Science, was sponsored by and conducted with the financial assistance of the National Advisory Committee for Aeronautics.

## X-RAY DETERMINATION OF STRESS DISTRIBUTION IN FLAT, NOTCHED TENSILE TEST BARS

### Previous History

The X-ray diffraction method of stress determination would seem to possess some outstanding advantages, accompanied by some disadvantages, when applied to the study of stress distribution in structural members. Structural parts frequently differ in section, shape, and size, sometimes very suddenly, resulting in a very nonuniform stress distribution close to the section change or "notch."[1] This stress state is characterized by steep stress gradients and high localized stress peaks, or "stress concentrations."

For this reason, a study of notched flat bars subjected to tension was undertaken in order to study the merits and possibilities of the X-ray method as applied to notched parts, particularly of metals used in aircraft.

In relation to stress measurements in notched sections, the X-ray method has the inherent advantages of using a small gage length, of providing a convenient method for determining the complete stress state, and of providing a method for the determination of stress not only in the elastic, but also in the plastic strain regions. Mechanical and

[1]The term "notch" is used generally for any type of sudden section changes.

photoelastic methods do not permit the determination of the stress in the plastic strain region. Photoelastic measurements, however, enable the analysis of the stress distribution in the elastic stress state very accurately. Such measurements and the results of theoretical investigations may serve as the basis for the evaluation of the X-ray method as applied to this problem.

Numerous attempts have been made to determine the effects of notches, holes, and so forth, on the stress distribution caused by elastic loading (see reference 2). The discussion here is restricted to investigations of flat and circular bars, provided with a local reduction of the section by an external notch, and subjected to pure tension in the uniform section.

The maximum value of longitudinal stress or "stress peak" which is created by elastic straining of round and flat bars of infinite width and provided with notches of hyperbolic profile has been calculated by Neuber (reference 3). This stress peak at the bottom is given by the expression:

For round bars: $S_{max} = S\sqrt{\frac{d}{r}}$

For flat bars: $S_{max} = 1.3\,S\sqrt{\frac{d}{r}}$

where

S average tension (load divided by the area of the notched section)

r radius at the notch bottom (apex of hyperbola)

d diameter or width of the unnotched section

These formulas, however, assume infinitely large bars and, therefore, approximate only the conditions created by very deep notches.

The effects of various factors, such as radius of notch, notch depth, and so forth, have been followed up by photoelastic investigations on flat bars of a transparent

material, such as Bakelite, by Coker and Filon (reference 4), Frocht (reference 5), and Wahl and Beeuwkes (reference 6). The following three types have been investigated:

1. V-notches of constant depth, having various bottom radii (figs. 1 and 2)

2. Semicircular notches of various radii (figs. 3 and 4)

3. Slot notches of various depths and widths having a half-circular bottom contour (of various radii) (figs. 5 and 6)

For the first two notch types, the distribution of the lateral stress has also been determined (figs. 1 and 3).

The last notch type should approximate the practical condition in notched bar tensile tests where the notch is usually a V-notch with a constant bottom radius. The measurements of Frocht evaluated for a bar of given thickness (= 100 percent) provided with notches of given bottom radii and varying depths are represented in figure 6. The stress concentration factor, that is, the ratio between the peak stress and the average longitudinal stress in the notched section, increases at first with increasing notch depth, then goes through a maximum and finally decreases again toward the value 1, representing uniform stress distribution for a notch which removes 100 percent of the cross-sectional area. The maximum value of the stress concentration factor occurs for a notch depth of somewhere between 20 and 50 percent, this depth being larger for sharper notches.

Regarding the transverse stress, the photoelastic measurements indicate that a high, but localized, transverse stress is present in the same region as the high longitudinal stress peak for shallow notches (fig. 1) while a more uniformly distributed transverse stress exists in a deeply notched section (fig. 3). The transverse stress is always zero at the notch bottom, as required by the theory of elasticity.

A few elastic measurements on flat steel bars with a semicircular notch have been carried out by Preuss (reference 7) (fig. 8) and by Coker and Filon (reference 4). Their results are in good agreement with those derived from photoelastic measurements.

Commercially, the two-dimensional stress state present in a flat bar is less important than the three-dimensional state present in a round bar or a more intricate structure. Little information is available on this problem.

Experiments regarding the stress distribution in round bars have been carried out by Berg (reference 8) on rubber and by Kraechter (reference 9) on steel bars by means of X-rays.

Both investigators agree, according to figure 7, that, with a notch of a given bottom radius, the stress concentration increases at first with increasing notch depth; however, the X-ray method, contrary to the rubber tests, shows a maximum stress concentration at a rather shallow notch and an increasingly uniform stress distribution with further increasing notch depth. These results are in qualitative agreement with the photoelastic measurements on flat bars.

Thus it appears possible to apply the information derived from the photoelastic investigations to a round bar in a semiquantitative manner. According to Neuber (reference 3), the stress peak in a round bar should be 30 percent higher than that in a flat bar having notches of the same profile on the flat sides.

## Material and Procedure

### Material and Preparation of the Specimens

The steel used for the investigation was commercial SAE X-4130 steel. It was provided in a sheet 0.120 inch thick through the courtesy of the American Steel and Wire Company.

The sheet was cut into strips of the approximate size desired, pickled down to 0.100 inch in thickness, cold-rolled to 0.035 inch, annealed at 1700° F for 15 minutes, and air-cooled. The cooling produced considerable warping; so the strips were given 3 percent strain on a tensile machine to straighten them.

After this heat treatment and straightening operation, the scale was pickled off and a diffraction pattern was made to determine whether or not the grain size was suitable to produce sharp lines. It was found that the $K_\alpha$ doublet

was unresolved indicating that the heat treatment was too severe (fig. 9). The strips were, therefore, stress relieved at various temperatures to determine the optimum grain condition for well-defined diffraction patterns. Temperatures of 1000° F, 1240° F, and 1320° F were used in the attempt to determine the optimum stress relieving temperature. Diffraction patterns (fig. 10) were made after each stress relief and showed that the most suitable temperature was 1320° F. In stress relieving, the strips were clamped between heavy steel plates to prevent warping, and packed in a mixture of powdered charcoal and burnt magnesia to prevent decarburization. The stress relieving was done in a Lindberg Cyclone furnace. The samples were held at the specified temperature for 4 hours, then furnace-cooled. All temperatures were maintained to ±5° F of the desired temperature.

The strips were then pickled to remove scale and any decarburization. After the pickling, the strips were made into tensile specimens. A final pickling operation was given to the finished specimen to remove any superficial cold work that might have taken place on the surface in the machining operation.

Tensile tests were run on standard size specimens that had been given the foregoing treatment, to determine the yield and ultimate strengths. The treatment resulted in a yield strength of 59,500 psi and ultimate strength of 81,500 psi. Figure 11 shows the stress strain curve for the SAE X-4130 steel in the condition in which it was used for the tensile specimens.

One duralumin specimen (fig. 12), was made from 24S-T duralumin sheet 0.033 inch thick. It was annealed for 1 hour at 400° F in order to increase the sharpness of the diffraction lines without appreciably decreasing the strength. The annealing conditions were selected on the basis of previous tests. The yield strength in the condition as tested was 56,000 psi.

It was decided to use, in the steel specimens, a 60° notch, and to hold the ratio of the notch radius to the maximum width of the specimen constant. This ratio was approximately 0.04 and produced theoretically (reference 5) a stress concentration factor of 3.5 for the 25-percent notch and of approximately 2.5 for the 5-percent notch (fig. 6).

Two notch depths were investigated 25 percent and 5 percent. The dimensions of the specimens are shown in figure 13.

Since the specimen was relatively short, and since the tensile machine applied the load by means of two pins passing through the ends of the specimen, there was some doubt as to whether or not the applied load would produce a uniform stress distribution in the unnotched portion of the specimen. To overcome this difficulty, cold-rolled steel plates were riveted to the ends of the specimen. This, in effect, increased the length of the specimen and produced a uniform stress distribution since the loading pins applied the load to the plates, and not to the specimen directly.

In the case of the duralumin specimen (fig. 12) a 60° notch also was used. However, in this specimen, a higher stress concentration factor was used. The ratio of the notch radius to the specimen width was approximately 0.02, and the notch depth was 20 percent. This set of conditions corresponds to a stress concentration factor of more than 4 (fig. 6). It was found necessary to rivet supporting plates to the ends of the specimen as in the case of the steel specimens.

## Straining the Tensile Specimens

A special tensile machine (fig. 14) designed and constructed in this laboratory especially for this investigation by Mr. Frank Miller, was used to obtain the various loads on the specimens. The load was applied through a worm-and-screw arrangement, and transmitted to the specimen by means of a "calibrating bar" made from tubular SAE X-4130 steel. Figure 15 shows the tensile machine in position for making diffraction patterns from the duralumin specimen. The tubular member served as a means of measuring load. For use in transmitting load to the duralumin specimen it was used in the hot-rolled condition, but for use with the steel specimens it was necessary to make it stronger, for carrying larger loads, by annealing at 1700° F, air cooling, and tempering at 700° F. This heat treatment produced a proportional limit corresponding to a load of 3200 pounds. The tensile machine itself could withstand a considerably higher load.

The change in length of this tube for any change in load was determined accurately on a standard Olsen tensile

machine. It was found that in the hot-rolled condition, 20 pounds produced an elongation of 0.0001 inch in a 2-inch gage length, while in the heat-treated condition, 37 pounds produced the same elongation. The load applied to the tensile test specimens during investigation by X-rays was measured by noting the change in length in a 2-inch gage length of this tube, and applying the foregoing calibration factors. To make sure that the same load was applied to the calibrating bar as to the specimen, they were connected in series. The elongation of the calibrating bar was measured with an Olsen gage, reading in ten-thousandths of an inch.

The tensile machine was equipped to produce a vertical movement of the specimen of 1 inch and also a complete rotation of the specimen about the horizontal axis of the machine.

On both steel specimens the first load was chosen in such a way that the peak stress would be approximately equal to the yield strength. Since the yield strength was 59,500 psi, and the stress concentration factor was 3.5, the first load corresponded to an average stress of 17,000 psi. The second load on the steel specimens was selected in such a way that there would be plastic flow at the notch bottom. If plastic flow occurs, there are residual stresses after unloading; so after the stress distribution corresponding to the second load was analyzed by means of diffraction patterns, the specimen was unloaded and the residual stresses were studied. The third load on the steel specimens was chosen in such a way that the average stress was greater than the yield strength, and thus, so that the whole sample had yielded. However, certain difficulties arose in the case of the specimen with the 5-percent notch, so that this load could not be attained. The final load for this specimen was, however, near the yield strength. Since the third load also caused residual stresses, a fifth series of patterns was made to analyze the residual stress state of each specimen.

All three loads for the duralumin specimen were chosen such that the average stress was below the yield strength for the duralumin. They corresponded to average stresses of 4300, 12,000, 33,700 psi.

After the application of the second load of 50,000 psi average stress to the 25-percent notch steel specimen, which was the first to be investigated, and after both the strains under load and the residual strains had been measured, a question arose as to the possibility of a decrease in load

when the specimen was kept in a state of strain over such a long period of time as is necessary for X-ray stress measurements. Mechanical tests showed that creep is very pronounced in SAE X-4130 steel, but that no creep occurs at a load which is 15 percent less than the maximum load to which the specimen has been previously subjected. Thus, to avoid possible changes of load during X-ray measurements, the following general procedure was used. The desired load was applied, and then backed off by 15 percent before making the X-ray exposures. To find what the stress distribution would have been at the desired load, elastic stresses corresponding to the 15-percent decrease of load were added to the measured stresses.

## X-ray Technique

Cobalt X-radiation is recommended for back-reflection work on steels; while copper X-radiation is best suited for aluminum and its alloys. Consequently, in making the diffraction patterns from the steel tensile bars, a Coolidge water-cooled cobalt target X-ray tube was used for the production of the X-ray beam and a Phillips-Metallix diffraction tube with a copper target was used for the duralumin specimen. Both tubes were operated at 35 kilovolts, but the cobalt tube required 10 milliamperes, while the copper tube could be operated at 20 milliamperes.

In the investigation of the steel specimens, cameras of the Sachs back-reflection type were used (fig. 16). These cameras were designed and constructed along with the plate on which they are mounted (described later) in this laboratory especially for this work by Mr. Frank Miller. They consisted of a flat circular cassette mounted normally on a hollow axle. The film, with a hole punched in the center and protected by black paper, was held in the cassette by means of a metal plate. The plate was provided with ports for the passage of the X-rays.

The cassette was mounted on grooved rollers which were fastened on a plate. The plate was adjustable with respect to the X-ray tube in horizontal and vertical movement, and in angle of inclination with the X-ray tube. By means of these adjustments, it was possible to pass the main beam of X-rays emanating from the tube through the pinhole system. The roller bearings permitted full rotation of the cassette about the X-ray beam as an axis. The pinhole system (fig. 16)

was held in a brass sleeve that fit snugly into the hollow axle of the cassette. The forward pinhole was 1 millimeter in diameter and was 2 inches from the target. The resultant beam was collimated to 0.10 inch by means of a collimating pinhole $1\frac{1}{2}$ millimeters in diameter placed $1\frac{1}{2}$ inches from the forward pinhole. The film to specimen distance was $3\frac{1}{2}$ inches. Figure 17 shows the plate and the cassette with the pinhole system in position.

After the first picture was taken, it was found that the silver calibration substance was too large grained to produce a uniform diffraction ring (fig. 18). It was necessary, therefore, to rock the film in order to obtain an accurately measurable silver ring. A rocking device was attached to the plate that held the cassette. The device gave a rocking motion of $\pm 10^{\circ}$ to the cassette. By releasing the cam action, it was possible to give the cassette a full 360° rotation. Figure 17 shows the cassette with the rocking mechanism attached.

In the case of the duralumin investigation the same type of camera was used (fig. 15). It was found that the duralumin was of such a grain size that rocking did not improve the pattern, and hence no rocking device was attached. The pinhole system which was used for the investigation of this specimen, was essentially the same as that used for the steel specimens, giving the same focusing conditions, but the pinholes were smaller. The forward pinhole was 0.025 inch in diameter, and the second pinhole collimated the beam to 0.075-inch diameter at the specimen surface.

The position of the X-ray beam on the surface of the specimen, where measurements were to be made, was located by placing a fluorescent screen across the notch. The screen was graduated in tenths of an inch by means of an X-ray-opaque ink. By locating the beam between successive graduations, its position relative to the sample could be determined. The thickness of the screen was taken into account when the specimen was in position for the oblique pictures.

Since the strain in the metal immediately adjacent to the notch bottom was of particular interest, attempts were made to produce patterns 0.05 inch from the notch bottom. With a beam 0.10-inch in diameter, the X-ray pattern yielded irregular results in this region, and usually stresses close to the average. This failure to register stress concentration might be explained by the fact that such stress concen-

tration occurs only within a small part of the exposed area and possesses a large gradient. Such stresses, apparently, have little influence on the stress pattern, and their effects are unconsciously disregarded in visual measurements. Some attempts were made to measure the peak stresses by restricting the beam to 0.02 inch, but with so small a beam, 24-hour exposures failed to produce measurable patterns. Because 24-hour exposures are not commercially useful, attempts in this direction were abandoned.

The (400) plane of silver produces $K_\alpha$ rings slightly greater in diameter than the rings produced by the (310) plane of iron, using cobalt radiation. It was decided to use silver as the calibration material (etalon) for the determination of the lattice parameter of the steel specimens. The silver was used in the form of chemically pure Mallinckrodt silver metal powder, a precipitated analytical reagent. It was found that the silver, when applied across the notch of the specimen in the form of strips, produced silver diffraction lines that were either too dark or too light (fig. 19). For that reason, the etalon was applied uniformly to the sticky side of cellulose tape, which was then glued to the specimen by means of glyptol with the silver in contact with the specimen. This method also produced a protective coating for the specimen which prevented the corrosion of the specimen surface.

For the duralumin test bar, gold powder (minus 300 mesh and 999.9 fine) was used as the calibration metal. It was supplied through the generosity of Handy and Harman of New York. The method of application was the same as for the application of the silver powder, with the exception that shellac was used to hold the cellulose tape to the specimen. The shellac was allowed to dry partially before the cellulose tape was applied. Several trials were necessary to get the gold powder of the right thickness to produce diffraction lines of the same intensity as those of the duralumin (fig. 20).

Assuming that the two principal stresses in the surface of the notched bar are always parallel and perpendicular to the longitudinal axis, three exposures in different directions must be taken in order to determine the complete stress state at each point. One of these exposures is usually made with the X-ray beam perpendicular to the surface, while the other two are oblique, and in the planes formed by the normal direction and the longitudinal and transverse axes, respectively.

The stress state was determined at five points across the specimen at the bottom of the notch. The stress state was assumed to be symmetrical about the longitudinal center line, so that the distribution of stresses over only half the width of the notched section was sufficient. These positions are shown in figure 13. For the duralumin specimen, the same assumptions were made, but only four positions were studied (fig. 12). For the oblique exposures, 45° was chosen as the angle between the surface and the incident beam for the steel specimens.

That part of the radiation from the target was used which made 6° with the horizontal plane perpendicular to the X-ray tube. Appropriate templets were made so that the specimen might be tilted to the proper angle to make the desired angle with the X-ray beam.

For the normal pictures, a templet of 90° − 6°, or 84°, with the horizontal was used. For the transverse patterns, a templet of 45° − 6°, or 39°, was used, and for the longitudinal pictures, the templet angle was 90° − 4°, or 86°. The templets were made of cold-rolled sheet and were such that when the flat side of the tensile specimen touched the inclined edge of the templet, the specimen was in the proper position.

In making the normal patterns, both the longitudinal and the transverse axes of the specimen were normal to the X-ray beam. For the oblique pattern necessary for determining the longitudinal stress, the longitudinal axis of the specimen was inclined 45° to the X-ray beam, while the transverse axis was perpendicular to it (fig. 21) and similarly for the oblique pattern necessary for determining the transverse stress (fig. 22).

All five positions across half the notch (fig. 13) were taken for one load and one orientation before the specimen was reoriented. For producing the patterns at different positions on the specimen, since the beam could not be raised and lowered, the specimen was raised or lowered with respect to the beam by means of the vertical adjustment on the tensile machine.

After the five exposures for one orientation of one particular load were completed, the specimen was unloaded, and reoriented. It was then reloaded to the same load, and diffraction patterns were made at the same positions. This process was repeated until the three patterns for each of

the five positions for one load were finished. The procedure was then repeated for the next load.

In exposing the film for the normal patterns, full rotation of the film was used. For the patterns made with oblique incidence, the film was rocked $\pm 10^{\circ}$ about its axis.

Thirty degrees was chosen as the angle of oblique incidence for the duralumin specimen. The method of specimen orientation was approximately the same, but the method of producing the diffraction patterns was slightly different. The chief difference occurred in the procedure for making the oblique patterns. Since the work on the duralumin specimen preceded the work on the steel specimens, not all the factors influencing the accuracy (reference 1) had been studied. In view of this fact, the following is the procedure that was used for the duralumin specimen. With the beam at normal incidence, the pattern was obtained in a single exposure (fig. 23a). For oblique incidence, that part of the beam farthest displaced from the normal was used (fig. 23b) in order to improve the accuracy. The remainder of the rays were blocked out with a lead baffle. This required two exposures with the film in two positions $180^{\circ}$ apart in order to obtain diametrically opposed segments for measuring.

In the steel sample investigation, both sides of the diffraction ring were obtained in one exposure by placing the film in such a position that each side fell on the focusing sphere at the intersection of the cone of diffraction and the focusing sphere.

Since the area of the specimen covered by the X-ray beam was of finite size, and since, for the oblique patterns, the specimen was inclined to the incident beam, the simple focusing conditions of the normal patterns (fig. 23a) were not obtainable. The incident beam did not pass along a major diameter of the sphere, but along one of the minor diameters (fig. 24a). Therefore, there was only one position of the film in which any two diametrically opposite points of the diffracted cone intersected the focusing sphere at equal distances from the specimen (fig. 24b). For the specimen orientation for determining transverse stress, the position of the film was such that the longitudinal axis of the film was parallel to the longitudinal axis of the specimen, while for the specimen orientation for determining longitudinal stress, the position was such that the longitudinal axis of the film was parallel to the transverse axis of the specimen.

In both cases, the film to specimen distance was the same as that for normal incidence. Although the rocking necessary to eliminate spottiness of the diffraction lines introduced an error because of the fact that this position was changed, the error was slight. The rocking was only 10° on either side of the true position so that the displacement of the line due to the effect of a strain in a slightly different direction was not great. For the normal patterns for the steel specimens, the same focusing conditions were used as were used in the case of the duralumin specimen (fig. 23a).

In making the diffraction patterns for the steel specimen exposure times of 25 to 30 minutes gave easily measurable films. It was thought that if the exposures had been made with an X-ray tube having beryllium windows instead of the conventional Linndeman glass, the exposure time might have been reduced to 10 minutes or less. The duralumin patterns required exposure times of $4\frac{1}{2}$ hours. This long exposure time might be accounted for partially by the small size of the pinholes, the extremely fine grained condition of the metal and an irregular metallic deposit on the Linndeman windows of the X-ray tube.

Agfa nonscreen X-ray film was used in both cases. It was developed in Eastman X-ray developer from $2\frac{1}{2}$ to 4 minutes depending upon the temperature of the developer. Although no attempt was made to control the temperature during the exposure time, it did not vary more than ±4° C of 25° C.

The films were fixed in Eastman X-ray fixer for about 20 minutes, then washed and dried in a horizontal position to prevent uneven shrinkage in the direction of measurement.

## Stress Calculations

Diffraction patterns for the steel specimens were measured with a comparator (fig. 25) consisting mainly of a metric scale and a sliding indicator carrying a vernier. The indicator rested almost directly on the film, thus avoiding parallax. Reflected light from beneath the film was used to illuminate the film. By this technique film expansion because of heating was eliminated. Readings to 0.01 centimeter were obtainable directly from the comparator, and readings to 0.003 centimeter could be obtained by averaging a sufficient number of readings.

In measuring the duralumin diffraction patterns, a slightly different comparator was used. It was capable of giving readings to 0.001 centimeter. A sketch of the comparator appears in figure 26. A series of settings was made with the indicator on each line until a consistent value was obtained. Three series were considered sufficient for each film to obtain an accurate average.

Each film was checked using the same technique. In more than half the total number of cases, a single check was sufficient to show the correctness of the value. In the remainder of the cases, the process was repeated until consistent values were obtained. When the lattice parameters agreed to within 0.00010 angstrom units, the values were averaged.

The checks were usually made on different days, and it was seen that temperature and humidity variations had little effect on the measured lattice parameter.

The duralumin strain patterns were measured on the comparator (fig. 26) mentioned previously. Each film was measured six times and an arithmetic mean taken as the true value.

In calculating the lattice parameter for steel the following method was used:

The diameters of the iron and silver rings were found by subtracting the readings obtained at each end of the film. The ratio of the silver diameter to the iron diameter ($D_{Ag}/D_{Fe}$) was found by the use of five-place log tables. From this ratio, the lattice parameter from each film was found graphically from the plot shown in figure 27a. (This graph was read to 0.00001 angstrom units.)

The same method was used for the duralumin specimen, with the exception that gold was used as the calibration material. The ratio of the diameters was then $D_{Au}/D_{Fe}$. The lattice parameter was determined by means of the group shown in figure 27b.

The lattice parameters of three films were used to determine the stress state at each point, as follows.

For the longitudinal or transverse stress, the normal and longitudinal or transverse parameters were substituted in the formula:

$$S = \left( \frac{(a_o)_{L,T} - (A_o)_n}{(a_o)_n} \right) \times \frac{E}{(1 + V) \sin^2 \Phi}$$

where

$S_{L,T}$ longitudinal or transverse stress

$(a_o)_{L,T}$ parameter which is oblique to the longitudinal or transverse direction

$(A_o)_n$ normal lattice parameter

$E$ modulus of elasticity

$V$ Poisson's ratio

$\Phi$ angle between the surface and the oblique incident beam

The modulus of elasticity for steel was taken as $E = 29,000,000$, Poisson's ratio as $V = 0.284$, and $\Phi$ was $45^\circ$.

For duralumin, the modulus of elasticity was taken as $E = 11,000,000$, Poisson's ratio was $V = 0.34$, and $\Phi$ was $39^\circ$.

Since everything, except $S_L$, $(A_o)$, and $(A_o)_n$, is constant, the formula reduces to:

$$S = [(A_o)_L - (A_o)_n] K$$

The constant $K$ was evaluated as

15,800,000 for the X-4130 steel specimens, and
4,670,000 for the duralumin specimen

Therefore, by multiplying the parameter difference by $K$ the stress could be computed directly. The accuracy of the lattice parameter measurements as well as the accuracy of the constants warranted only slide rule accuracy in this last calculation.

If the calculated stress was positive, the stress was considered to be tension. If it was negative, it was considered as compression.

Corrections were then applied to the calculated stress values of the steel specimens.

These corrections were calculated from the following formulas:

Longitudinal stress

$$(S_L)_T = (S_L)_C + 0.056\ (S_L)_C - 0.030\ (S_T)_C$$

Transverse stress

$$(S_T)_T = (S_T)_C - 0.030\ (S_L)_C + 0.056\ (S_T)_C$$

where

$(S_L)_T$ true longitudinal stress

$(S_L)_C$ calculated longitudinal stress

$(S_T)_T$ true transverse stress

$(S_T)_C$ calculated transverse stress

The stresses for the duralumin specimen appear in table I and are plotted in figures 28 to 33. The stresses for the steel specimens appear in tables II and III and are plotted in figures 34 to 46.

## Experimental Results

The X-ray diffraction patterns permit the determination, for each set of three exposures in different directions, of the surface stresses in the longitudinal and transverse directions. The investigation was limited to a number of points on the surface in the notched section for a given specimen under given conditions of straining. The individual values of stress are assembled into the respective distribution

curves of the longitudinal and the transverse (or lateral) stresses, for each condition investigated (figs. 28 to 46).

A considerable importance is ascribed both to the longitudinal and to the transverse stresses in relation to the theory of failure of metals, in particular to the theory of failure of brittle metals. Regarding the longitudinal stress, the most significant feature is the maximum value or stress peak, as previously discussed, while it is the average value of transverse stress which is of major importance.

In discussing the results of this investigation, it must be kept in mind constantly that the measured values are surface stresses only and it is subject of considerable argument as to their significance regarding the stress state in the interior of the metal.

## Duralumin

One duralumin specimen was investigated, illustrating the change of the stress pattern on loading through the elastic range (figs. 28 and 29) up to a load halfway between that expected of yielding at the notch bottom and that for total yielding (table I). The yield strength of the metal was 56,000 psi, the stress concentration factor approximately 4.

The distributions of the longitudinal and transverse stress under a presumably elastic load (figs. 28 and 29) agree with the expected stress distributions. Figure 31 illustrates the general trend of the stress pattern occurring after and during plastic flow in notched tensile specimens (reference 10).

However, the accuracy of the stress pattern for purely elastic conditions was revealed by the X-ray measurements. It would be necessary to increase the number of exposures a prohibitive extent in order to draw an accurate trend curve through the experimental points. Furthermore, X-rays are apparently not suitable for the determination of a very steep stress gradient, as will be discussed later.

The distribution of longitudinal stress under an average load stress of 33,700 psi, or 60 percent of the yield strength, (fig. 30) illustrates one point in the spread of plastic flow from the notch bottom to the center of the specimen, resulting in a considerable decrease of the stress concentration at the

notch bottom. Also, the distribution of the longitudinal stress does not conform to that expected, in that the stress at the notch bottom is definitely less than the stress at that point at the moment of yielding. This may be due to an effect of creep similar to relaxation.

This stress pattern rather corresponds to that of the specimen loaded up to an average stress of 43,000 psi and unloaded to the actual average stress of 33,700 psi. Assuming that such an unloading by 10,000 psi average stress creates only elastic stresses of three-fourths the amount shown in figure 29, the assumed stress distribution under a load of 43,000 psi average would be obtained from the actual distribution under the load of 33,700 psi (fig. 30) plus approximately three-fourths of the stresses under the load corresponding to 12,000 psi average (fig. 29). A test of this type on steel yielded a stress distribution (fig. 34a) quite similar to that obtained on the duralumin specimen which was subjected to the high load for a long time.

The residual stress distribution curve (fig. 32) agrees well with that expected, in that it can be constructed from the curve corresponding to a load of 33,700 psi average by subtracting a hypothetical elastic stress distribution for the same load (fig. 33). In the process of unloading to zero load, there should be some plastic flow at the notch bottom. The peak stress of the elastic distribution, which must be subtracted to represent the process of unloading, is very high. If it is greater than twice the yield strength, then the yield strength in compression will be reached before complete unloading has occurred, and plastic flow will take place. However, this effect should be insignificant insofar as it relates to the general shape of the residual stress pattern, except for the points in the immediate vicinity of the notch bottom which cannot be investigated readily by X-ray stress measurement.

### SAE X-4130 Steel

Two steel specimens, provided with notches of 5 and 25 percent, respectively, were investigated in some detail.

The stress distribution of the 25 percent notch specimen under a presumably elastic load was not determined accurately. The study of this load was the first attempt in this direction, so far as steel specimens were concerned, and the calculated values scattered to a larger extent than

those of later determinations, yielding no definite stress pattern. This scattering was attributed to the spottiness of the diffraction lines because of mechanical difficulties in the rocking mechanism of the camera. The absence of a definite stress peak in these tests (table II) might be attributed, also, to the fundamental difficulty that steep stress gradients are likely to be missed by X-ray stress determinations. This will be discussed in more detail.

Longitudinal stress for 25-percent notched specimen.

The longitudinal stress distribution for the 50,000 psi average load on the 25-percent notched specimen (fig. 34a) is in good agreement with the theoretical distribution. The spread of the stress peak toward the center of the specimen indicated that the metal at the notch bottom had flowed plastically, while the metal in the center of the specimen was still under an entirely elastic strain. This is verified by the diffraction patterns for this series of tests (fig. 47), which became blurred in the vicinity of the notch, while they remained sharp in the center of the specimen. Since the metal at the very notch bottom showed a stress of approximately the yield strength, it might be assumed that the extent of plastic flow was limited. If the metal flow had been extensive, the metal adjacent to the notch would have strain hardened, and would have been capable of bearing a stress in excess of the yield strength of 59,500 psi.

The longitudinal residual stress distribution for the 50,000 psi average load is shown in figure 36a. Residual stress results from plastic flow and in the usual case is the difference between the actually measured stress distribution under load, and the elastic distribution that would have resulted had the specimen been able to carry the load elastically. In other words, the residual stress distribution might be obtained approximately by subtracting the theoretical elastic stress distribution from the measured stress distribution. However, such a hypothetical elastic stress distribution for a high load cannot be determined experimentally, while the actual stress distribution under load and the residual stress are subject to actual stress measurement. Consequently, by subtracting the residual stresses from the actual stresses, the fictitious elastic stress distribution is obtainable.

Figure 37a shows this fictitious (elastic) stress distribution that resulted from subtraction of the residual stresses for the 50,000 psi average load (fig. 36a) from the

actual stress distribution for the same load (fig. 34a). This curve agrees quite well with the proposed theoretical distribution. Here again, however, it was impossible to determine the height of the peak accurately. From the trend of the curve, it can be seen readily that the stress peak might rise to three times the average stress, which is in agreement with the stress concentration factor of 3.5.

It might also be noted that the integration of the stress distribution curve (fig. 34a) determined by actual X-ray measurement was 50,000 psi average, or equal to the actually applied load.

Figure 35 illustrates the experimental stress distribution obtained when the 25 percent notch specimen was loaded to 70,000 psi and then unloaded to 59,500 psi average. The reasons for the unloading were twofold. First, it was thought that the stress distribution obtained from this procedure represented a more stable stress state than the probably changing stress distribution under high loads, which results in "creep" of the metal. It has been discussed previously that the stress distribution resulting from the high load on the duralumin test bar (fig. 30a) gave a distribution curve that did not conform to the expected shape. The method of partial unloading gives some control over the stress state of the notch section. The nominal load of 70,000 psi average was maintained for only a few seconds so that creep was negligible. Experiments discussed previously in the experimental procedure showed that unloading by approximately 15 percent of the applied load would prevent creep. With the elimination of creep, the stress state becomes stable, so that the diffraction patterns for the applied load represented the true stress distribution for the applied load.

The second advantage of partial unloading was that the stress distribution obtained would serve as additional evidence as to the validity of previous conceptions regarding the stress distribution in a notched and overstrained bar and its changes on unloading.

However, before entering into the discussion of partial unloading, another phenomenon must be mentioned which is apparent from figure 35a. The average longitudinal stress in this case does not agree with the stress to which the load was relieved, 59,500 psi average, but is much lower, approximately 50,000 psi. As such a discrepancy has been

observed only after loading to the high load which caused plastic flow throughout the notched section, the observed low average stress must be attributed to a nonuniformity of the stress through the thickness of the specimen. In other words, the deficiency of the stress found in the surface layers must be compensated for by a higher stress in the inner fibers. This conclusion is in agreement with the general conception of plastic flow in a polycrystalline aggregate, the crystals of which are more restrained in the interior than at the surface.

Such a relation would explain, also, that the residual longitudinal stress usually does not average out to zero, but to a small compressive stress. This is explained by the fact that, subtracting an elastic stress distribution from a distribution which shows higher tensions in the interior than at the surface, the total resultant of the difference being zero, would create compression at the surface.

These relations do not destroy the validity of the previous manipulations, regarding the 70,000 psi average load, but it should be borne in mind considering the stress distributions. Furthermore, since these discrepancies were noted only for the highest average load, and since the phenomena that explain them result from plastic flow throughout a major portion of the notched section, this discussion will apply only to that load which produced a large amount of plastic flow, that is, the 70,000 psi average load.

The distribution of longitudinal stresses for the 70,000 psi average load which was relieved by 10,500 psi average (fig. 35a) shows that the stress peak is not at the notch bottom as in figure 34a, but is at a position approximately 0.25 inch from the notch bottom. This difference in the location of the stress peaks can be accounted for by the fact that the unloading, which was presumably elastic, caused a greater decrease in stress at the notch bottom than elsewhere, thus leaving stress peaks at a point below the notch bottom. Since the specimen was relieved by 15 percent of the initial load, this relief must be taken into account before the stress distribution at the initial load can be calculated. Because the 15 percent unloading constituted an elastic relief, an elastic stress distribution for an average stress of 15 percent of 70,000 psi, or of about 11,000 psi, had to be added to the actual distribution curve (fig. 35a) in order to determine the distribution before the unloading. As there was no way of actually determining the elastic stress distribution, the theoretical elastic curve for the 50,000 psi average load

(fig. 37a) was taken as representative of an elastic distribution.

Figure 38a shows the hypothetical distribution of the elastic longitudinal stress for an average stress of 11,000 psi, which was constructed from the theoretical elastic distribution for the 50,000 psi average load by reducing all the ordinates proportionately. This curve was added to the actual stress distribution curve as determined by the X-ray measurements, and the curve that represented the actually applied load was obtained (fig. 39a). The metal adjacent to the notch bears a load in excess of the original yield strength of 59,500 psi average. This is in keeping with the theory that the metal at the notch bottom flowed plastically and so underwent some degree of strain hardening. The center elements of the specimen carry a load slightly below the original yield strength. This would seem to indicate that although the average stress was well beyond the yield strength of the material, the distribution was such that the center elements of the specimen were still under elastic stress.

Another possible explanation of this dip in the center of the stress distribution curve might be the previously discussed phenomenon that the surface crystals of a crystalline aggregate bear less stress than the average stress for the aggregate.

The integration of the curve representing the longitudinal stress while under load (fig. 39a) gave an average stress of 60,000 psi, while the applied stress was 70,000 psi average. This is again in keeping with the theory of uneven distribution of the stress along a line perpendicular to the surface.

Figure 40a shows the longitudinal residual stress distribution for the 70,000 psi average load. The curve is similar to that of the longitudinal residual stress curve for the precious load of 50,000 psi average (fig. 36a). The compression at the notch bottom is much higher, as would be anticipated from the fact that the stress peak of the corresponding fictitious elastic stress distribution is proportionately higher for the higher load. However, the increase in actual stress with increasing load is relatively uniform over the cross section because of the effects of plastic flow. Thus, when a much higher elastic stress peak is subtracted from an actual stress that is only slightly higher, the resulting residual stress would have a larger value in compression.

In the residual stress curve for the 70,000 psi average load, the tension peaks have moved in farther toward the center of the specimen than is the case for the 50,000 psi average load. This, too, can be accounted for by the shape of the fictitious elastic stress distribution curve. The tension peaks have a wider base, and consequently when they are subtracted, the tension peaks remaining in the residual stress curve are farther from the notch bottom.

When the longitudinal residual stress was subtracted from the actual longitudinal stress for the 70,000 psi average stress load, the fictitious elastic stress distribution curve shown in figure 41a resulted. This curve bears a striking similarity to the theoretical elastic stress curve for the 50,000 psi average stress load (fig. 37a). The stress peaks again rise to a value that might be 3.5 times the average stress of the fictitious elastic distribution for the 70,000 psi average stress. The average stress determined by integrating the curve was 69,000 psi. This is in close agreement with the actually applied load of 70,000 psi average. In other words, the total unloading causes changes of stress which are practically only of an elastic nature, and, consequently, for the surface do not differ materially from those for the interior fibers.

Transverse stress for the 25-percent notched specimen. Figure 34b illustrates the transverse stress distribution for the 25-percent notched specimens, strained to the average load of 50,000 psi. The transverse stress is zero at the notch bottom, becomes a maximum at a point 0.15 inch from the notch bottom, and then again decreases to a very low value in the center of the specimen. Such a stress distribution agrees with both theoretical conceptions and photoelastic measurements, as previously discussed.

Figure 36b shows the residual transverse stress distribution for the 50,000 psi average load. It will be noted that the transverse residual stress has approximately the same distribution curve as the longitudinal residual stress, with two exceptions. The first is that the stress at the notch bottom must be zero for the transverse stress, while it is probably high in compression for the longitudinal stress. The second is that the longitudinal residual stress in the center is compression, while the residual transverse stress in the center is tension.

Subtracting the residual stresses from the actual stresses in order to determine the fictitious elastic stress distribu-

tion was also used in regard to the transverse stress. Figure 37b shows the resultant distribution which is again in agreement with the generally accepted conceptions.

The distribution of the transverse stress under an average load of 59,500, after unloading from an average load of 70,000 psi (fig. 35b) shows two significant phenomena. First, the stress peak has moved closer to the center, appearing at 0.25 inch from the notch bottom, and secondly, the average transverse stress was increased, almost in proportion to the average longitudinal stress.

The effect of unloading by 15 percent is presumably purely elastic, as illustrated in figure 38b. When this curve was added to the actual stress distribution as determined by X-rays, the curve shown in figure 39b resulted. This curve represents the lateral distribution for the applied load of 70,000 psi average.

Figure 40b shows the transverse residual stresses for the 70,000 psi average load. This curve is similar to the lateral residual stress curve for 50,000 psi average load. However, as expected, the distribution of the 70,000 psi average lateral residual stress curve shows greater compression peaks and higher tension in the center of the specimen.

When these lateral residual stresses for the 70,000 psi average load (fig. 40b) were subtracted from the curve representing the lateral stress distribution for the total load of 70,000 psi average (fig. 39b) a fictitious elastic distribution for the lateral stresses under a load of 70,000 psi average was obtained (fig. 41b). This curve agrees with the one representing the fictitious elastic distribution for the 50,000 psi average load. The stress peak is in both instances at approximately the same place, while the tension in center is increased more than in proportion to the applied load.

Stresses for the 5-percent notched specimen.- The 5-percent notched specimen did not exhibit the sharp stress peaks (figs. 42 to 46) that the 25-percent notched specimen did. Although the stress peaks probably did exist, their presence could not be detected. This was ascribed to the limited sensitivity of the X-ray method. In this case, the stress peak was thought to be of sufficiently narrow width that it was not apparent in the diffraction patterns. Since the beam covered 0.10 inch of the notch width, the displaced diffrac-

tion line due to a sharp peak might not be apparent when included with the more intense line due to a uniform stress in the larger region of adjacent metal.

Figure 42 shows the stress distribution for an average stress of 17,000 psi. With the stress concentration factor being approximately 2.5, this load was well within the elastic range of the steel. The longitudinal stress distribution (fig. 42a) shows no stress peaks, but an average value of 18,000 psi, in agreement with the applied load of 17,000 psi. The transverse distribution curve (fig. 42b) shows a uniform scattering about the zero line.

Figure 43 shows the distribution for the 30,000 psi average load which was unloaded by 15 percent to 25,500 psi average. The specimen was unloaded again with the thought that there was plastic flow at the notch bottom, and the relief of a portion of the load would prevent creep. The curves show a uniform stress distribution in the case of the longitudinal stresses, and again no lateral stress. The X-ray measurements yielded an average stress of 22,000 psi, which is not sufficiently different from the applied average load of 25,500 psi average to draw any definite conclusions.

Since it was thought that plastic flow had occurred, the specimen was unloaded entirely after having been subjected to an average stress of 30,000 psi, and residual stress determinations were made (fig. 45). No residual stress exceeding the accuracy of the method was found. The scattering might be attributed to experimental error, or to slight residual stresses introduced in the process of making the specimen.

It was desired to have the highest load exceed the yield strength of the material, but the difficulties of producing sufficient strain to cause appreciable strain hardening prohibited loading the specimen to the desired load. The specimen was loaded to 50,400 psi average, then unloaded 15 percent to 41,400 psi average. Figure 44 shows the distribution curves that resulted. Again no stress peak or lateral stress was apparent. The X-ray measurements yielded an average stress of 39,000 psi, which did not sufficiently differ from the applied average stress of 41,400 psi average to permit the formation of any definite conclusion.

Residual stress determinations for this load (fig. 46) also yielded scattering along the zero line.

# X-RAY DETERMINATION OF RESIDUAL STRESSES IN A BUTT-WELDED SAE X-4130 STEEL TUBING

## Previous History

The X-ray diffraction method of stress determination would seem to possess unique advantages when applied to the study of residual stresses in welded structures. For this reason a study of a welded tube was undertaken, in connection with the present report, in order to study the merits and possibilities of the X-ray method as applied to welds in aircraft materials in particular.

In relation to welds, the X-ray method has the inherent advantage of using a small gage length, of being nondestructive, and of providing a convenient method of determining the complete stress state. Since it is well known that the residual stress state in and near a weld is characterized by large stress gradients, the first feature is of some importance in determining the effect, which is unknown as yet, of residual stress on weld strength. Since mechanical methods for the determination of residual stress necessarily involve the removal of material, which may greatly alter the stress picture where steep stress gradients exist, the nondestructive feature of the X-ray method is an important advantage even for experimental work, and especially for possible routine use of the method. Finally, mechanical methods generally will not lead to the determination of the complete stress state.

The problem of weld stresses has attracted many investigators, resulting in a large amount of information on this subject (reference 11). However, only few attempts have been made to derive, from experimentation or theory, a general and accurate pattern of stress distribution in a particular assembly. The conclusion can be drawn from the previous work that the stress state in a welded structure, particularly in the most frequently investigated structure, welded plate, is very involved and not readily explained.

It may be expected that the residual stresses in a welded structure will follow some general pattern depending upon the geometry of the welded pieces, but that local fluctuations will be superimposed on this pattern. In order to keep the general pattern of residual stress as simple as possible, the cylindrical geometry of thin-walled, butt-welded tubes was chosen.

Previous investigations of various types have been carried out in this laboratory on such welded tubes of the same material. These investigations have resulted in the collection of data on the microstructures found in the weld and base materials, the hardness values in the same regions and data on the average circumferential stress at different sections of the tube as obtained by a mechanical method. The data of Sachs and Graham (reference 12) on the residual circumferential stress (fig. 48) confirm the general conception of the development of residual stress in a welded structure. The welded bead, being the hottest part, tends to contract more than the parent metal. This contraction introduces circumferential tension in the deposited metal. This tension is counterbalanced by compression in the base metal, in agreement with theoretical conception. The magnitude of this compression decreases with increasing distance from the weld, presumably according to a logarithmic function. A comparison of this stress distribution with macrographs (fig. 49) shows that the residual stress in such an externally unrestrained weld is limited approximately to the heat-affected zones, that is, the regions that were heated above the critical range. Hardness results of Mastenbrook and Steffan (reference 13) showed considerable local variations in a circumferential section at the center line of the weld. These variations were not so pronounced in sections removed from the center of the weld. The average hardness along an element of the tube (fig. 50) showed a minimum of 82 Rockwell B in the weld metal. The hardness rose to a maximum of 105 Rockwell B at a distance of 1/4 inch from the weld. From this value, the hardness decreased to 87 Rockwell B at 3/4 inch and finally increased again to a value of 100 Rockwell B at 1½ inches from the weld, in the base alloy steel. The microstructure of the butt-welded tube (fig. 51) was found by the same authors to be a Widmanstatten structure of varying grain size at the center of the weld, which changed gradually with increasing distance from the weld through a coarse-grained to a fine-grained normalized structure, then to a recrystallization structure, and eventually to that of the parent metal.

## Material and Procedure

### Material and Preparation of Specimen

Commercial SAE X-4130 steel tubing, 1¾-inch outside diameter and 0.084-inch wall thickness was supplied for the

investigation by the Ohio Seamless Tube Company. This steel, in the as-received condition, had an ultimate strength of approximately 110,000 psi, a yield strength of 90,000 psi, and an elongation of 15 percent. The tubing was stress relieved, and the absence of residual stress was determined by the split-ring method (reference 14).

Pieces 6 inches in length were cut from the tubing and end-faced on a lathe. Two such pieces were butt-welded by the oxyacetylene process in the production line of a company producing aircraft parts and accustomed to welding such material. Welding rod of SAE 1006 steel 1/8 inch in diameter was used. The welds were tacked on opposite sides. The welding was started between the two tacks and was then made continuous. Thus the warpage was maintained at a minimum. The specimens were only locally preheated with the torch, and after welding were allowed to cool in air, then sandblasted to remove the scale.

The tubular specimen was then machined inside and outside to a truly cylindrical shape. By this procedure the wall thickness was reduced from 0.084 to 0.050 inch average thickness, the original thickness of the welded bead being 1/8 inch. A circumferential gage line was scribed around the tube at one end to serve as a longitudinal reference line. Similarly, longitudinal gage lines were scribed at one end, at intervals of $5^{\circ}$ on the circumference to serve as reference lines for the circumferential "position" of the points of measurement.

The scale was carefully pickled off a considerable area around the tube in the vicinity of the weld. The cleaned area was then covered with an extremely thin coat of lacquer to prevent subsequent rusting.

## X-Ray Technique

In order to obtain precise lattice parameter values, it is necessary to apply some calibration material of known lattice parameter to the surface of the specimen. The material used was Mallinckrodt silver metal, precipitated analytical reagent grade. This powder was sprinkled on a long strip of Scotch tape and then brushed to a uniform layer with a camel's hair brush. In the process, all excess powder not adhering to the tape was brushed off. The Scotch tape was then attached to the weld with thinned lacquer.

For a complete stress determination, at each selected point on the surface, diffraction patterns with the incident beam making a number of different angles with the normal to the surface are required. The directions shown in figure 52 were chosen, corresponding to method G-1-A of reference 1. The longitudinal stress is determined by a normal picture and a picture taken in the direction L (fig. 52) with the incident beam in the plane defined by the normal N and the tube axis A and at 45° with the normal. The transverse, or circumferential, stress is determined from a normal picture and another picture in the direction C (fig. 52) taken with the incident beam in the plane normal to the tube axis but with the beam making an angle of 45° with the surface normal at the point in question. In order to make a complete stress determination, still another pattern is necessary, preferably one making an angle of 45° with the normal and such that the projection of the incident beam on the tangent plane also makes an angle of 45° with the similar projections of the C and L beams.

A goniometer was constructed to hold the welded tube in position on the X-ray tube table. This goniometer (fig. 53) allowed two translational and two rotational degrees of freedom, and a third translational degree of freedom was available by shimming the tube to different heights on the table. This combination of motions enabled any spot in the tube to be X-rayed at any angle, although the actual computation of the necessary coordinates was in some cases tedious.

The X-ray camera used was a Sachs back-reflection camera equipped with a device for rocking or rotating the film. (See figs. 16 and 53.)

The collimation system was set up to obtain the focusing condition for a normal picture and the same setup was also used for the oblique pictures. A focusing pinhole 0.040 inch in diameter was used with a front pinhole 0.080 inch in diamoter. The combination produced an X-ray spot on the surface of the tubing 0.10 inch in diameter.

A General Electric X-ray tube with Lindemann glass windows and a cobalt target was employed. The tube was operated at 35 kilovolts and 10 milliamperes. Exposures were 1/2 hour.

The patterns were measured on a visual comparator having a least count of 0.02 millimeter.

The first step in the stress analysis of the welded tube was to determine at what points in and near the weld significant X-ray measurements could be made, and where they were impossible because of the unfavorable condition of the metal. For this purpose a series of patterns was taken on the center line of the weld at 5° intervals completely around the weld. Furthermore, a series of patterns was taken across the weld at several circumferential positions. These patterns were all normal patterns and were made with complete rotation of the film.

The 72 normal patterns taken at 5° intervals around the circumference on the center line of the weld were then measured, and lattice parameters were computed by the methods outlined in reference 1. The measurement was necessarily of poor precision in the frequent cases where the diffraction lines were broad. However, a measurement of sorts was obtained. Repeated measurements on different patterns showed that the maximum error in lattice parameter was about 0.0002 angstrom unit. This is greater than the maximum error which occurs when "sharp line" diffraction patterns are measured.

From the lattice parameter $\bar{a}$ measured on a normal pattern taken under full rotation, the sum of the principal stresses can be computed using the expression:

$$S_L + S_C = \frac{E}{a_o \upsilon}(\bar{a} - a_o) = 36.2\ (\bar{a} - a_o) \times 10^6 \text{ psi}$$

where:

$$E = 29 \times 10^6 \text{ psi}$$

$$\upsilon = 0.28$$

$$a_o = 2.86100 \text{ angstrom units}$$

This expression is approximate, being subject to a 5-percent correction because of the fact that the parameter $\bar{a}$ is not the true normal parameter. The expression is accurate enough, however, in view of the over-all precision of the measurements in this particular case. Using this relation, the

sum of the principal stresses was computed under the assumption that the lattice paramenter $a_o$ of the stress-free material was 2.86100. This assumption is reasonable, since the material in the weld (SAE 1006 steel) contained no alloying elements except carbon, which has a negligible effect on the lattice parameter. Further, the sum obtained in this way agreed with that obtained by adding the longitudinal and circumferential stresses, wherever they were obtained individually.

In a circumferential region at the center of the weld (positions 125° to 160°) longitudinal and transverse 45° pictures were taken in order to determine the longitudinal and circumferential stresses. The pictures were taken with ±15° rotation of the film. This was necessary to smooth out the slight spottiness of the silver lines; the iron lines were in no cases spotty. In the oblique films the diameter of the film normal to the plane of incidence was used. The films were measured in a manner identical with that in which the normal pictures were measured. The resulting parameters $a_L$ or $a_c$ may be used in the expressions:

$$S_L = \frac{E}{(1 + \nu)a_o} \frac{(a_L - \bar{a})}{\sin^2 45^\circ}$$

$$S_C = \frac{E}{(1 + \nu)a_o} \frac{(a_c - \bar{a})}{\sin^2 45^\circ}$$

to compute the respective stresses. These equations reduce to:

$$S_L = 15.4 \times 10^6 (a_L - \bar{a})$$

$$S_C = 15.4 \times 10^6 (a_c - \bar{a})$$

using the same constants as before.

Two positions, 60° and 275°, were chosen to investigate the situation across the weld. Normal, longitudinal, and

transverse patterns were made across the weld on these two longitudinal elements, at 0.05-inch intervals. The investigation extended 0.15 inch on one side of the estimated center line and 0.20 inch on the other, being stopped in each case by the previously mentioned metal condition. Parameters were calculated and stresses computed in the manner just described.

## Experimental Results

There has been considerable previous work on welded parts using the X-ray diffraction method. (See reference 1.) This work has been concerned entirely with plain, low carbon steels; however, this material is of little interest in the aircraft industry. The present investigation, on the contrary, has been concerned with a chrome-moly steel (SAE X-4130), which is one of the principal aircraft metals. This is mentioned now because the results of the investigation show that the type of material concerned plays a very important part as to the usefulness of the method. While previous investigators have been able to report favorable results of X-ray stress measurements on plain carbon steels, in the present investigation it was found impossible to determine stresses in the base material, the alloy steel, by any of the methods applied. This result is due to the condition of the metal.

It was possible, however, to make accurate determinations in restricted regions of the weld metal, and to this extent only the X-ray method has proved successful, yielding some new information on the stress conditions in welded structures.

### Metallurgical Conditions

In order to make accurate stress measurements, any steel to be investigated must be in a suitable metallurgical condition. This, in turn, depends mainly upon the response of the particular steel to the heating and cooling cycle at any point of the weldment during and after the welding.

A welded steel part consists fundamentally of four structurally distinct regions:

(1) The weld proper, possessing a cast structure

(2) The adjacent region which has been heated to a temperature above the critical temperature of the particular steel and cooled comparatively rapidly

(3) The region heated below the critical but above the stress-relieving temperature of the steel

(4) The region practically unaffected by the welding process

If a weldment is not restrained, such as in this investigation, weld stresses are restricted to the weld proper and to the adjacent metal, regions (1) and (2), according to previous investigations. In the case of a restrained weldment, long range residual stress may be developed also in the metal farther from the weld bead (reference 15).

Of the two regions of the investigated tube presumably containing residual stress, only the weld bead (region (1)) was found to yield X-ray diffraction patterns which permitted a stress measurement by the selected method. The patterns showed the $K_\alpha$-doublet in varying sharpness, ranging from clearly separated $K_1$ and $K_2$ lines to a rather broad line with a single maximum.

A semiquantitative method of specifying the breadth of the diffraction lines was adopted for convenience. The films were rated on a 1-to-6 basis, 1 being the good extreme and 6 the poor extreme (fig. 54). Roughly, a rating 1 was assigned to a line if the doublet was resolved distinctly. The rating 6 corresponded to a line so broad as to raise the question if it were indeed present. In this investigation, lines rated as 1 to 3 could be measured with a good accuracy, while some measurements of doubtful accuracy were made on lines of poorer accuracy. Approximately 50 percent of the circumference of the weld bead was rated 3 or better, and 50 percent was 4 or worse (see fig. 58).

Thus, even the low-carbon steel of the weld proper was distorted during the welding procedure to such an extent that the accuracy of X-ray stress measurements is seriously impaired in a considerable portion of the bead.

Some further difficulties resulted from the large grain size of some surface areas of the welded bead, which did not yield uniform diffraction lines even when the film was rocked, but resulted in streaks within the $K_\alpha$-doublet (references 16

and 17). However, this applied only to a few exposures. One out of approximately two hundred films was impossible to measure because of this difficulty. In all other cases, rocking of the film during exposure produced measurable lines.

In all cases the metal adjacent to the weld yielded X-ray patterns composed of such broad, diffuse lines that stress determinations by the method applied were not successful. It is possible that some method might be applied, which, however, would be extremely tedious and time-consuming (reference 18). The change along two selected elements is shown in figure 55, in which the ratings are plotted for a number of films, illustrating the previously discussed variations of the metallurgical condition. If exposures are taken a certain distance away from the welded bead (in region (3)), the heating has been sufficient to remove the effects due to cold work, but not sufficient to cause effects by cooling from above the critical, and sharp diffraction lines are obtained.

## Stresses across the Weld

The changes of the longitudinal and circumferential stresses across the weld were determined for two elements at 60° and 275° (table IV and fig. 56). Exposures were taken in intervals of 0.05 inch on both sides of the visual center of the weld. The width of the weld proper, as apparent to the eye after machining and etching, was approximately 0.30 inch. However, width and position of the weld vary for different points around the tube, and consequently the assumed center line has no physical significance. Furthermore, it is clearly recognized from figure 56 that the stress state is not symmetrical about the assumed center line or about any other possible position of a center line. A suggestion of symmetry can be seen in the readings for the 60° position but none for the 275° position.

Both the longitudinal and transverse stresses change with the position across the weld. Apparently the stress pattern is characterized by a fairly slow change of the stress, as compared with the rapid fluctuations around the tube, as will be discussed later.

However, a displacement of the point of exposure by 0.05 inch might cause in some cases a change of one of the stresses of as much as 30,000 to 40,000 psi.

## Longitudinal and Circumferential Stresses around the Tube

Figure 57 shows that accurately measurable X-ray patterns were restricted to two large and several small regions around the tube.

The two large regions were selected for the measurement of both the longitudinal and circumferential stresses in intervals of 5° along the center line of the weld. In addition, such stress measurements were made also for each interval of 45°. The results are represented in table V and figure 58, showing what regions yielded accurately measurable films.

No attempt was made to draw trend lines through the experimental points in figure 58. The individual points would deviate from any possible trend line by as much as ±10,000 psi. These variations exceed the presumable accuracy of the stress measurement by two to three times.

As the accuracy of locating a desired part is estimated to be considerably better than 0.0005 inch, these variations can be explained only as actual fluctuations of the residual stress in the welded bead. Consequently, in order to obtain a fairly complete stress pattern around the tube, exposures must be taken in very small intervals, say of 0.010 inch along the circumference. To do this, the technique used in the present investigation would have to be changed, the width of the exposed area being too large in relation to the expected frequency of the fluctuations.

The slightly reduced scattering in the range of 125° to 160° in comparison with that in the range 15° to 65° can be attributed to two factors. First, the rating of the lines was better, and second, the film measurements were repeated several times in order to improve the accuracy. However, since these measures caused only a slight reduction of the fluctuations, the fluctuations were considered as real.

Neither the longitudinal nor the circumferential stress shows an average which is either definitely tension or definitely compression. From the thermal conditions of welding, a considerable average tension in the circumferential direction should be expected in the welded bead, while the average longitudinal stress should be zero. The determined surface stresses certainly do not offer any confirmation of this expectation.

### Sum of Principal Stresses

In many X-ray investigations, only one exposure, perpendicular to the surface at each point, was made, and the sum of the two principal stresses $S_1 + S_2$ in the surface was determined. Such a procedure assumes the knowledge of the stress-free lattice parameter $a_0$.

On the contrary, three exposures made at each point permit the calculation of the stress-free lattice parameter $a_0$ at this point, as well as two stresses in the surface, according to the following equation:

$$a_0 = \bar{a}\left(\frac{1+\nu}{E}\right)(S_L + S_C)$$

The stress-free parameters were calculated for all points where the longitudinal and circumferential stresses were measured. The values (table VI) vary to a considerable extent, the average value being 2.86110 ± 0.00020 angstrom units; and some values deviate as much as ±0.0004 angstrom unit from this average. This accuracy is as good as can be expected, even for regular determinations of lattice parameters by the back-reflection method (reference 19). Consequently, it cannot be decided whether the variations are caused by random errors or possibly by differences in the steel composition. This second explanation is suggested by the fact (apparent from table III) that within any one restricted interval the values agree considerably better than the values from different intervals.

It might be assumed that by making a single exposure perpendicular to the surface, the sum of the principal stresses can be measured with sufficient accuracy, when the stress-free lattice parameter is taken as 2.86100 angstrom units. A large number of such X-ray patterns were taken, therefore, and the sum of the principal stresses determined (table VII and fig. 58).

However, the sum of the principal stresses $S_1 + S_2$, obtained in this manner, is not the same as that determined by addition of the longitudinal and circumferential stresses $S_L + S_C = S_1 + S_2$ without using the stress-free lattice parameter (fig. 58). The values determined by the two methods agree comparatively well, considering the uncertainty regarding the stress-free parameter and the difficulty of reproducing

the exposed area in two independent series of tests. The deviations from a trend line can be kept below approximately ±10,000 psi. It is apparent from these results that the single exposure method does not yield sufficiently accurate and lucid stress values.

The sum of the principal stresses (fig. 58) again illustrates the rapid fluctuations of the stress state around the tube. No correlation is apparent between the surface stresses and the mechanism of the welding process.

## Individual Principal Stresses

Utilizing independently the two sides of each film obtained in the two oblique directions, four values of lattice parameter are obtained which permit the determination of the magnitude and direction of the two principal stresses (see reference 1, method G4). This method is not very accurate, and the following results (assembled in fig. 59 and table VIII) are therefore open to considerable argument. The measurements were restricted to one region, 125° to 160°, which yielded readily measurable films.

Regarding the directions of the principal stresses, figure 59a shows that they scatter irregularly about the longitudinal and transverse directions. The accuracy of these angles is very limited and consequently the results cannot be taken as a proof either that the principal directions coincide approximately or diverge considerably from the longitudinal and circumferential directions.

The principal stresses (fig. 59b) differ from the longitudinal and circumferential stresses (fig. 59c) but not to a sufficient extent to warrant any other conclusion but that the longitudinal and circumferential stresses are the principal stresses. The distribution of the one principal stress $S_c$ over the investigated range agrees with that of the circumferential stress $S_C$, and the distribution of the other principal stress $S_a$ corresponds to that of the longitudinal stress $S_L$.

A more accurate X-ray stress measurement method must be used to obtain more decisive information regarding the magnitude and, in particular, the directions of the principal stresses.

## CONCLUSIONS

Measurements by means of X-ray diffraction techniques of the principal stresses in flat notched tensile bars of SAE X-4130 steel and 24S-T aluminum alloy have demonstrated the following:

1. X-ray diffraction methods can be used to determine surface stresses in metals in which the stress gradients are not steep, provided the condition of the metal is suitable. Measurement of stresses in the interior of a metal is not possible at present except by inference from the surface stresses. The measurement of highly localized stresses cannot be achieved by X-ray diffraction without extensive experimental precautions.

2. The longitudinal stress in a flat-notched specimen was found to be in agreement with the results of previous theoretical and photoelastic investigations so long as the metal was elastically strained. The changes of longitudinal stress have been determined for the range in stress in which the notched section becomes progressively plastic. These stress changes were found to confirm previously developed theories.

3. In the range of elastic stress, the ratio of the average transverse to longitudinal stresses was found to be independent of stress but varied with the degree of notching.

4. When the average stress exceeds the elastic range and progressive plastic flow occurs without further increase in load, the stress distribution changes gradually because of yielding, the change being of the same type as that caused by partial unloading. It was further noted that surface stress does not increase as rapidly as the stress in the interior when the average stress is beyond the elastic range.

Attempts to determine the residual stresses in a butt-welded joint in SAE X-4130 steel tubing by means of X-ray diffraction showed that:

(a) The residual stresses present in a structure welded from the alloy steel SAE X-4130 cannot be measured in the regions of the parent metal, affected by the heat. These heat-affected regions presumably contain large residual stresses.

(b) Only if the weld bead is made from low-carbon steel can accurate stress measurements be made in the bead. However, the structure of the deposited metal varies considerably; and some parts may be in such a condition that the accuracy of the measurements becomes very small.

(c) Large variations of the surface stresses in both the longitudinal and circumferential directions were observed, both around the weld and across the weld.

(d) In the longitudinal direction, the highest stress values measured were 12,000 psi in tension and 20,000 psi in compression. The average stress was a small compressive stress. As the butt-welded tubing is not restrained in the longitudinal direction, little longitudinal stress was expected.

(e) In the circumferential direction, the highest stress values measured were 30,000 psi in tension and 15,000 psi in compression. The average stress was approximately 6000 psi in tension. This corresponds to the value expected from previous measurements by mechanical methods. The low magnitude of the peak values of stress may possibly be explained by the machining operation which relieves the surface stress somewhat; the low magnitude of the average stress may be explained by the fluctuations of stress and the limitation that no residual stress should exceed the yield strength of the metal.

(f) This investigation reveals a rather restricted applicability of the X-ray diffraction method for the measurement of residual stress in weldments.

Department of Metallurgical Engineering,
Case School of Applied Science,
Cleveland, Ohio, October 11, 1944.

## REFERENCES

1. Sachs, George, Smith, Charles S., Lubahn, Jack D., Davis, Gordon E., and Ebert, Lynn, J.: Nondestructive Measurement of Residual and Enforced Stresses by Means of X-ray Diffraction. I - Correlated Abstract of the Literature. NACA TN No. 986, 1945.

2. Sachs, G., and Lubahn, J.: Effects of Notching on Strained Metals. The Iron Age, vol. 150, 1942, Oct. 8, pp. 31-38, Oct. 15, pp. 48-52.

3. Neuber, H.: (Exact Elastic Solutions Concerning the Notch Effect on Plates and Bodies of Rotational Symmetry.) Z.f.a.M.M., vol. 13, 1933, pp. 439-442.

4. Coker, E. G., and Filon, L. N. G.: A Treatise on Photoelasticity. The University Press, London, 1931, pp. 562, 597.

5. Frocht, M. M.: Factors of Stress Concentration Photoelastically Determined. Jour. Appl. Mech., vol. 2, 1935, pp. A67-A68.

6. Wahl, A. M., and Beeuwkes, R., Jr.: Stress Concentration Produced by Holes and Notches. Trans. A.S.M.E., vol. 56, 1934, pp. 617-625.

7. Preuss, E.: Experiments Regarding the Stress Distribution in Notched Tensile Test Bars. Z.V.D.I., vol. 57, 1913, pp. 664-667.

8. Berg, S.: Forschungsarbeiten auf dem gebiete des Ingenieurwesens, no. 331, 1930.

9. Kraechter, H.: X-ray Determination of the Stress Concentration Factor of Notched Cylindrical Test Bars. Zeitschr. Metallkunde, vol. 31, 1939, pp. 114-115.

10. Sachs, George, and Lubahn, J. D.: Notched Bar Tensile Tests on Heat Treated Low Alloy Steels. Am. Soc. Metals, Convention, 1942, Preprint No. 8.

11. Spraragen, W., and Claussen, G. E.: Shrinkage Stresses in Welding. Trans. Am. Welding Soc., vol. 16, Res. Supp., 1934, pp. 2-62.

12. Sachs, G., and Graham, T.: Residual Stress in Butt-Welded SAE X-4130 Tubing - Part I. Jour. Am. Welding Soc., vol. 7, no. 3, 1942, pp. 122s-125s.

13. Mastenbrook, H. J., and Steffan, H. J.: Structure of Butt-Welded Steel Tubing. Bachelor's Thesis, Case School of Appl. Sci., 1942.

14. Sachs, G., and Campbell, C. H.: Residual Stress in SAE X4130 Steel Tubing. Jour. Am. Welding Soc., vol. 6, 1941, pp. 553-558.

15. Sachs, G., and Davis, W. E.: The Effects of Residual Stress and External Restraint on Some Welding Characteristics of SAE X-4130 Steel Tubing. Jour. Am. Welding Soc., vol. 7, 1942, pp. 427s-433s.

16. Brandenberger, E.: Variations of the Lattice Parameter in Crystalline Aggregates. Schweizer Archiv für angewandte Wissenschaft und Technik. vol. 5, 1939, pp. 354-356.

17. Bollenrath, F., and Osswald, E.: X-ray Stress Measurement on Unalloyed Steels beyond the Compression Yield Point. Z.V.D.I., vol. 84, 1940, pp. 539-541.

18. Staeblein, F.: Interesting Examples of Residual Stress. Tech. Mitteilungen Krupp Forschungsbericht, vol. 2, 1939, pp. 33-34.

19. Sachs, G., and Weerts, J.: The Lattice Parameters of Gold-Silver Alloys (A New Method for the X-Ray Precision Measurement of Lattice Parameters), Ann. der Phys., vol. 60, 1930, pp. 481-490.

TABLE I

20% NOTCHED DURALUMIN SPECIMEN

| LOAD AND AV. STRESS | POSITION | NORMAL PARAMETER IN A° | LONGITUDINAL PARAMETER IN A° | TRANSVERSE PARAMETER IN A° | LONGITUDINAL STRESS PSI | TRANSVERSE STRESS PSI |
|---|---|---|---|---|---|---|
| 140 lbs. (4,300 psi) | 1 | 4.0402 | 4.0421 | 4.0405 | +10,000 | + 1,500 |
| | 2 | 4.0404 | 4.0418 | 4.0403 | + 6,000 | + 500 |
| | 3 | 4.0408 | 4.0422 | 4.0407 | + 7,000 | - 500 |
| | 4 | 4.0409 | 4.0416 | 4.0417 | + 3,500 | + 4,000 |
| 400 lbs. (12,000 psi) | 1 | 4.0370 | 4.0426 | 4.0391 | +29,000 | +11,000 |
| | 2 | 4.0394 | 4.0419 | 4.0398 | +14,500 | + 2,000 |
| | 3 | 4.0401 | 4.0426 | 4.0397 | +13,000 | - 2,000 |
| | 4 | 4.0395 | 4.0417 | 4.0401 | +11,500 | + 3,000 |
| 1110 lbs. (33,700 psi) | 1 | 4.0368 | 4.0418 | 4.0385 | +26,000 | + 9,000 |
| | 2 | 4.0350 | 4.0422 | 4.0382 | +37,000 | +16,500 |
| | 3 | 4.0363 | 4.0422 | 4.0379 | +31,000 | + 8,500 |
| | 4 | 4.0364 | 4.0427 | 4.0378 | +33,500 | + 7,000 |
| Residual Stress Unloaded from 1110 lbs. | 1 | 4.0452 | 4.0413 | 4.0442 | +20,000 | - 5,000 |
| | 2 | 4.0408 | 4.0413 | 4.0416 | + 2,000 | + 3,500 |
| | 3 | 4.0409 | 4.0413 | 4.0412 | + 2,000 | + 1,500 |
| | 4 | 4.0416 | 4.0414 | 4.0418 | - 1,000 | + 1,000 |

TABEE II

25% NOTCHED S.A.E.X4130 STEEL

| LOAD AND AV. STRESS | POSITION | NORMAL PARAMETER IN A° | LONGITUDINAL PARAMETER IN A° | TRANSVERSE PARAMETER IN A° |
|---|---|---|---|---|
| 527 lbs. (17,000 psi) | 1 | 2.86061 | 2.86147 | 2.86003 |
| | 2 | 2.86044 | 2.86150 | 2.86052 |
| | 3 | 2.86059 | 2.86118 | 2.86071 |
| | 4 | 2.86062 | 2.86124 | 2.86044 |
| | 5 | 2.86022 | 2.86128 | 2.86050 |
| 1550 lbs. (50,000 psi) | 1 | 2.85908 | 2.86253 | 2.86003 |
| | 2 | 2.85885 | 2.86196 | 2.86035 |
| | 3 | 2.85924 | 2.86173 | 2.86019 |
| | 4 | 2.85945 | 2.86189 | 2.86002 |
| | 5 | 2.85972 | 2.86215 | 2.86020 |
| Residual Stress Unloaded from 1550 lbs. | 1 | 2.86143 | 2.86099 | 2.86100 |
| | 2 | 2.86083 | 2.86096 | 2.86103 |
| | 3 | 2.86095 | 2.86089 | 2.86089 |
| | 4 | 2.86095 | 2.86071 | 2.86097 |
| | 5 | 2.86095 | 2.86072 | 2.86097 |
| Loaded to 2170 lbs. (70,000 psi) Unloaded to 1960 lbs. (59,000 psi) | 1 | 2.85996 | 2.86230 | 2.86057 |
| | 2 | 2.85893 | 2.86233 | 2.86008 |
| | 3 | 2.85879 | 2.86200 | 2.86008 |
| | 4 | 2.85907 | 2.86224 | 2.86022 |
| | 5 | 2.85927 | 2.86204 | 2.86000 |
| Residual Stress Unloaded from 2170 lbs. | 1 | 2.86179 | 2.86052 | 2.86093 |
| | 2 | 2.86092 | 2.86101 | 2.86114 |
| | 3 | 2.86077 | 2.86100 | 2.86097 |
| | 4 | 2.86073 | 2.86066 | 2.86109 |
| | 5 | 2.86089 | 2.86085 | 2.86112 |

TABLE II (CONT'D)

25% NOTCHED S.A.E. X4130 STEEL

| LOAD AND AV. STRESS | POSITION | LONGITUDINAL STRESS-PSI MEASURED | TRANSVERSE STRESS-PSI MEASURED | LONGITUDINAL STRESS-PSI CORRECTED | TRANSVERSE STRESS-PSI CORRECTED |
|---|---|---|---|---|---|
| 527 lbs. (17,000 psi) | 1 | +13,600 | - 9,200 | +14,700 | -10,100 |
| | 2 | +16,800 | + 1,300 | +17,700 | + 900 |
| | 3 | + 9,300 | + 1,900 | + 9,800 | + 1,500 |
| | 4 | + 9,800 | - 2,800 | +10,400 | - 3,300 |
| | 5 | +16,800 | + 4,400 | +17,600 | + 4,200 |
| 1550 lbs. (50,000 psi) | 1 | +54,500 | +15,000 | +57,600 | +14,200 |
| | 2 | +49,200 | +23,700 | +51,300 | +23,700 |
| | 3 | +39,400 | +15,000 | +41,100 | +15,000 |
| | 4 | +37,200 | + 7,600 | +39,100 | + 6,900 |
| | 5 | +38,400 | + 7,600 | +40,400 | + 6,800 |
| Residual Stress Unloaded from 1550 lbs. | 1 | - 7,000 | - 6,800 | - 7,200 | - 7,000 |
| | 2 | + 2,100 | + 3,200 | + 2,100 | + 3,200 |
| | 3 | - 900 | - 900 | - 1,000 | - 1,000 |
| | 4 | - 3,800 | + 300 | - 4,000 | + 400 |
| | 5 | - 3,600 | + 300 | - 3,800 | + 400 |
| Loaded to 2170 lbs. (70,000 psi) Unloaded to 1960 lbs. (59,500 psi) | 1 | +37,000 | + 9,600 | +38,800 | + 9,000 |
| | 2 | +53,000 | +18,200 | +56,200 | +17,600 |
| | 3 | +50,700 | +20,400 | +52,900 | +20,000 |
| | 4 | +50,000 | +18,200 | +52,300 | +17,700 |
| | 5 | +43,800 | +11,500 | +46,000 | +10,800 |
| Residual Stress Unloaded from 2170 lbs. | 1 | -20,100 | -13,600 | -20,800 | -13,800 |
| | 2 | + 1,400 | + 3,500 | + 1,400 | + 3,700 |
| | 3 | + 3,600 | + 3,200 | + 3,700 | + 3,300 |
| | 4 | - 1,100 | + 5,200 | - 1,400 | + 5,500 |
| | 5 | - 600 | + 3,600 | - 700 | + 3,800 |

TABLE III

5% NOTCHED S.A.E. X4130 STEEL

| LOAD AND AV. STRESS | POSITION | NORMAL PARAMETER IN A° | LONGITUDINAL PARAMETER IN A°. | TRANSVERSE PARAMETER IN A°. |
|---|---|---|---|---|
| 578 lbs. (17,000 psi) | 1 | 2.86025 | 2.86129 | 2.86003 |
| | 2 | 2.86039 | 2.86145 | 2.86037 |
| | 3 | 2.86032 | 2.86141 | 2.86040 |
| | 4 | 2.86015 | 2.86125 | 2.86033 |
| | 5 | 2.86041 | 2.86155 | 2.86038 |
| Loaded to 1020 lbs. (30,000 psi) Unloaded to 870 lbs. (25,500 psi) | 1 | 2.86021 | 2.86138 | 2.86013 |
| | 2 | 2.86034 | 2.86140 | 2.86008 |
| | 3 | 2.86020 | 2.86156 | 2.86013 |
| | 4 | 2.86016 | 2.86151 | 2.85988 |
| | 5 | 2.86005 | 2.86128 | 2.86009 |
| Residual Stress Unloaded from 1020 lbs. | 1 | 2.86089 | 2.86069 | 2.86086 |
| | 2 | 2.86070 | 2.86097 | 2.86069 |
| | 3 | 2.86074 | 2.86048 | 2.86072 |
| | 4 | 2.86074 | 2.86058 | 2.86064 |
| | 5 | 2.86073 | 2.86070 | 2.86072 |
| Loaded to 1713 lbs. (50,400 psi) Unloaded to 1405 lbs. (41,400 psi) | 1 | 2.85971 | 2.86207 | 2.85973 |
| | 2 | 2.85982 | 2.86203 | 2.85970 |
| | 3 | 2.85957 | 2.86196 | 2.85979 |
| | 4 | 2.85981 | 2.86210 | 2.85984 |
| | 5 | 2.85954 | 2.86195 | 2.85967 |
| Residual Stress Unloaded from 1713 lbs. | 1 | 2.86092 | 2.86103 | 2.86079 |
| | 2 | 2.86088 | 2.86057 | 2.86101 |
| | 3 | 2.86070 | 2.86042 | 2.86039 |
| | 4 | 2.86068 | 2.86086 | 2.86073 |
| | 5 | 2.86070 | 2.86071 | 2.86089 |

TABLE III (CONT'D.)

5% NOTCHED S.A.E. X4130 STEEL

| LOAD AND AV. STRESS | POSITION | LONGITUDINAL STRESS-PSI MEASURED | TRANSVERSE STRESS-PSI MEASURED | LONGITUDINAL STRESS-PSI CORRECTED | TRANSVERSE STRESS-PSI CORRECTED |
|---|---|---|---|---|---|
| 578 lbs. (17,000 psi) | 1 | +16,400 | -3,500 | +17,400 | -4,200 |
| | 2 | +16,800 | - 300 | +17,700 | - 800 |
| | 3 | +17,200 | +1,300 | +18,200 | + 900 |
| | 4 | +17,400 | +2,800 | +18,300 | +2,500 |
| | 5 | +18,000 | - 500 | +19,000 | -1,000 |
| Loaded to 1020 lbs. (30,000 psi) | 1 | +18,500 | -1,300 | +19,500 | -2,000 |
| | 2 | +16,700 | -4,100 | +17,700 | -4,800 |
| Unloaded to 870 lbs. (25,500 psi) | 3 | +21,500 | -1,100 | +22,700 | -1,800 |
| | 4 | +21,300 | -4,400 | +22,600 | -5,200 |
| | 5 | +19,400 | + 600 | +20,500 | 0 |
| Residual Stress Unloaded from 1020 lbs. | 1 | - 3,200 | - 500 | - 3,400 | - 400 |
| | 2 | + 4,300 | - 200 | + 4,500 | - 300 |
| | 3 | - 4,100 | - 300 | - 4,300 | - 200 |
| | 4 | - 2,500 | -1,600 | - 2,600 | -1,800 |
| | 5 | - 500 | - 200 | - 500 | - 200 |
| Loaded to 1713 lbs. (50,400 psi) | 1 | +37,300 | + 300 | +39,300 | - 300 |
| | 2 | +35,100 | -1,900 | +37,200 | -3,100 |
| Unloaded to 1405 lbs. (41,400 psi) | 3 | +37,800 | +3,500 | +39,700 | +2,600 |
| | 4 | +36,200 | + 500 | +38,200 | - 600 |
| | 5 | +38,100 | +2,100 | +40,100 | +1,100 |
| Residual Stress Unloaded from 1713 lbs. | 1 | + 1,700 | -2,100 | + 1,400 | -2,300 |
| | 2 | - 4,900 | +2,100 | - 5,300 | +2,300 |
| | 3 | - 4,400 | -4,900 | - 4,500 | -5,100 |
| | 4 | + 2,800 | + 800 | + 3,000 | + 700 |
| | 5 | + 200 | -3,000 | + 300 | -3,200 |

TABLE IV

Longitudinal and Circumferential Stresses at Various Positions Across the Weld (Along the Length of the Tube)

| Distance from Center Line of Weld Inches | $S_L$ - 1000 psi | $S_C$ - 1000 psi | $S_L + S_C = S_1 + S_2$ 1000 psi | $S_1 + S_2$ -(from normal exposure)- 1000 psi |
|---|---|---|---|---|
| At the 60° Position of Circumference | | | | |
| -.10 | - 5* | -14* | -19* | -35* |
| -.05 | -14 | - 3 | -17 | -28 |
| 0 | - 2 | + 7 | + 5 | + 7 |
| +.05 | - 1 | + 3 | + 2 | + 2 |
| +.10 | - 8 | - 1 | - 9 | - 4 |
| +.15 | -10 | - 5 | -15 | -26 |
| +.20 | +22* | +12* | +34* | +27* |
| At the 275° Position of Circumference | | | | |
| -.15 | -32.6 | -11.6 | -44.2 | -40 |
| -.10 | -39.8 | - 8.9 | -48.7 | -42 |
| -.05 | -42.5 | - 4.1 | -46.6 | -40 |
| 0 | -15.4 | - 4.5 | -19.9 | -16 |
| +.05 | - 6.0 | - 2.0 | - 8.0 | - 8 |
| +.10 | - 6.8 | - 4.0 | -10.8 | -11 |
| +.15 | - 3.4 | - 4.5 | - 7.9 | - 8 |
| +.20 | - 3.0 | - 6.5 | - 9.5 | - 5 |

*doubtful - large rating

TABLE V

Longitudinal and Circumferential Stresses at Various Positions Around the Center Line of the Weld

| Angular Position Degrees | $S_L$ - 1000 psi | $S_C$ - 1000 psi | $S_L + S_C = S_1 + S_2$ 1000 psi | $S_L + S_C$ from normal exposure - 1000 psi | |
|---|---|---|---|---|---|
| | | | | Observer 1 | Observer 2 |
| 15 | + 3 | +20 | +23 | +27 | + 4 |
| 20 | +10 | +12 | +22 | +28 | +18 |
| 25 | - 2 | + 4 | + 2 | +19 | +18 |
| 30 | + 9 | + 7 | +16 | +23 | +25 |
| 35 | + 9 | + 2 | +11 | +18 | +36 |
| 40 | - 3 | + 9 | + 6 | +11 | +27 |
| 45 | + 6 | +11 | +17 | + 6 | +40 |
| 50 | -15 | + 4 | -11 | 0 | 0 |
| 55 | + 3 | +19 | +22 | +18 | +12 |
| 60 | - 2 | + 7 | + 5 | + 7 | + 5 |
| 65 | -18 | +10 | - 8 | +12 | +10 |
| 105 | + 6 | +25 | +31 | +25 | +18 |
| 125 | + 1 | + 2 | + 3 | - 2 | - 3 |
| 130 | + 6 | + 8 | +14 | +13 | - 4 |
| 135 | + 3 | 0 | + 3 | 0 | -40 |
| 140 | - 3 | +12 | + 9 | + 3 | -31 |
| 145 | -17 | + 4 | -13 | -21 | -18 |
| 150* | -20 | - 5 | -25 | -37 | -27 |
| " | -15 | - 5 | -20 | -24 | |
| 155 | -18 | -14 | -32 | -31 | -27 |
| 160 | -10 | - 3 | -13 | -22 | -25 |
| 195 | +13 | +30 | +43 | +45 | +40 |
| 240 | + 9 | -14 | - 5 | + 9 | -18 |
| 285 | -18 | + 2 | -16 | -21 | -40 |
| 330 | -17 | + 1 | -16 | -12 | +25 |

*Two independent exposures taken

TABLE VI

Stress-free Lattice Parameters at Various Points Across and Around the Weld.

| Around the Weld | | Across the Weld at the 275° Position | |
|---|---|---|---|
| Angular Position Degrees | Lattice Parameter - A° | Distance from Center Line of Weld - Inches | Lattice Parameter - A° |
| 15 | 2.86101 | | |
| 20 | 2.86095 | | |
| 25 | 2.86086 | -.15 | 2.86079 |
| 30 | 2.86092 | -.10 | 2.86101 |
| 35 | 2.86093 | -.05 | 2.86103 |
| 40 | 2.86097 | 00 | 2.86104 |
| 45 | 2.86138 | +.05 | 2.86111 |
| 50 | 2.86083 | +.10 | 2.86112 |
| 55 | 2.86119 | +.15 | 2.86112 |
| 60 | 2.86105 | +.20 | 2.86100 |
| 65 | 2.86059 | | |
| | | Across the Weld at the 60° Position | |
| 105 | 2.86124 | | |
| 125 | 2.86123 | -.10 | 2.86149 |
| 130 | 2.86113 | -.05 | 2.86137 |
| 135 | 2.86117 | 00 | 2.86105 |
| 140 | 2.86124 | +.05 | 2.86109 |
| 145 | 2.86131 | +.10 | 2.86098 |
| 150 | 2.86141 | +.15 | 2.86148 |
| 150 | 2.86121 | +.20 | 2.86127 |
| 155 | 2.86106 | | |
| 160 | 2.86132 | | |
| 195 | 2.86106 | | |
| 240 | 2.86075 | | |
| 285 | 2.86123 | | |
| 330 | 2.86100 | | |

2.86093 average

2.86123 average

TABLE VII

Principal Stress Sum at Various Positions Around the Center Line of the Weld

| Angular Position Degrees | $S_1 + S_2$ 1000 psi First Value | Second Value | Angular Position Degrees | $S_1 + S_2$ 1000 psi First Value | Second Value |
|---|---|---|---|---|---|
| 0 | -19.0 | | 180 | - 2.0 | + 6.0 |
| 5 | 0.0 | | 185 | -18.0 | |
| 10 | -42.5 | | 190 | -39.0 | -39.0 |
| 15 | + 4.0 | | 195 | +40.0 | +40.0 |
| 20 | +18.0 | | 200 | -16.0 | |
| 25 | +18.0 | | 205 | - 9.0 | |
| 30 | +25.0 | | 210 | -14.0 | |
| 35 | +36,0 | +29.0 | 215 | - 4.0 | |
| 40 | +27.5 | +23.0 | 220 | - 9.0 | -13.0 |
| 45 | +40.0 | +40.0 | 225 | -31.0 | -31.0 |
| 50 | 0.0 | - 9.0 | 230 | -18.0 | |
| 55 | +12.0 | | 235 | -12.0 | |
| 60 | + 5.0 | | 240 | -18.0 | |
| 65 | +10.0 | | 245 | 0.0 | |
| 70 | -23.5 | | 250 | -14.0 | |
| 75 | -21.5 | | 255 | - 3.0 | |
| 80 | - 7.0 | | 260 | -14.0 | |
| 85 | 0.0 | | 265 | -31.0 | |
| 90 | +12.0 | | 270 | -26.5 | |
| 95 | +31.0 | | 275 | -20.0 | |
| 100 | +41.5 | | 280 | -36.0 | |
| 105 | +18.0 | | 285 | -40.0 | |
| 110 | 0.0 | | 290 | -16.0 | |
| 115 | 0.0 | | 295 | - 4.5 | |
| 120 | - 1.0 | | 300 | -50.0 | |
| 125 | - 3.0 | | 305 | -40.0 | |
| 130 | - 4.0 | | 310 | -18.0 | |
| 135 | -40.0 | -40.0 | 315 | -16.0 | |
| 140 | -31.0 | -36.0 | 320 | -14.0 | |
| 145 | -18.0 | | 325 | +22.0 | |
| 150 | -27.0 | | 330 | +25.5 | |
| 155 | -27.0 | | 335 | +45.0 | |
| 160 | -25.0 | | 340 | +31.0 | |
| 165 | -14.0 | | 345 | +12.0 | |
| 170 | -14.5 | | 350 | + 7.0 | |
| 175 | -23.0 | -27.0 | 355 | - 4.5 | |

TABLE VIII

Magnitude and Direction of the Principal Stresses at Various Points Along One Portion of the Center Line of the Weld

| Angular Position Degrees | $S_1$ 1000 psi | $S_2$ 1000 psi | Angle from $S_L$ to $S_1$ Degrees |
|---|---|---|---|
| 125 | + 3,000 | 0 | 48 |
| 130 | +25,000 | -10,000 | 133 |
| 135 | + 8,000 | - 6,000 | 39 |
| 140 | +16,000 | - 7,000 | 71 |
| 145 | +11,000 | -24,000 | 66 |
| 150 | - 2,000 | -22,000 | 106 |
| 155 | -11,000 | -21,000 | 59 |
| 160 | - 2,000 | -12,000 | 72 |

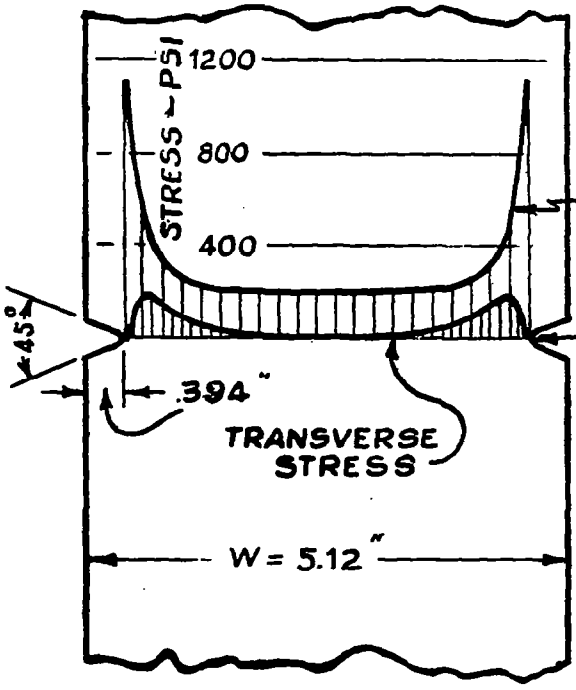


Figure 1.- Stress distribution in a notched flat bar under tension (Coker and Filon).

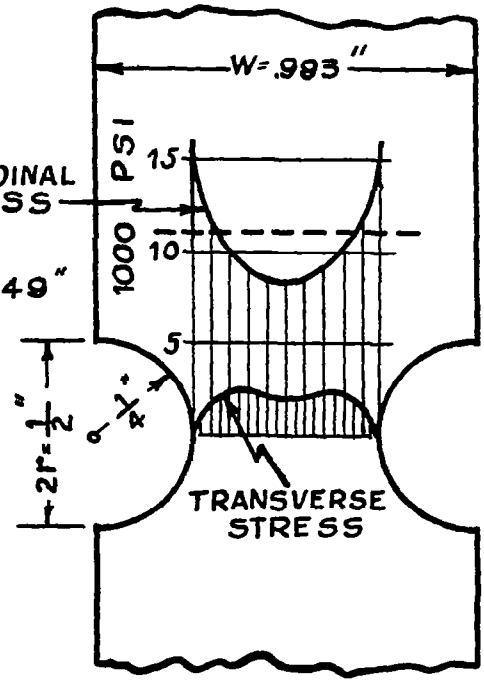


Figure 3.- Stress distribution in a notched flat bar under tension (Coker and Filon).

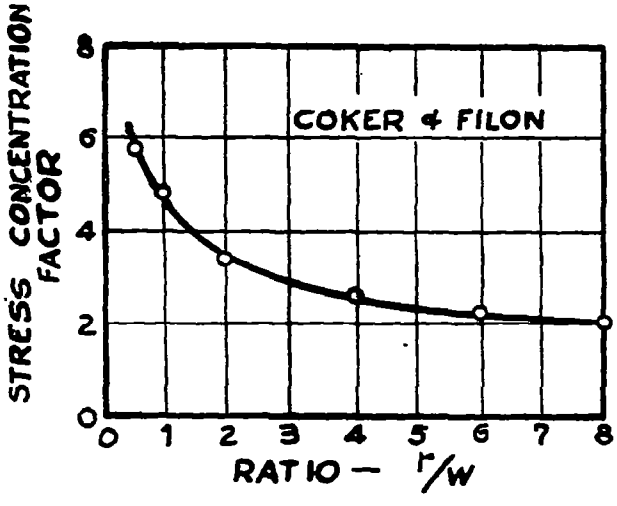


Figure 2.- Effect of bottom radius on stress concentration in a flat bar having V notches as shown in Figure 1.

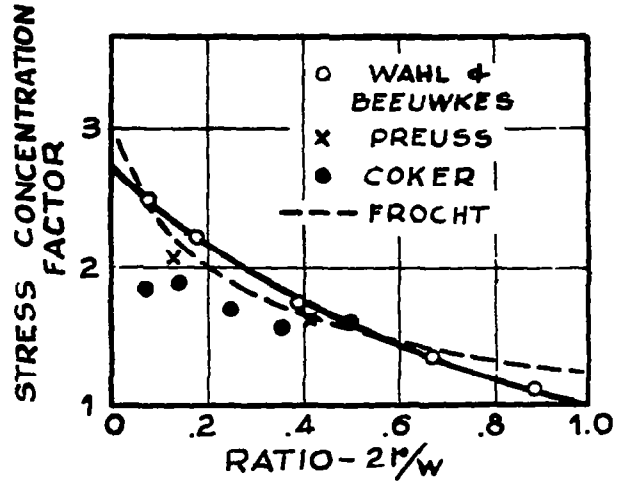


Figure 4.- Effect of notch depth on stress concentration in a flat bar having semicircular notches as shown in Figure 3.

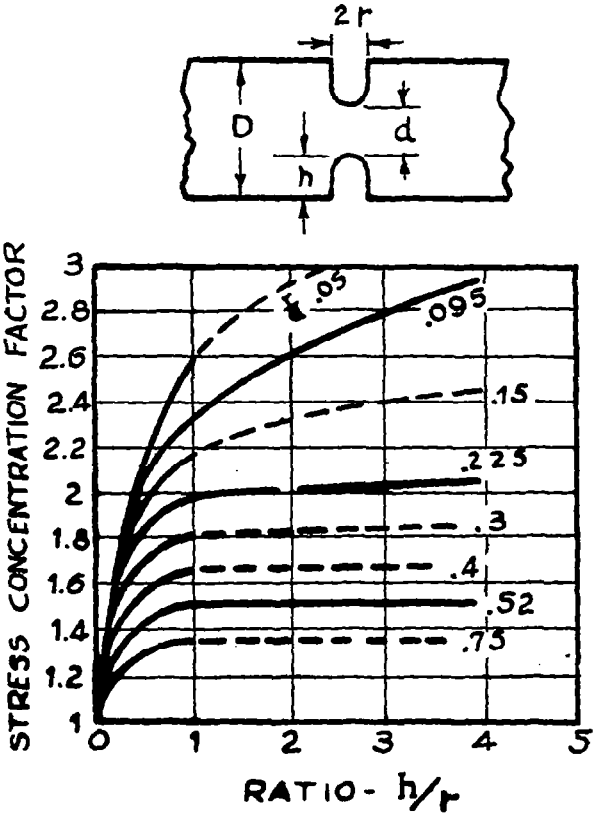


Figure 5.- Effect of depth and radius of notch on stress concentration in a flat notched bar (derived from Frocht).

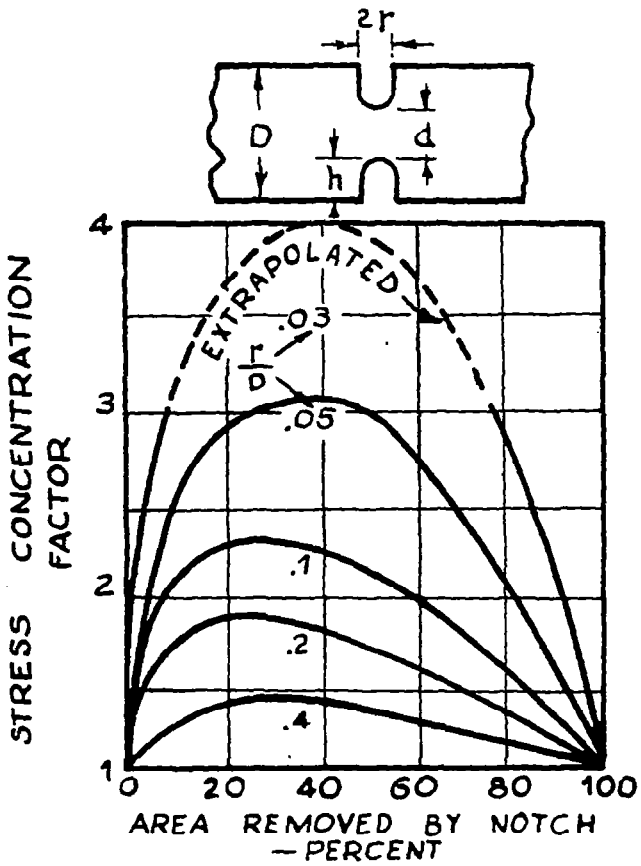


Figure 6.- Effect of depth and radius of notch on stress concentration in a flat notched bar (derived from Frocht).

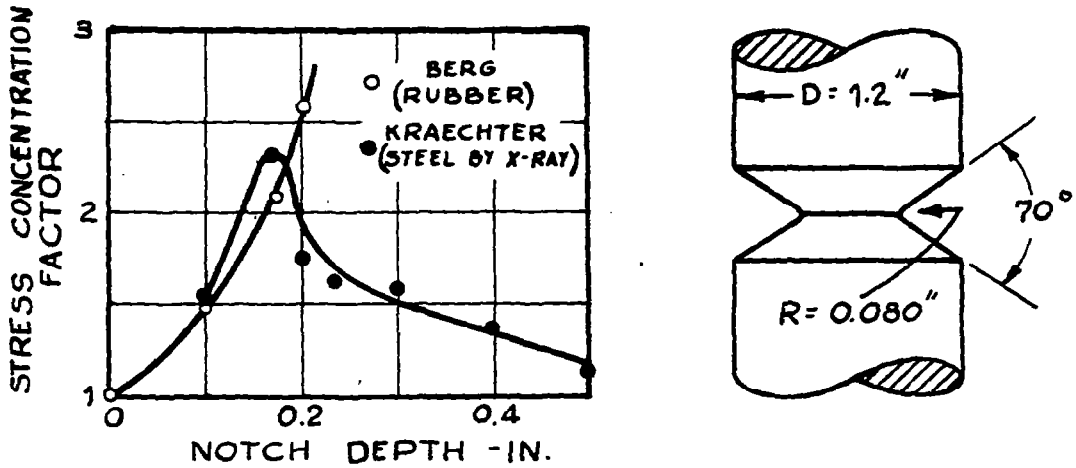


Figure 7.- Effect of notch depth on stress concentration in round notched bars.

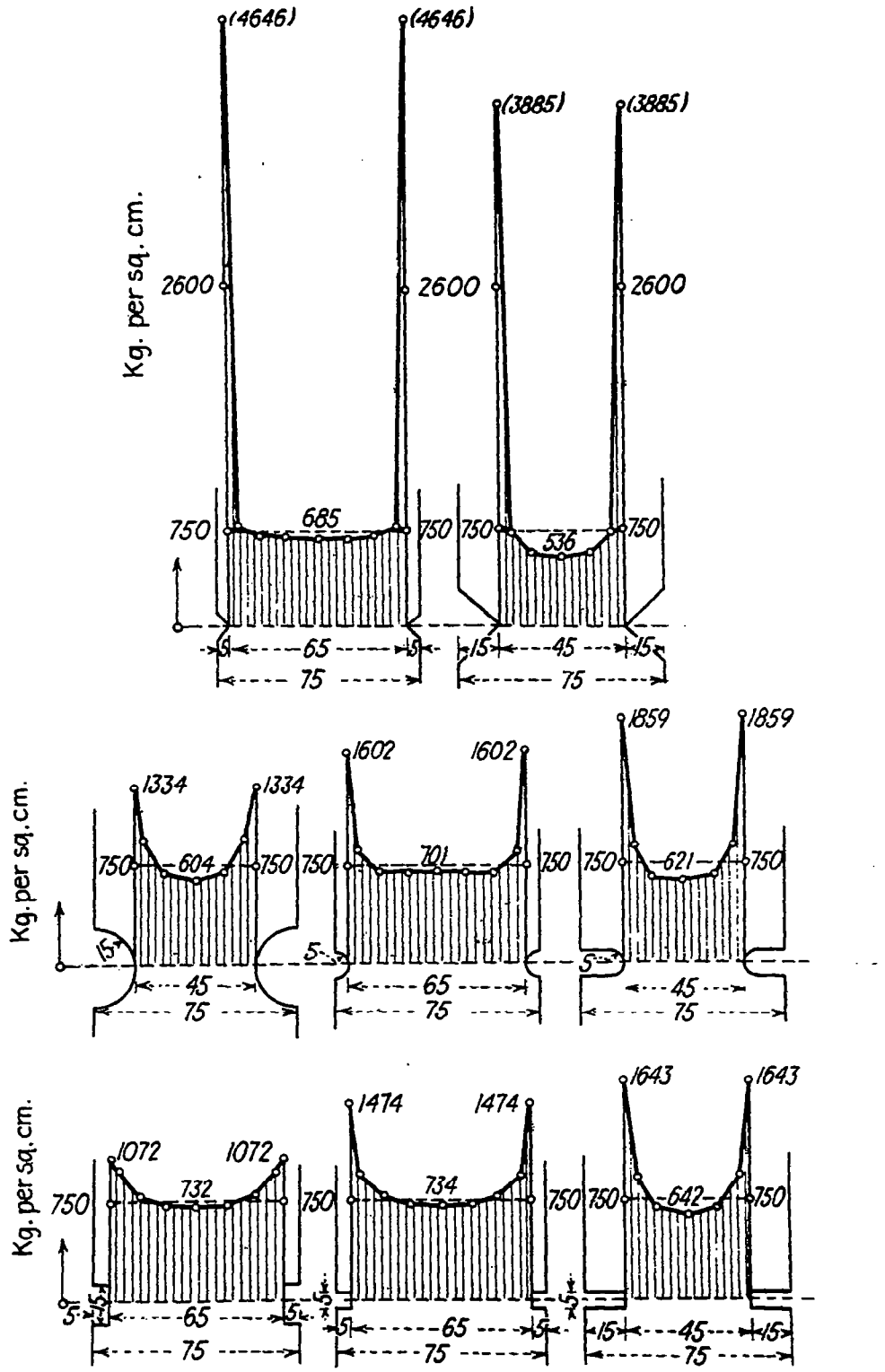


**Figure 8.- Elastic longitudinal stress distribution for various notches of different depths.**

FIGURE 9.—Mergence of $K_\alpha$ doublet on normalizing from 1700° F.

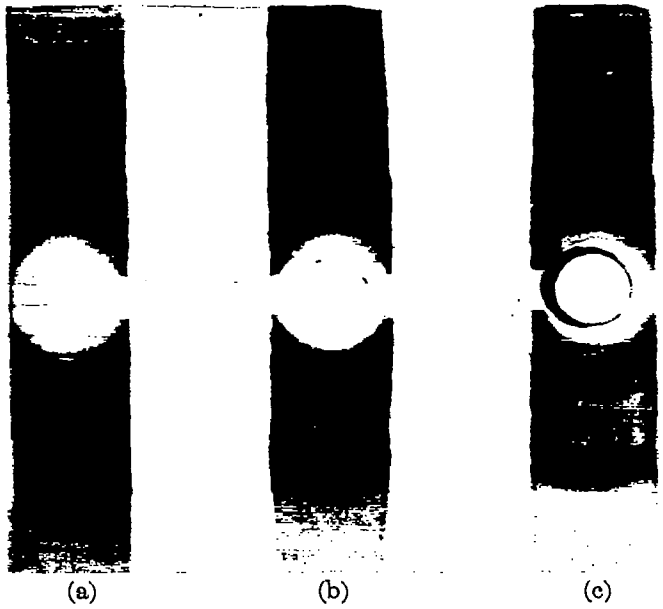

(a) (b) (c)

FIGURE 10.—Diffraction patterns of SAE X4130 steel, stress relieved at (a) 1000° F., (b) 1250° F., and (c) 1320° F., after normalizing from 1700° F.

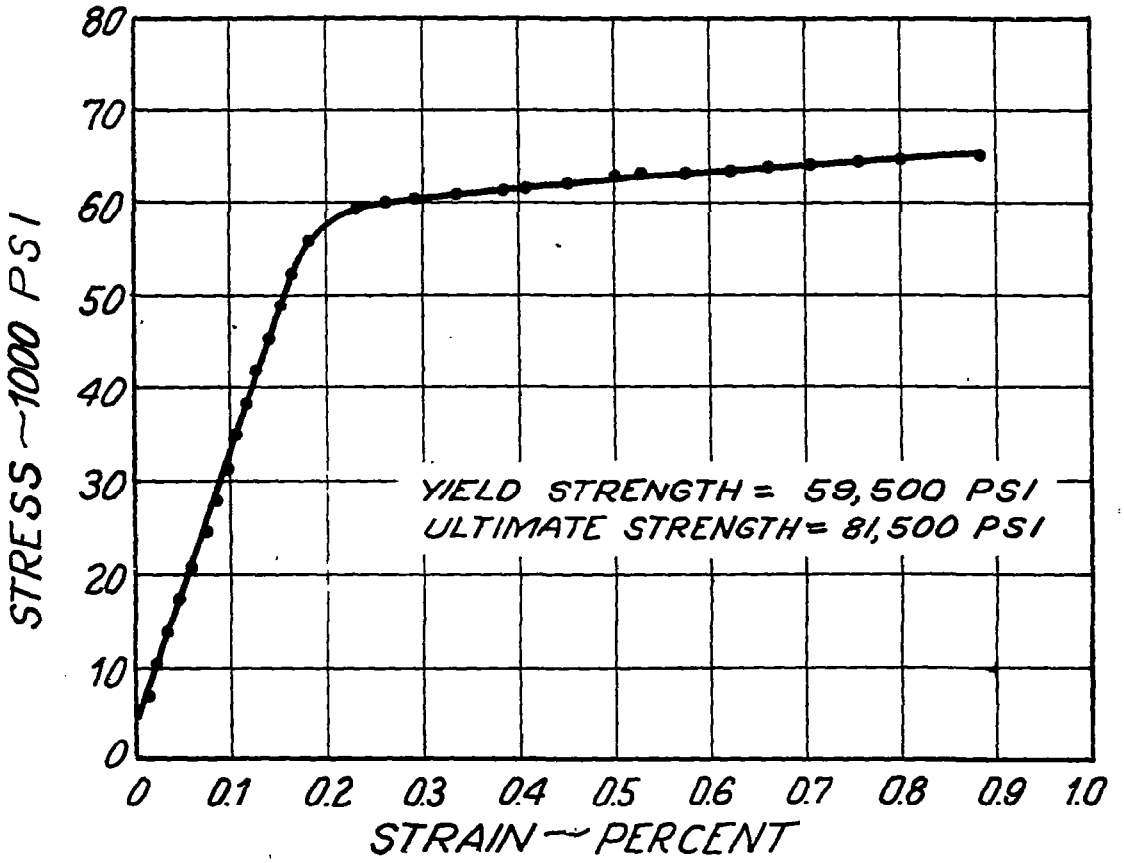


Figure 11.- Stress strain curve for SAE X4130 steel strip air cooled from 1700° F and stress relieved at 1320° F.

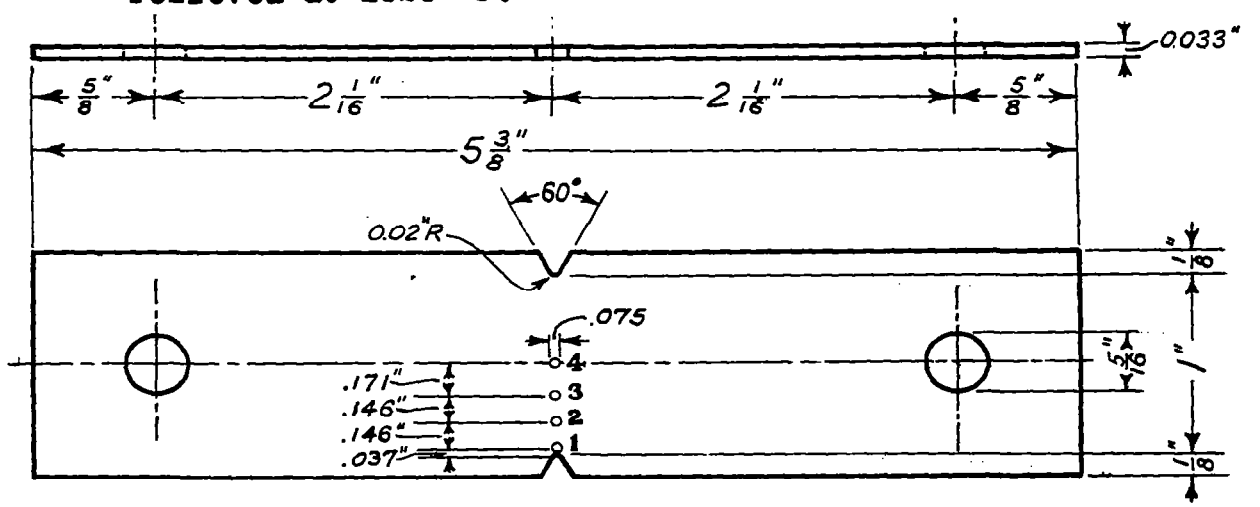


Figure 12.- Tensile specimen. 1,2,3,4 - location of spots studied.

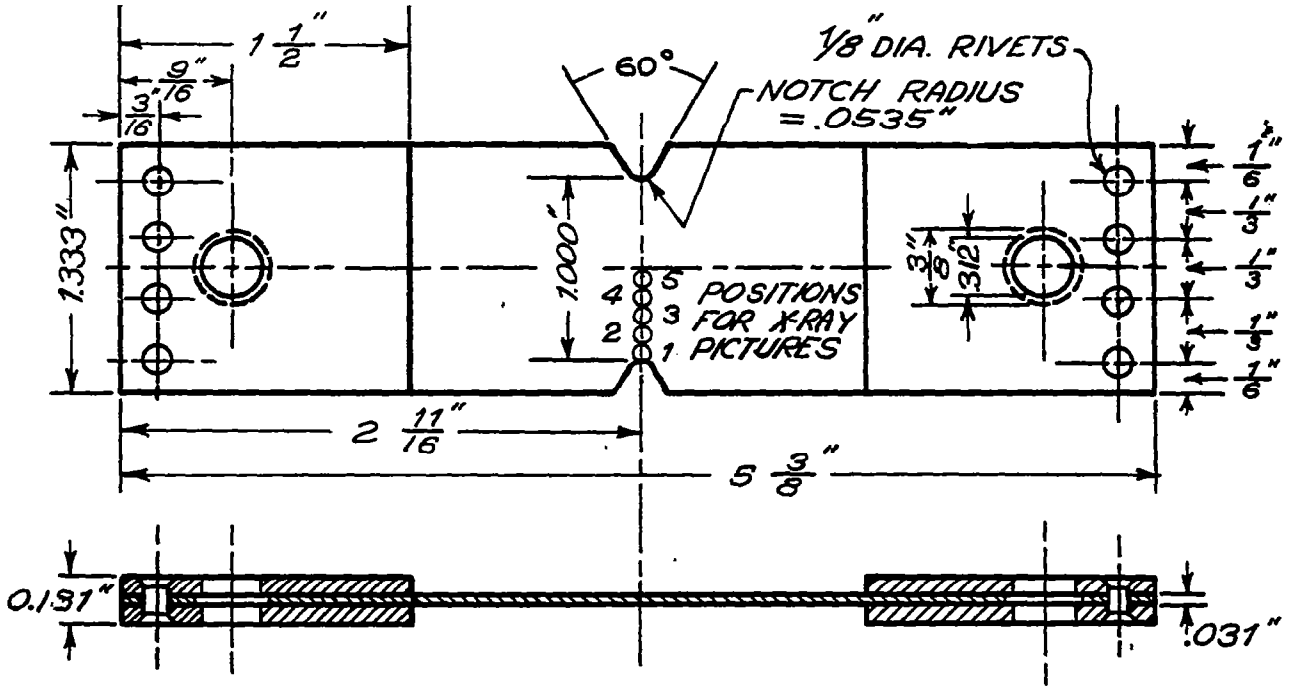


25 % NOTCH SPECIMEN

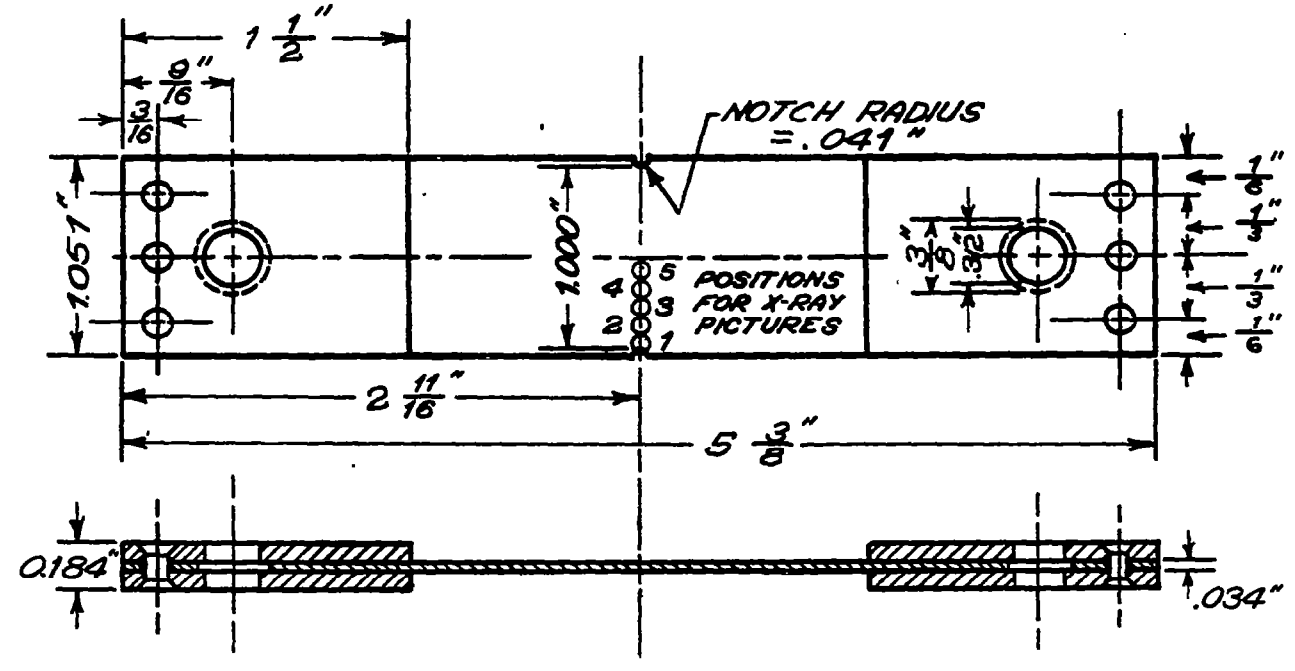


5 % NOTCH SPECIMEN

Figure 13.- SAE X4130 steel flat tensile test specimens.

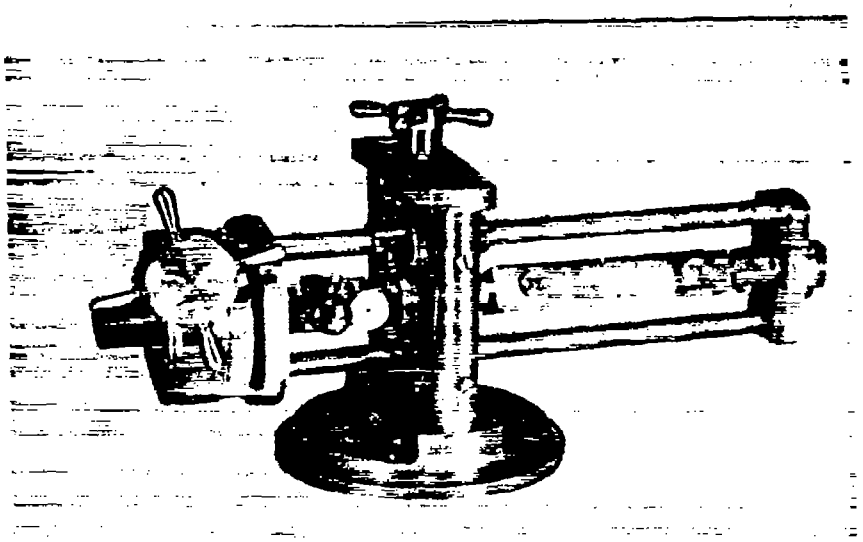

FIGURE 14.—Special tensile testing machine.

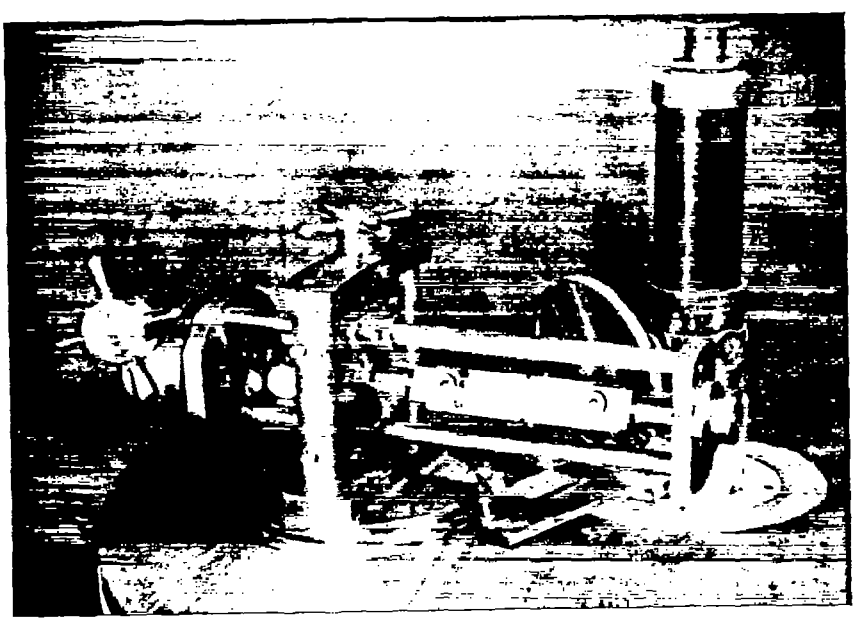

FIGURE 15.—Special tensile testing machine in position to make oblique diffraction patterns of duralumin tensile bar.

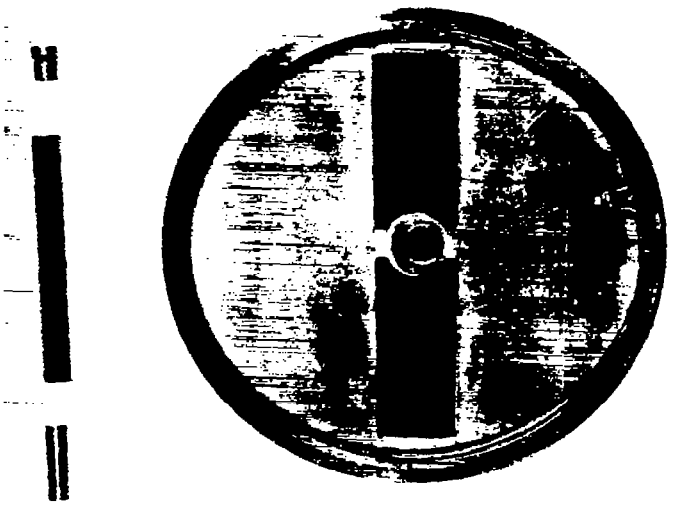

FIGURE 16.—Back reflection cassette and pinhole system.

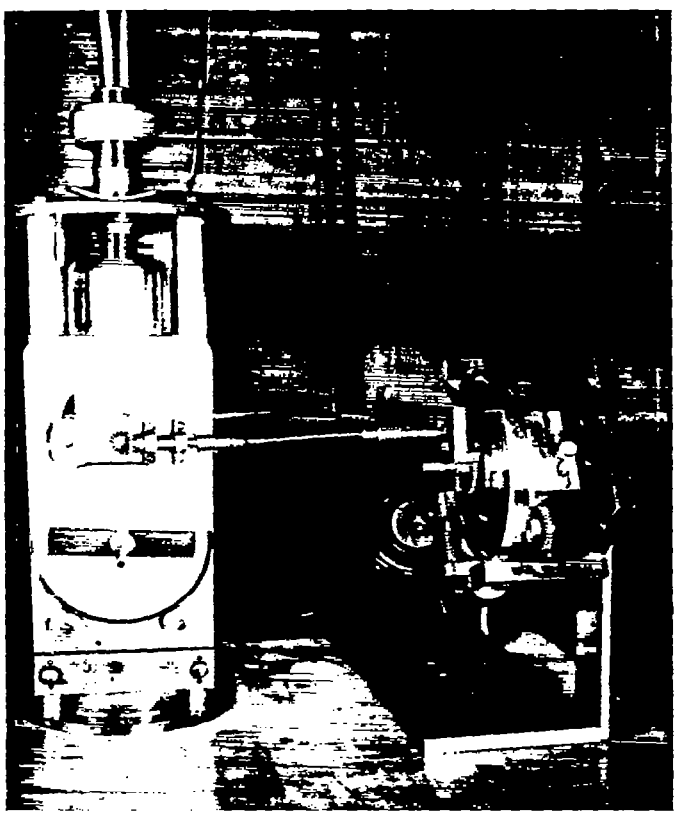

FIGURE 17.—Back reflection camera with pinhole system in place and rocking mechanism.

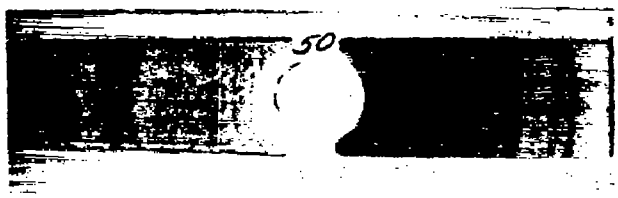

FIGURE 18.—Diffraction pattern showing spotty silver lines.

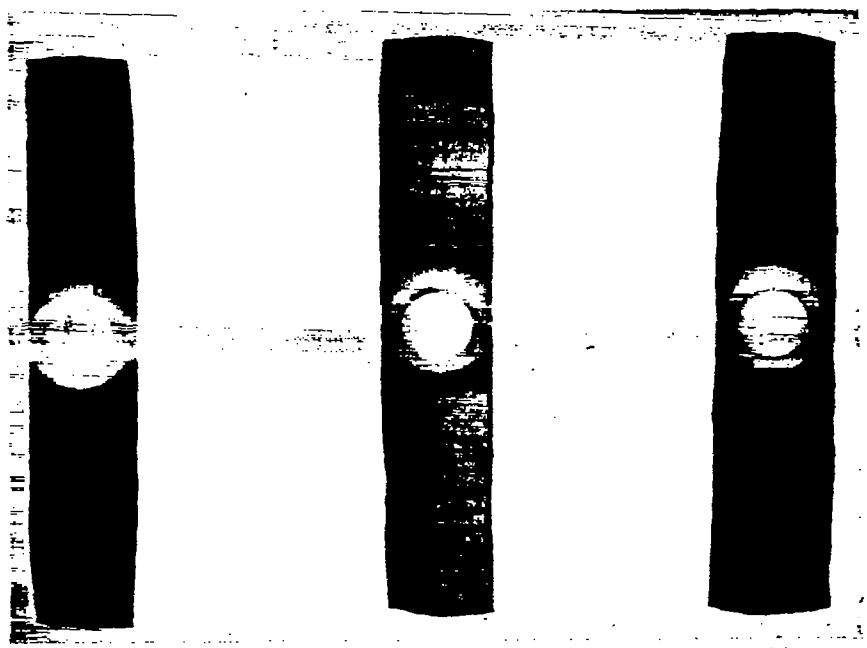

(a) (b) (c)

FIGURE 19.—Diffraction patterns showing (a) too little, (b) proper amount, and (c) too much silver.

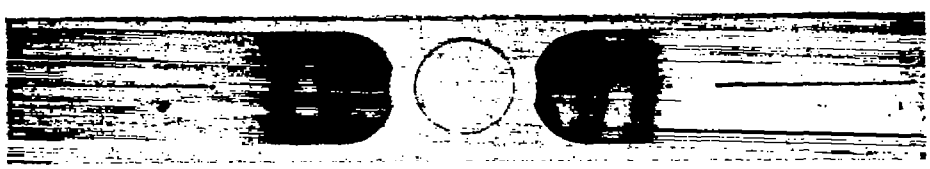

FIGURE 20.—Typical duralumin diffraction pattern.

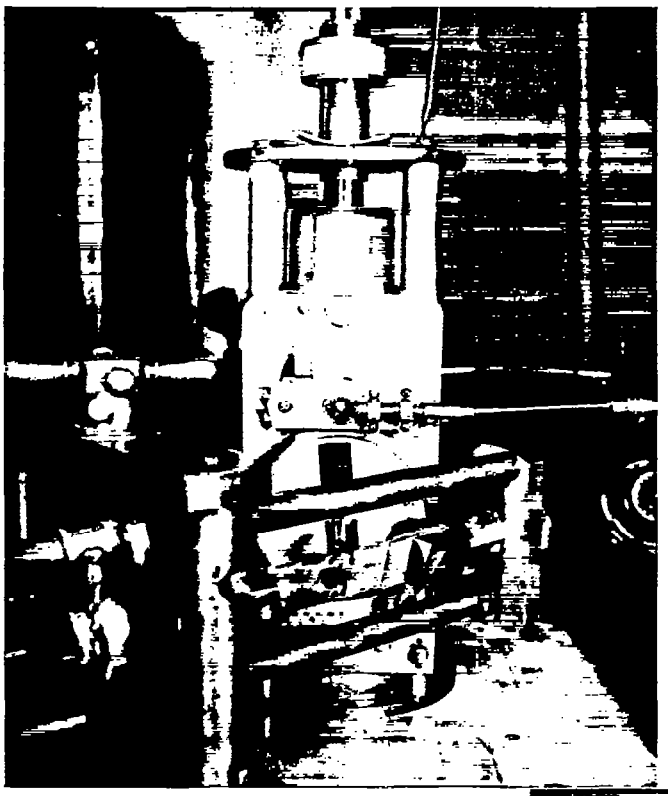

FIGURE 21.—Special tensile machine in position for making longitudinal strain diffraction patterns from SAE X4130 steel tensile bars.

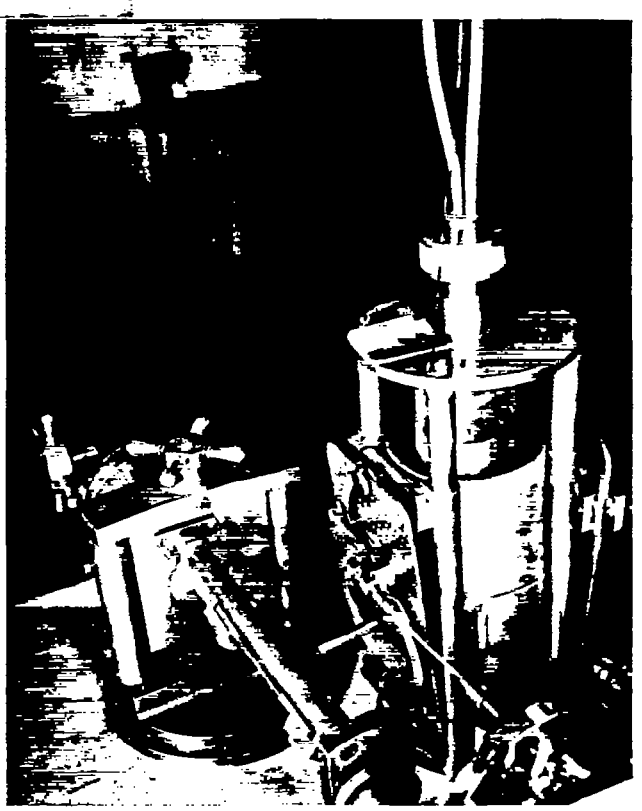

FIGURE 22.—Special tensile machine in position for making transverse strain diffraction patterns from SAE X4130 steel tensile bars.

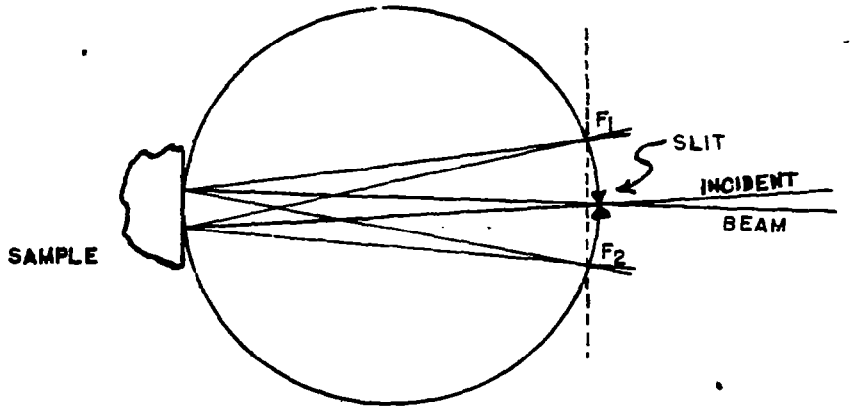


(a).-Normal Incidence

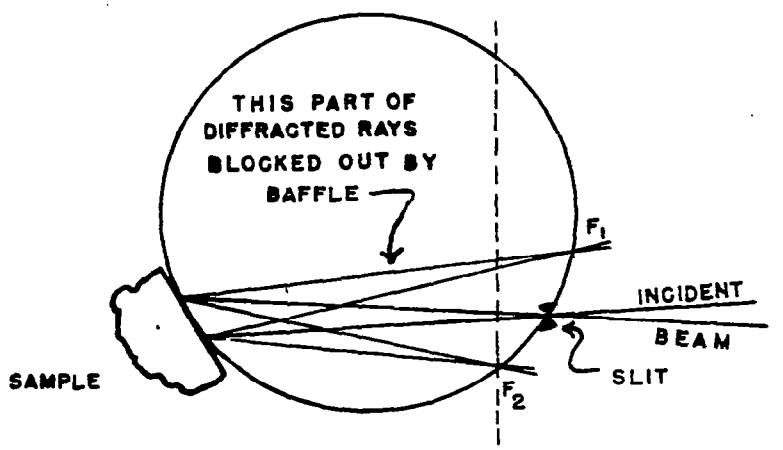


(b).-Oblique Incidence

Figure 23a,b.- Focusing conditions.

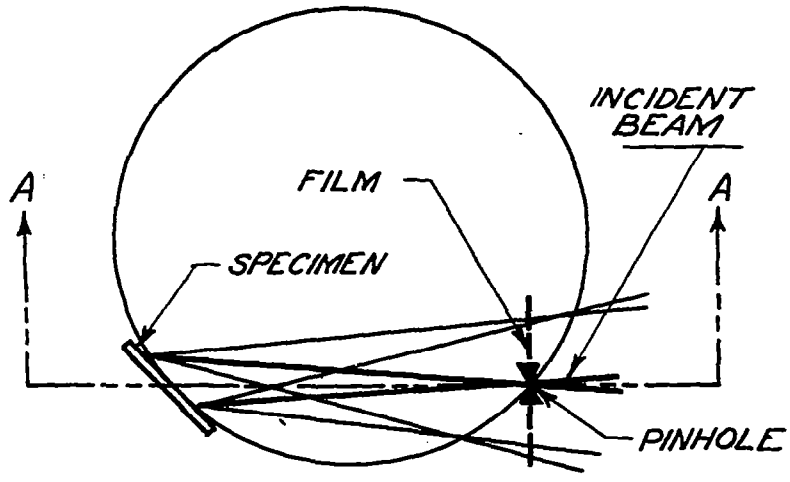


Figure 24a.- Side view of focusing sphere showing non-focusing conditions for oblique incidence.

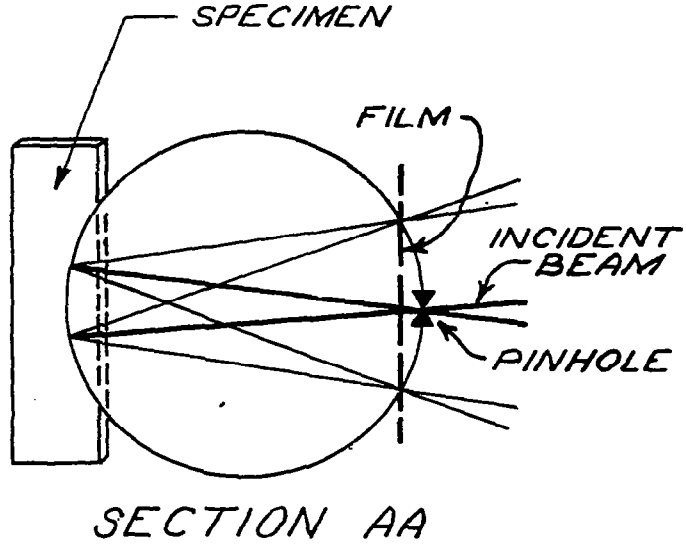


Figure 24b.- Top view of section through minor diameter of focusing sphere showing focusing conditions for oblique incidence.

FIGURE 25.—Comparator used in measuring steel diffraction patterns.


FIGURE 26.—Viewing tube for comparator used in measuring duralumin diffraction patterns.

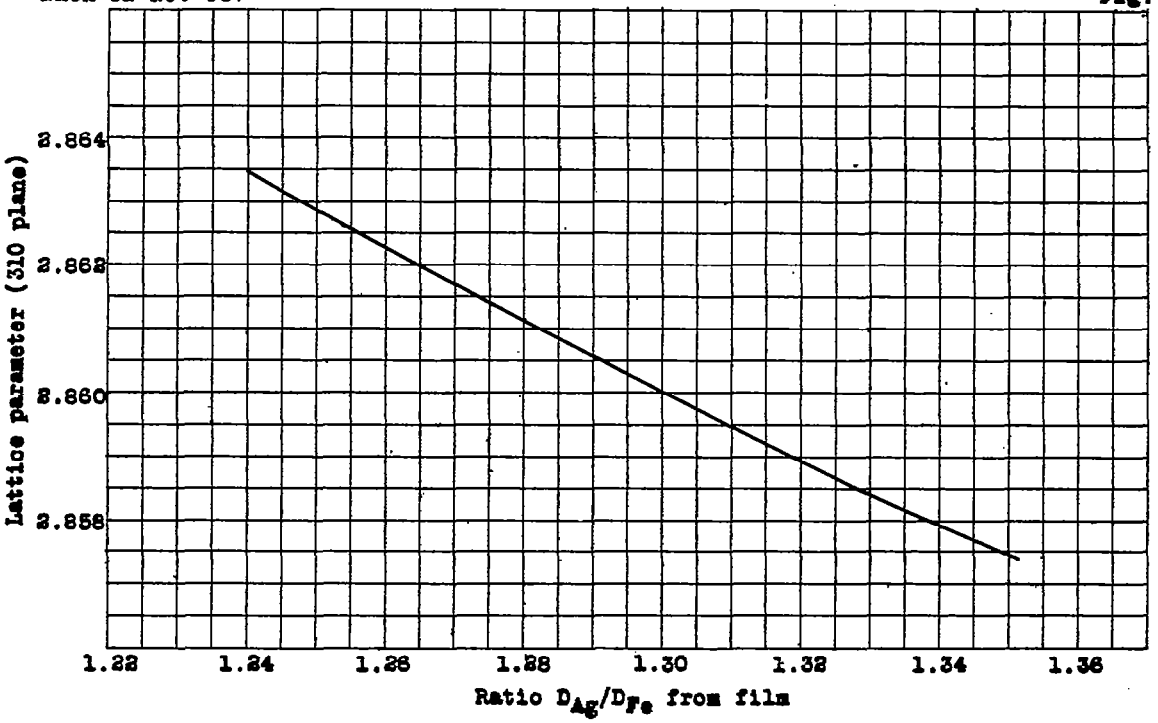


Figure 27a.- Chart for calculation of iron lattice parameter from measured diffraction ring diameters $D_{Ag}$ and $D_{Fe}$.

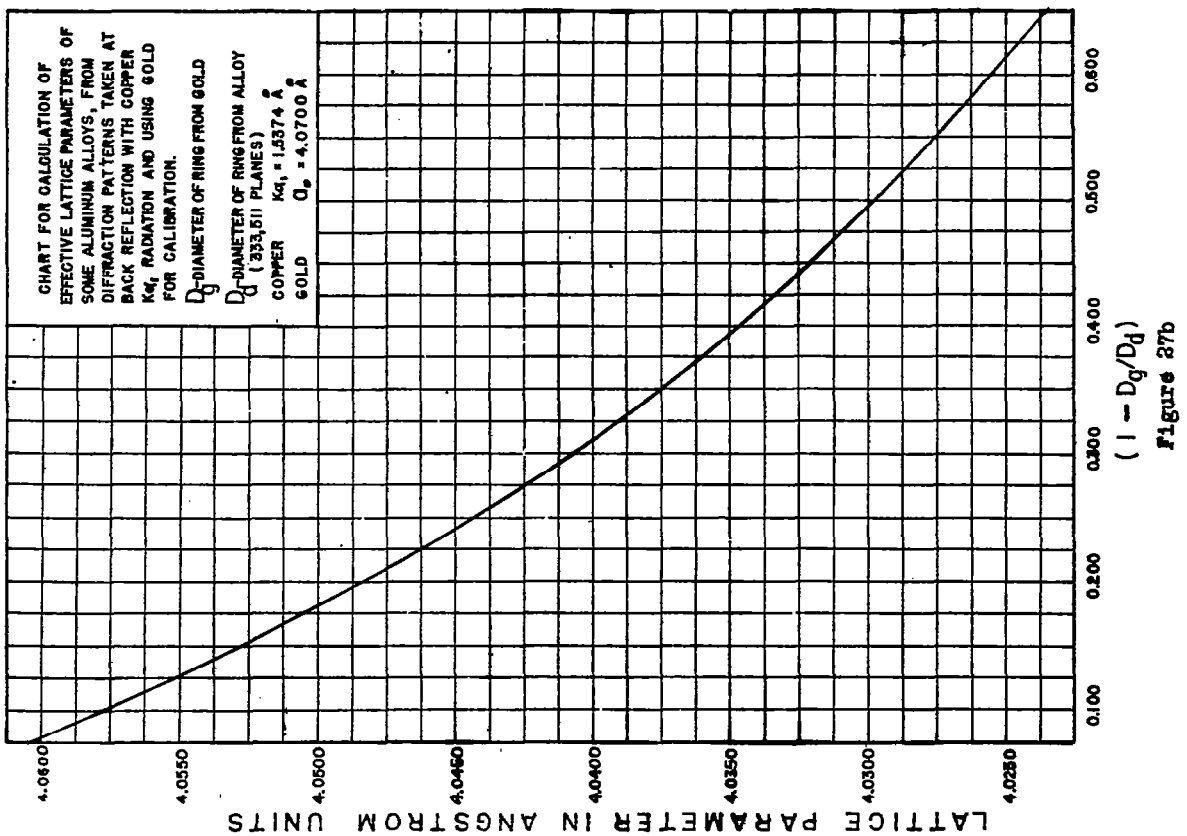


Figure 27b

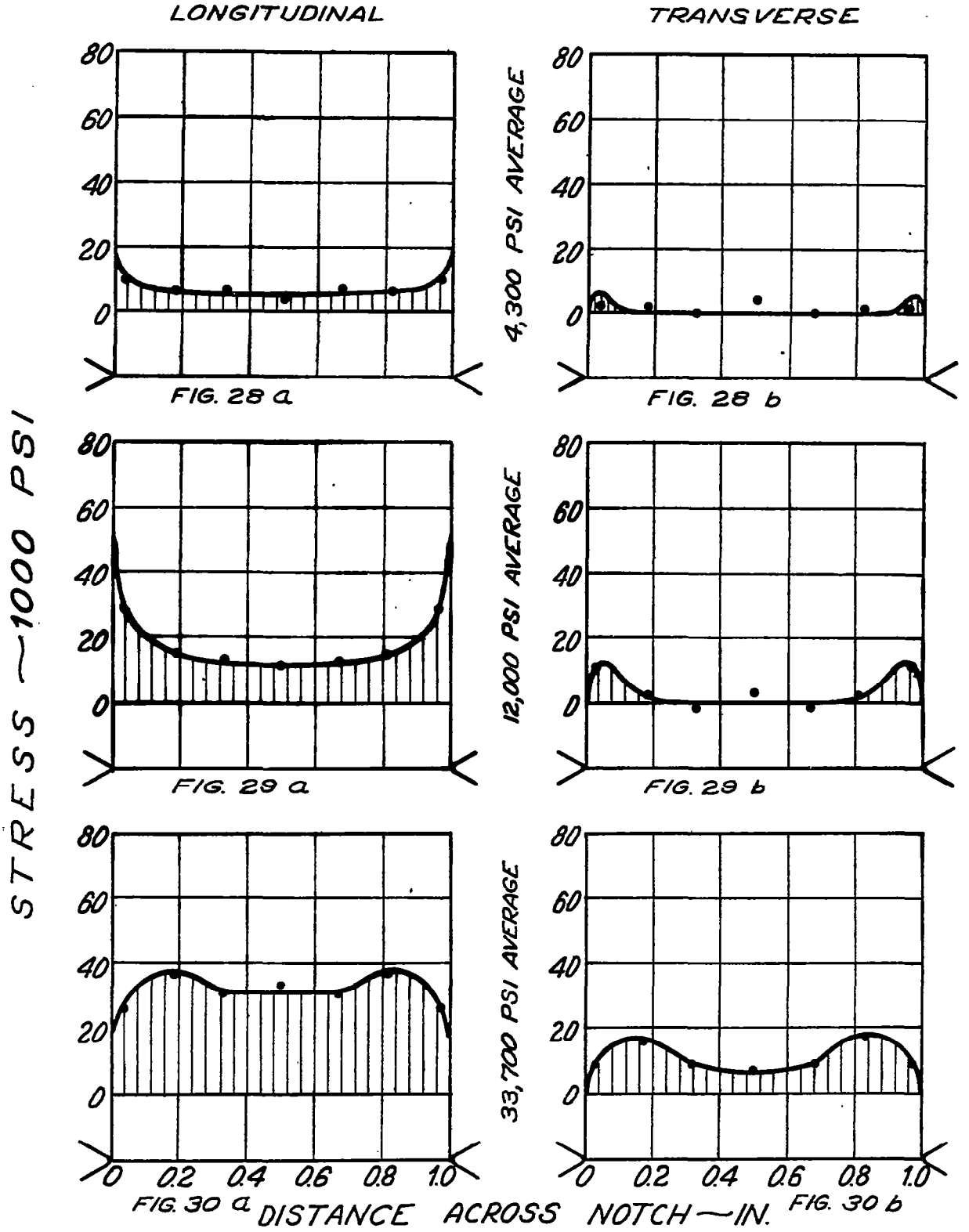


FIG. 28 a FIG. 28 b

FIG. 29 a FIG. 29 b

FIG. 30 a FIG. 30 b

Figures 28,29,30.- Measured stress distributions in 20% notched 24-SH duralumin flat tensile bar.

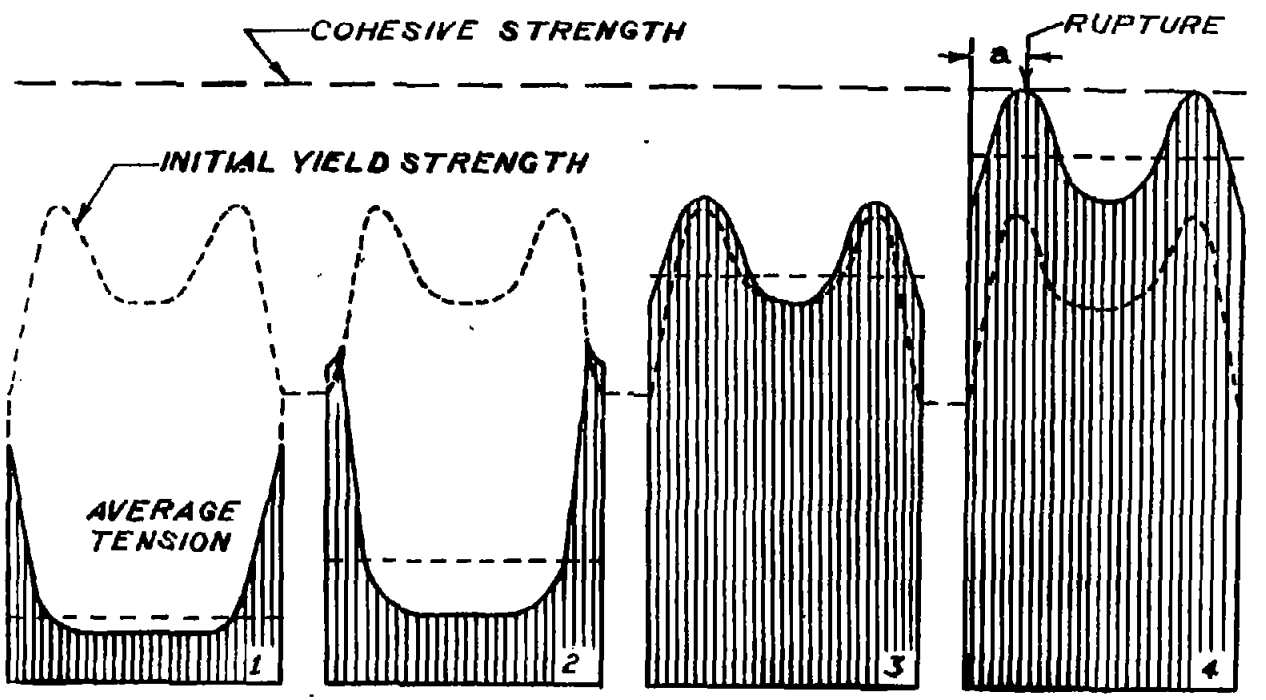


Figure 31.- Proposed elastic longitudinal stress distributions in notched tensile test bars with increasing applied loads. (Sachs and Lubahn)

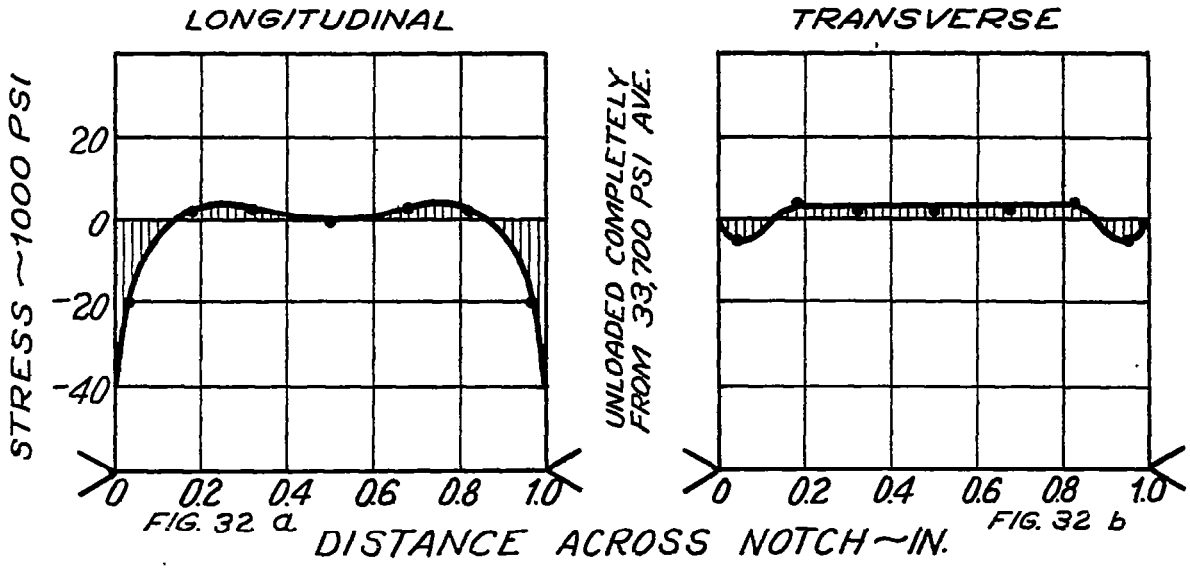


Figure 32.- Residual stress distribution in 20% notched 24-SH duralumin flat tensile bar.

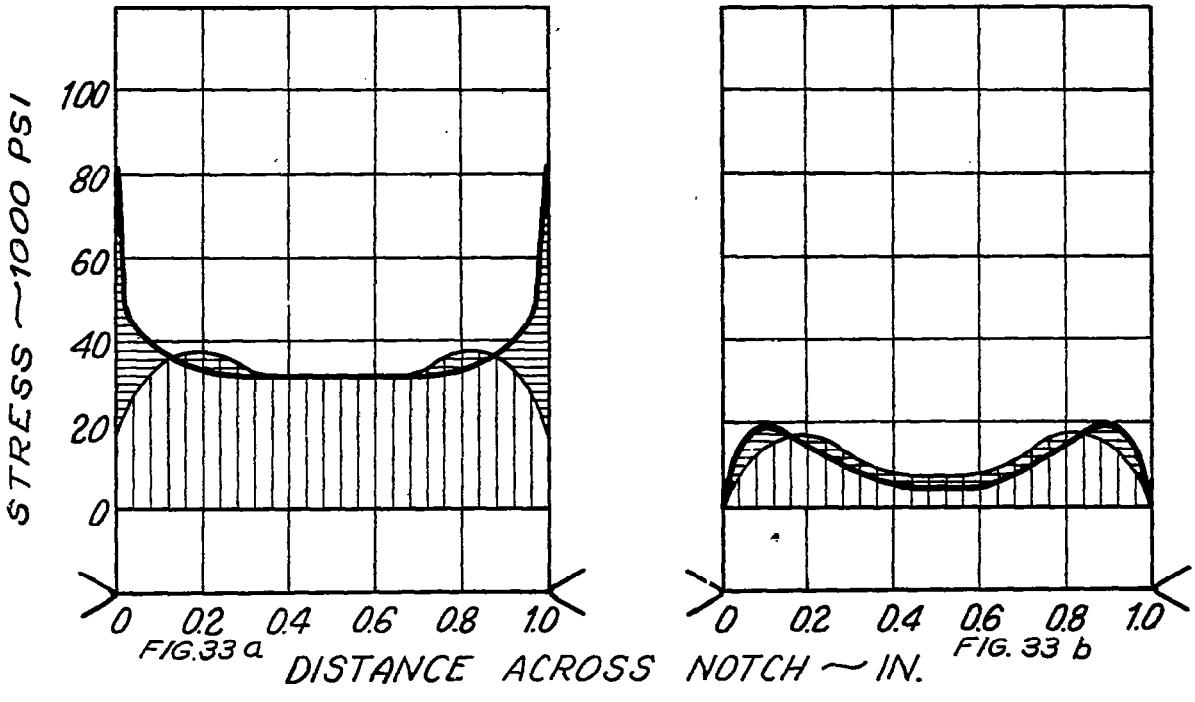


Figure 33.- Ficticious elastic stress distribution for 33,700 psi average load in 20% notched 24-SH duralumin flat tensile bar. (Actual distribution minus residual distribution)

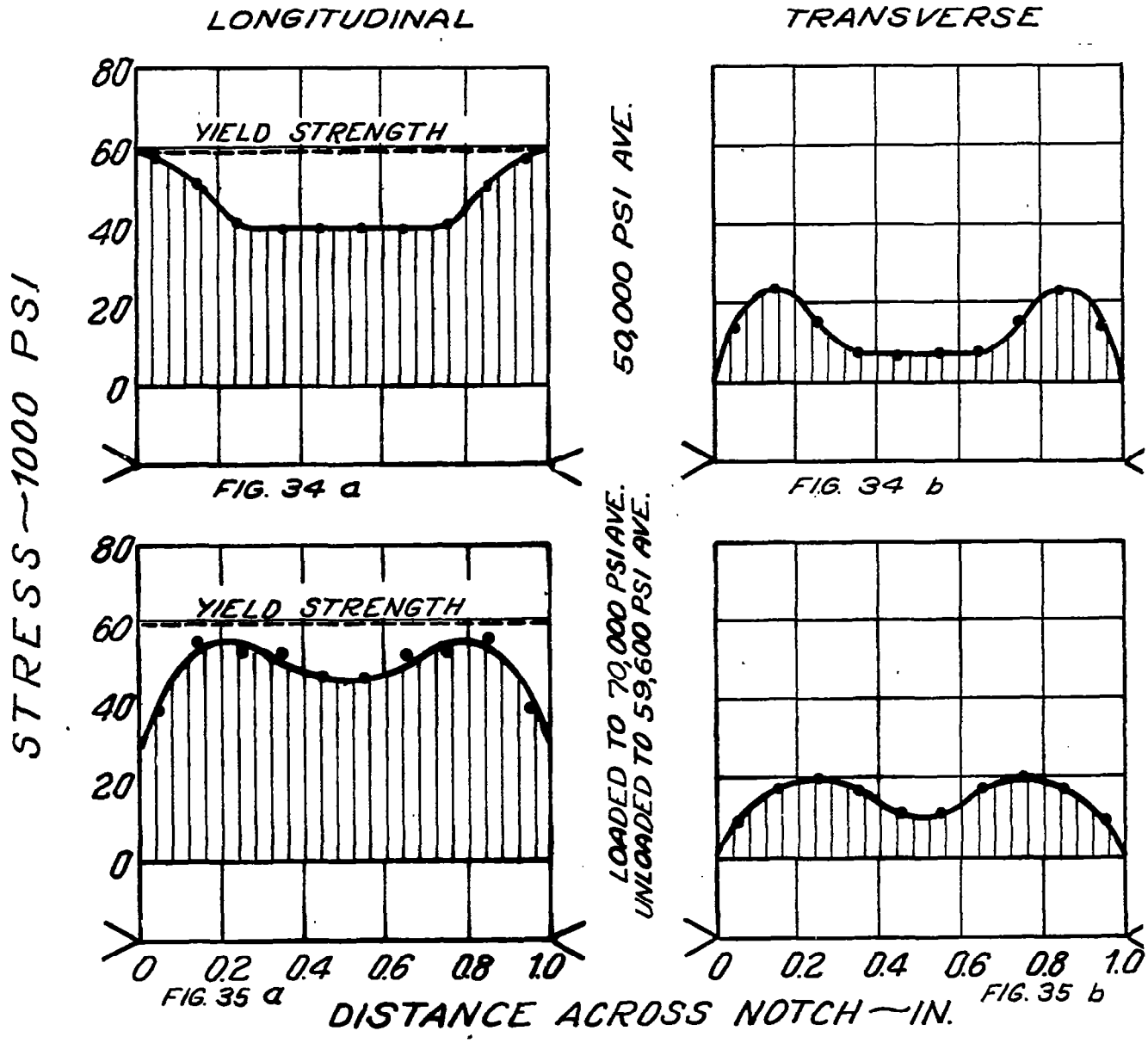


Figures 34,35.- Measured stress distributions in 25% notched SAE X4130 steel flat tensile bar.

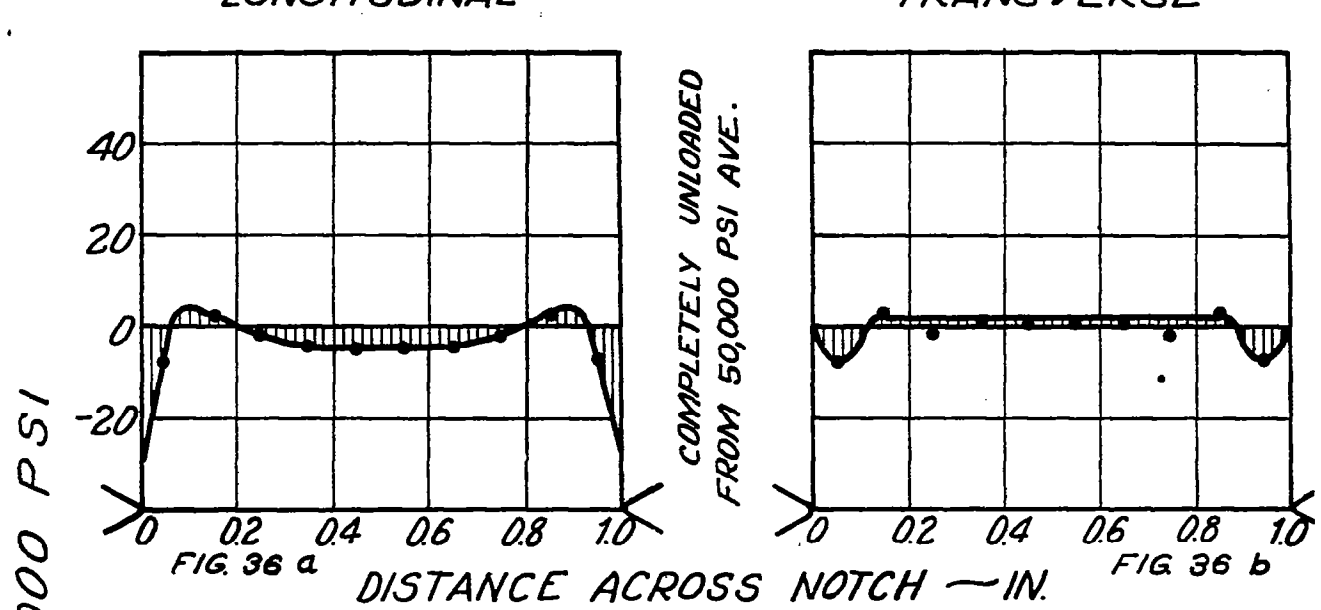


Figure 36.- Residual stress distribution in 25% notched SAE X4130 steel flat tensile bar.

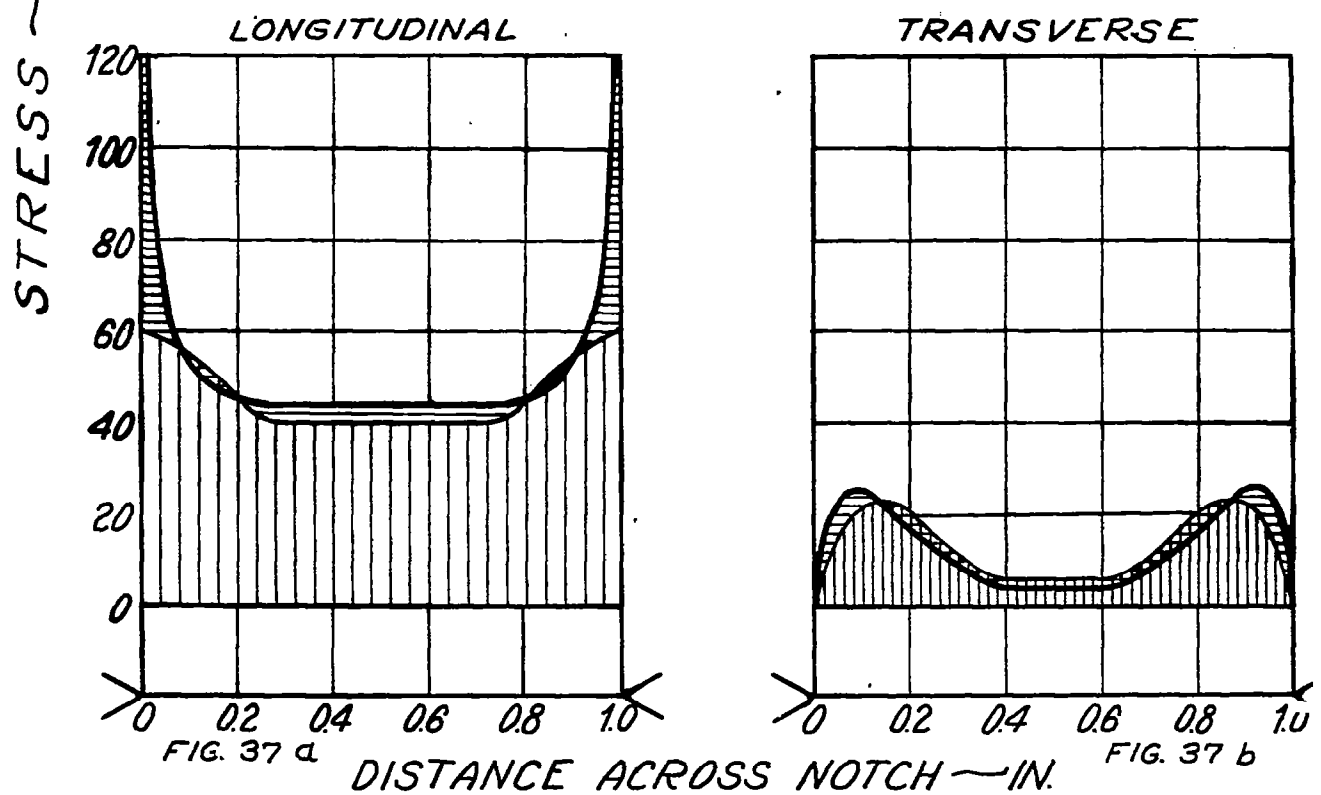


Figure 37.- Ficticious elastic stress distribution for 50,000 psi average load on 25% notched SAE X4130 steel flat tensile bar. (Actual distribution minus residual distribution).

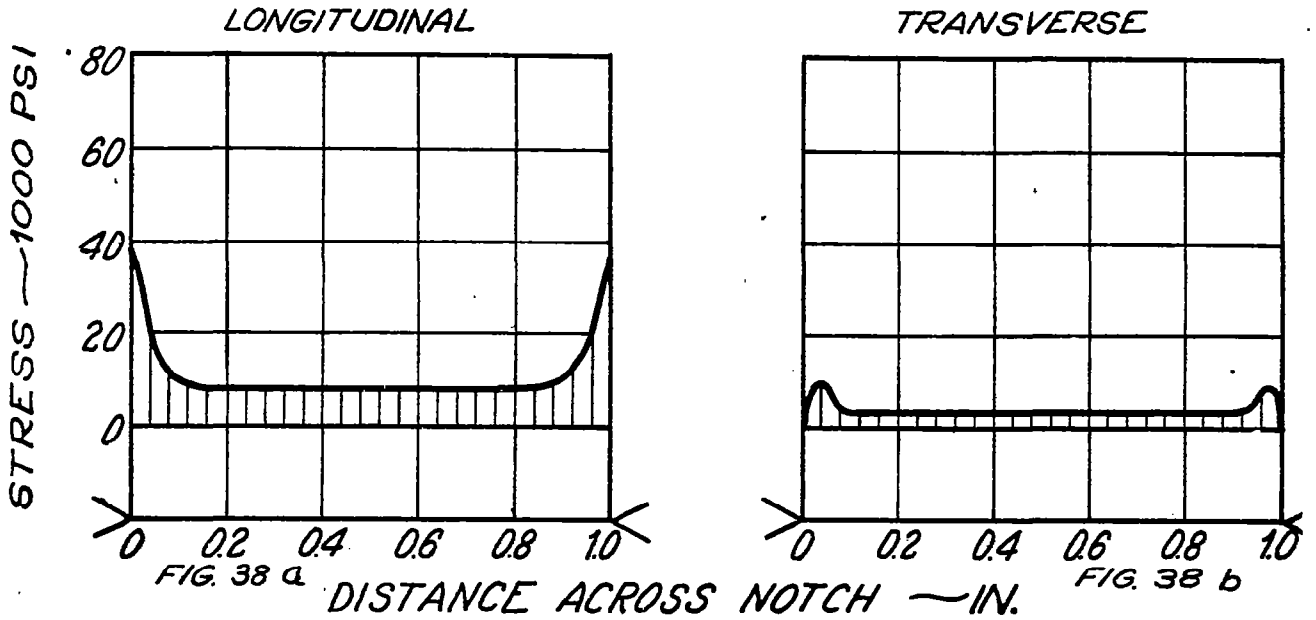


Figure 38.- Hypothetical stress distribution for 10,500 psi average elastic relief of 70,000 psi average load on 25% notched SAE X4130 flat tensile bar.

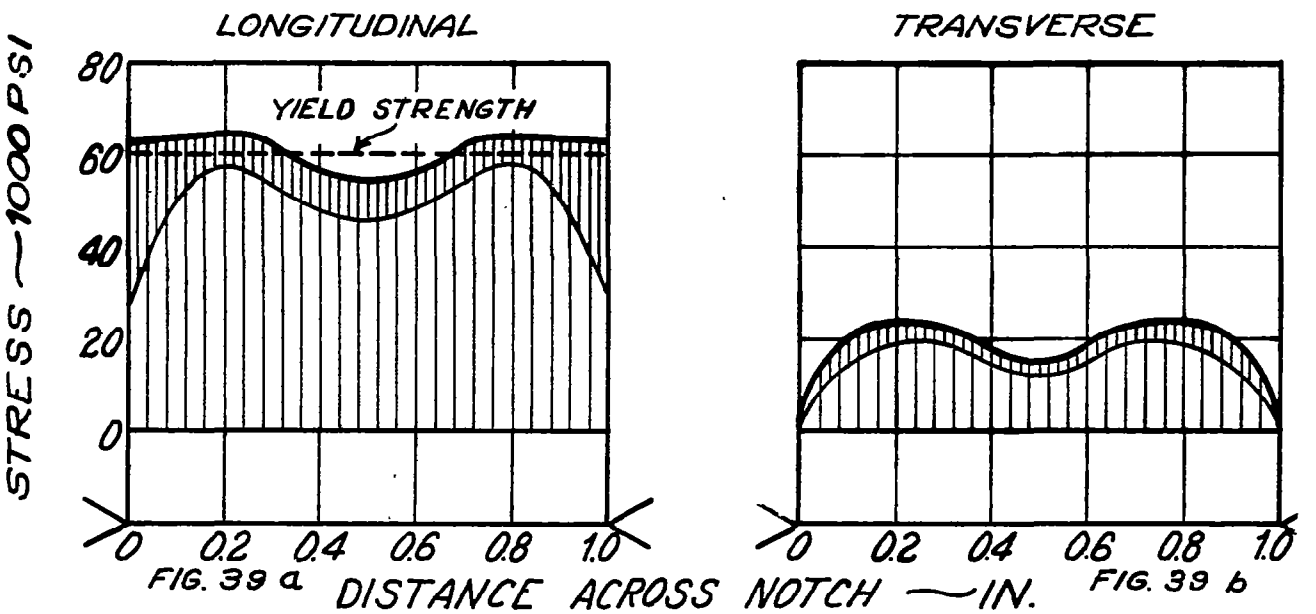


Figure 39.- Actual stress distribution curve for 70,000 psi average load on 25% notched SAE X4130 flat tensile bar (measured distribution plus hypothetical distribution).

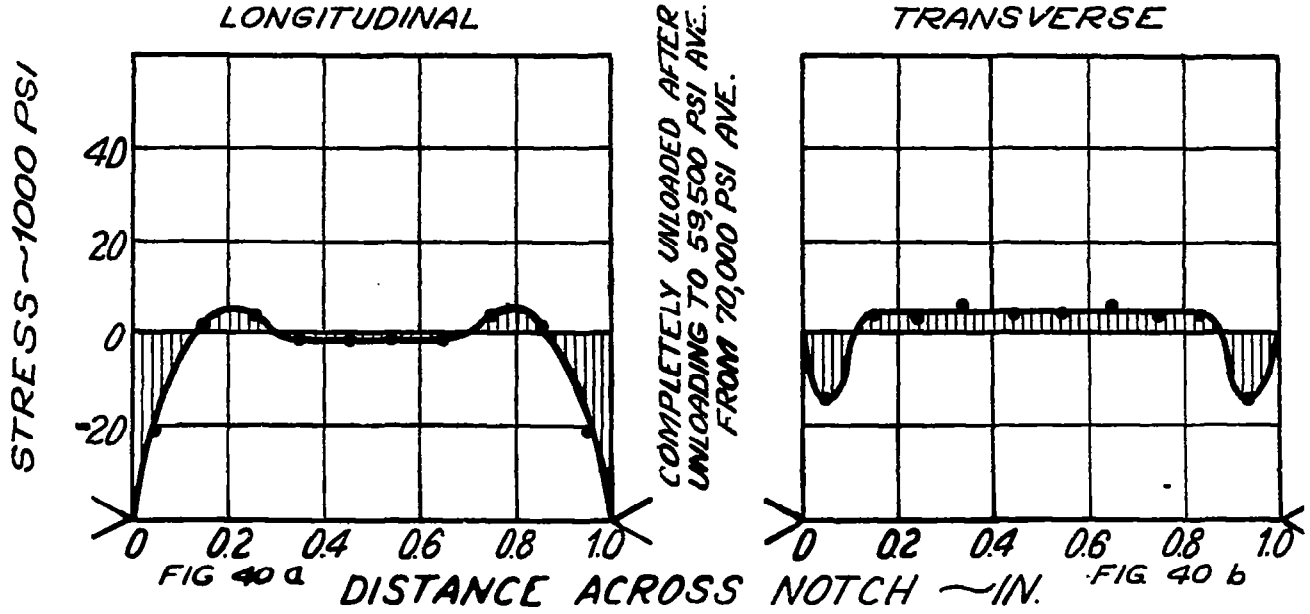


Figure 40.- Residual stress distribution in 25% notched SAE X4130 steel flat tensile bar.

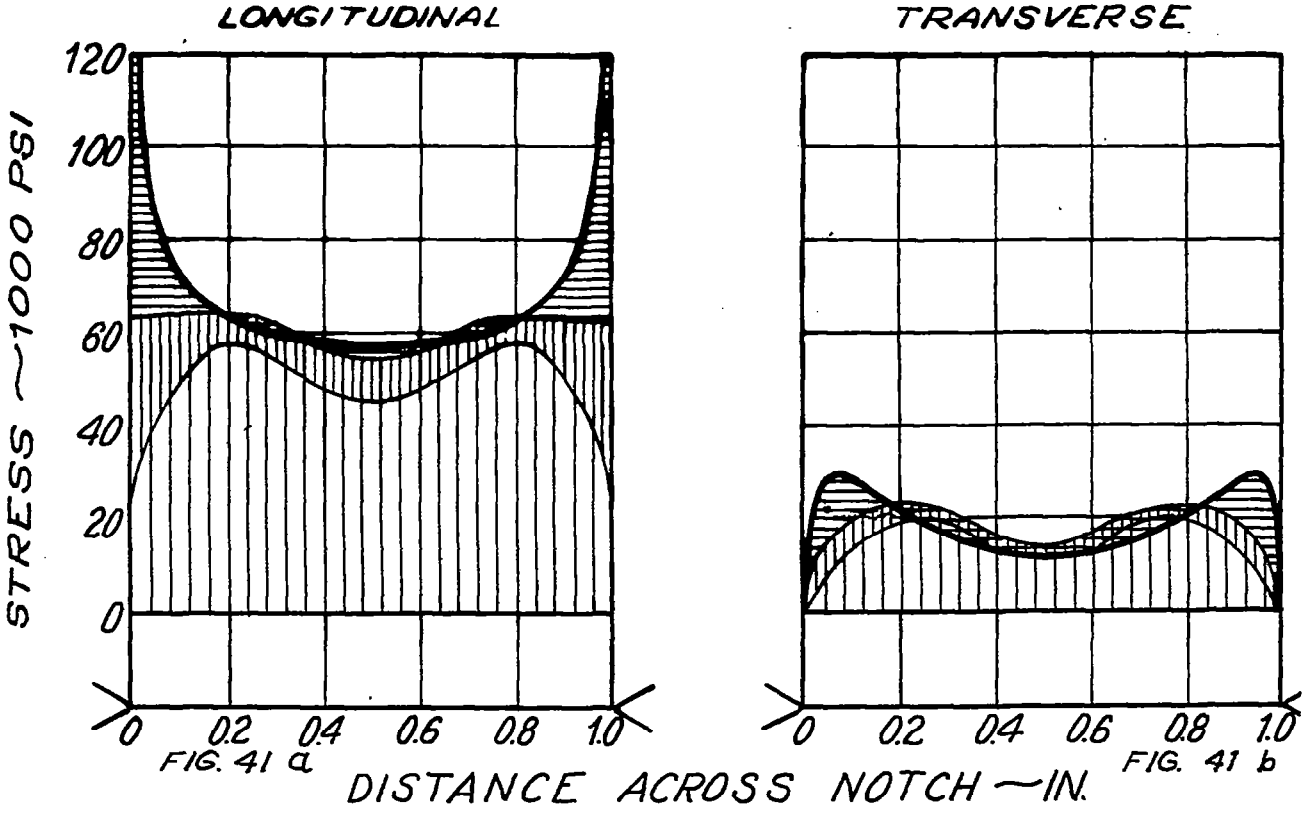


Figure 41.- Ficticious elastic stress distributions for 70,000 psi average load on 25% notched SAE X4130 flat tensile bar. (Actual distribution minus residual distribution).

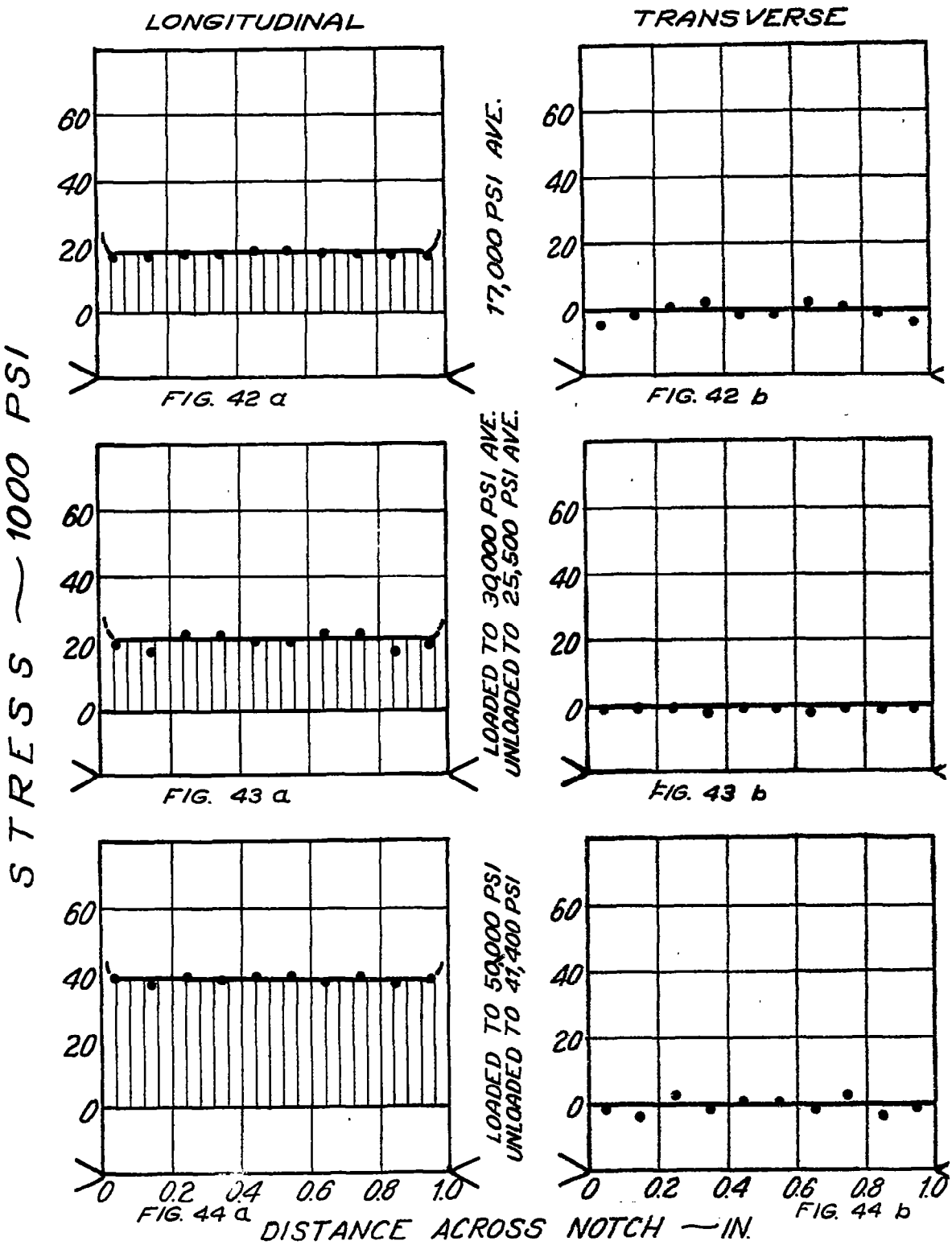


Figures 42,43,44.- Measured stress distribution in 5% notched SAE X4130 steel flat tensile bar.

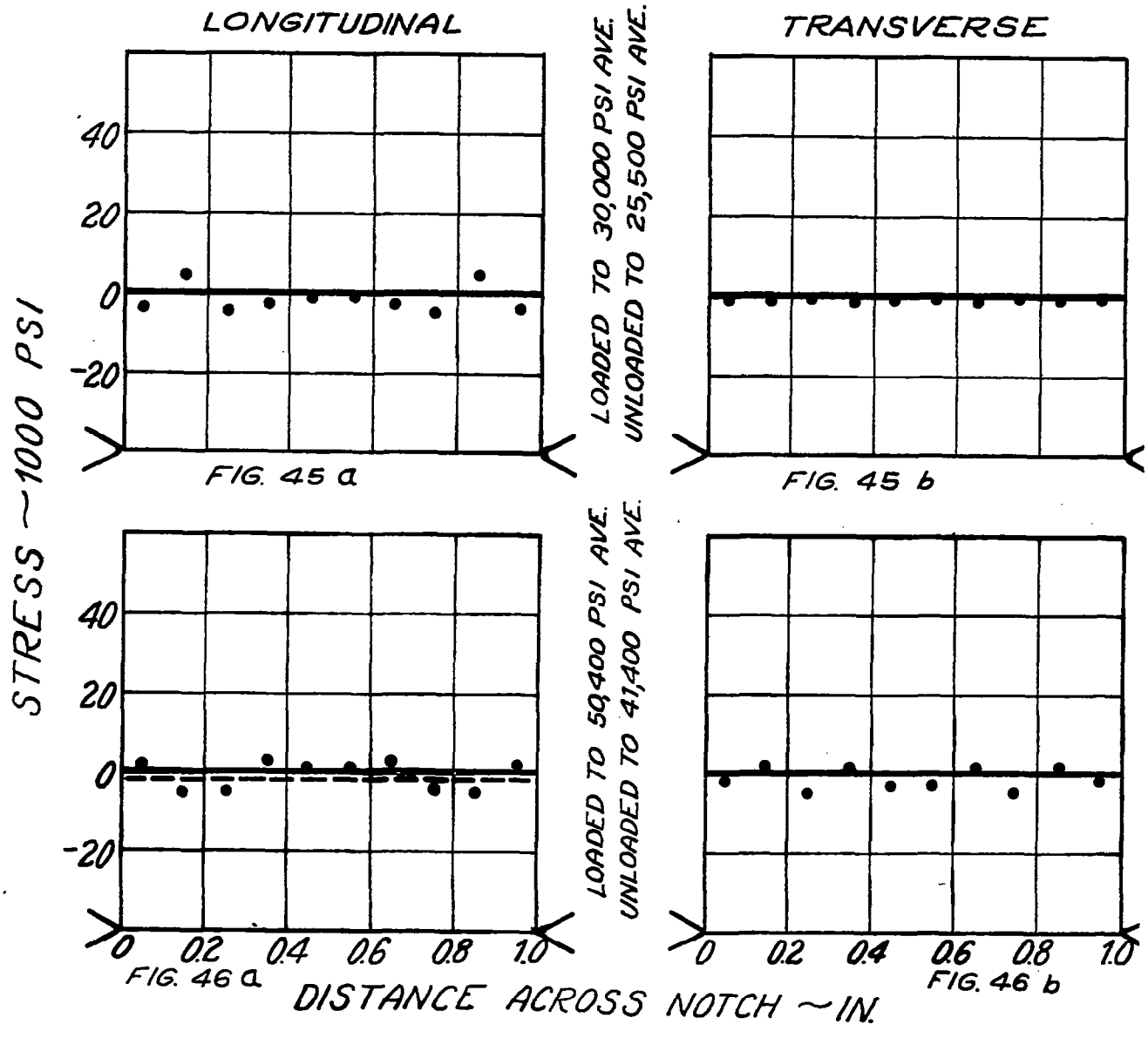


Figures 45,46.- Residual stress distribution in SAE X4130 steel 5% notched flat tensile bar.

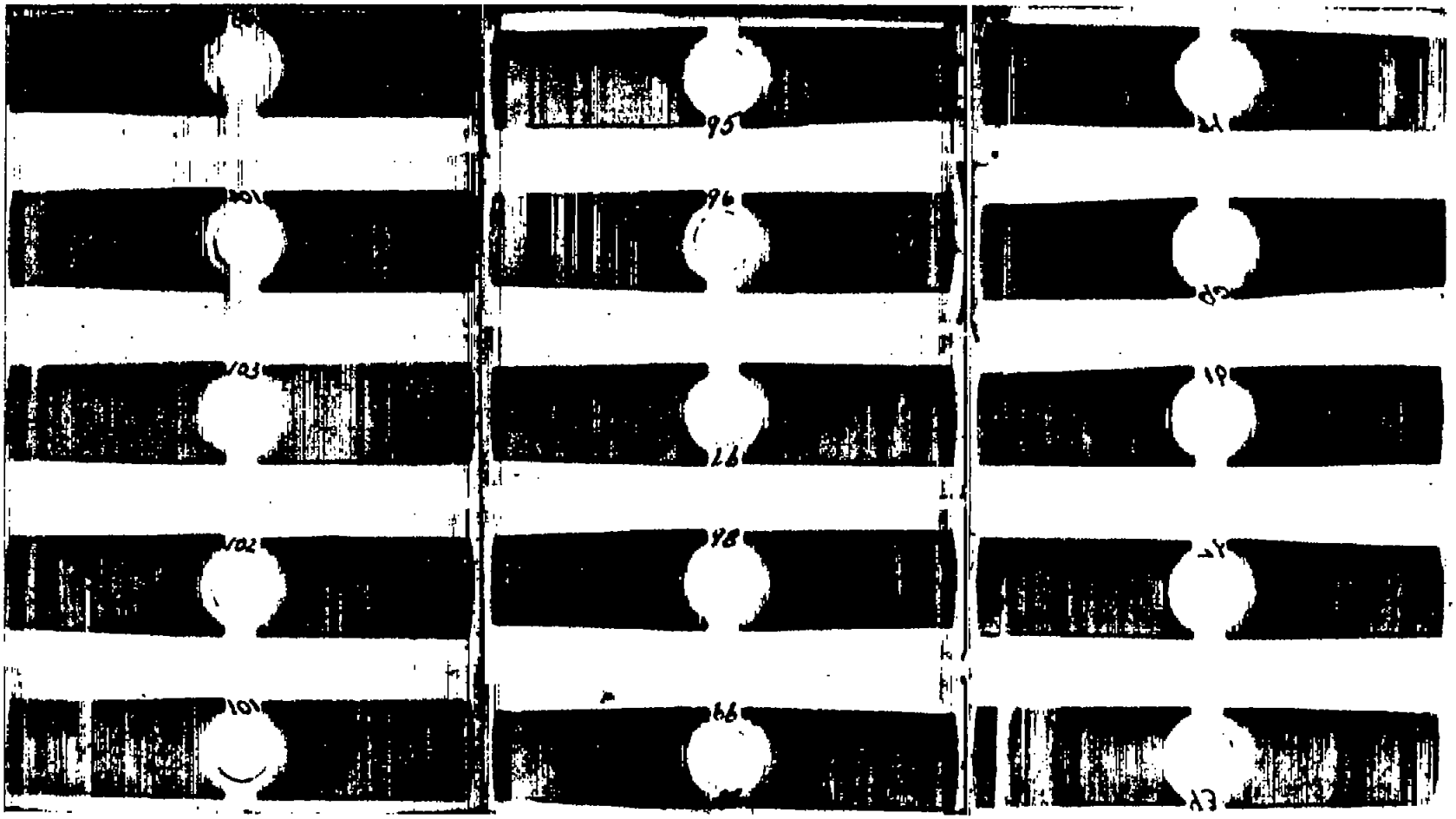

Oblique transverse | Oblique longitudinal | Normal

FIGURE 47.—Diffraction patterns from notch bottom to center of specimen (top to bottom) for 50,000 psi average load on 25 percent notched SAE X4130 steel tensile specimen.

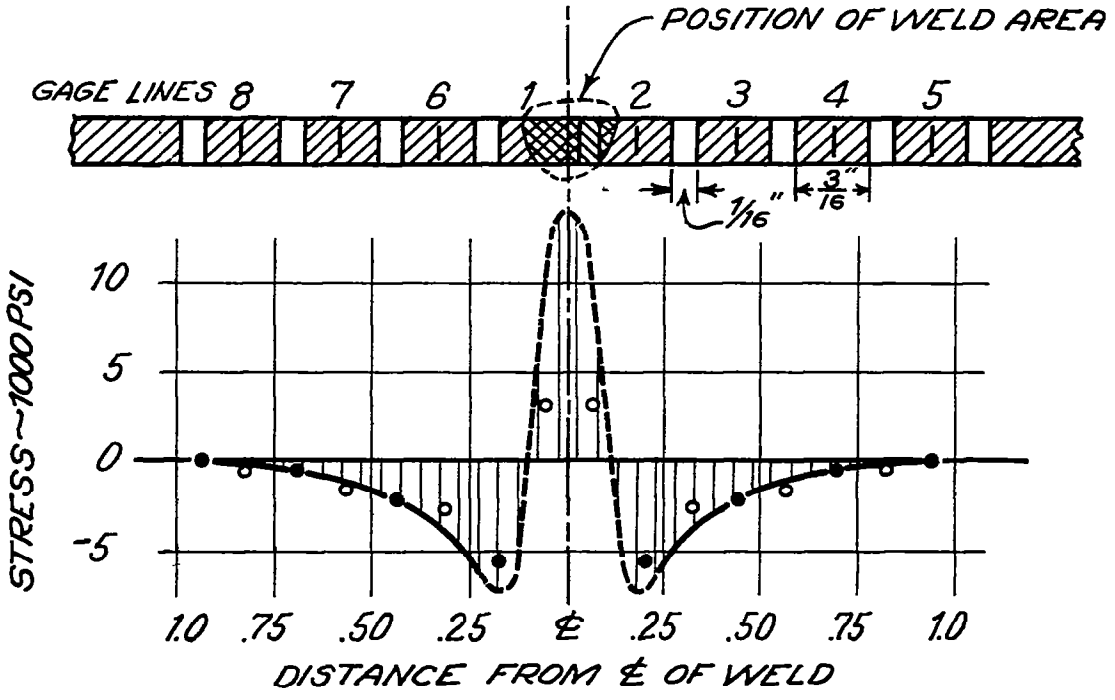


FIGURE 48.—Average circumferential stress values of butt-welded SAE X4130 tubing. After acetylene welding, tube was machined inside and out to .050″ wall thickness.

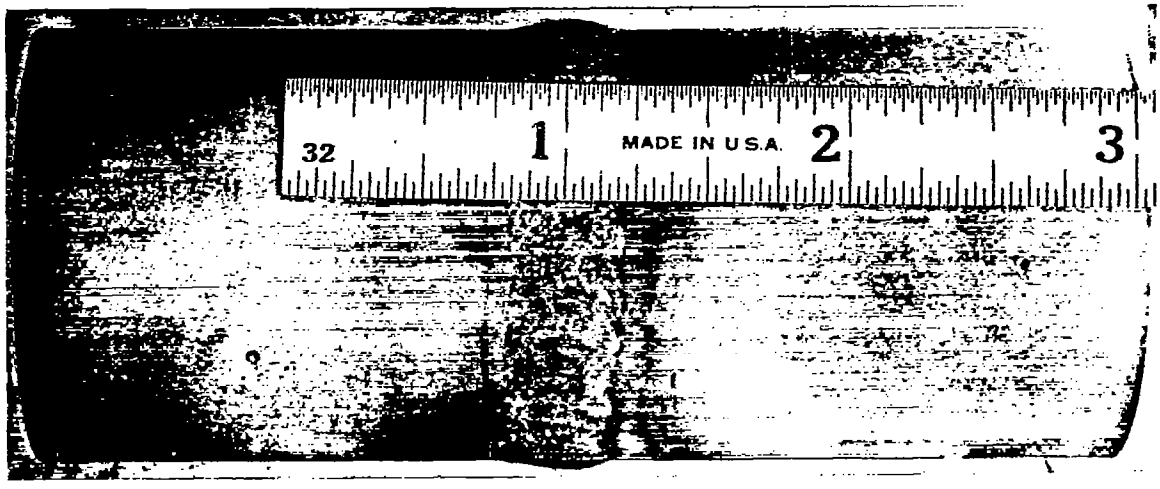


FIGURE 49.—Macrostructure of the weld and adjacent material, showing the various heat-affected zones.

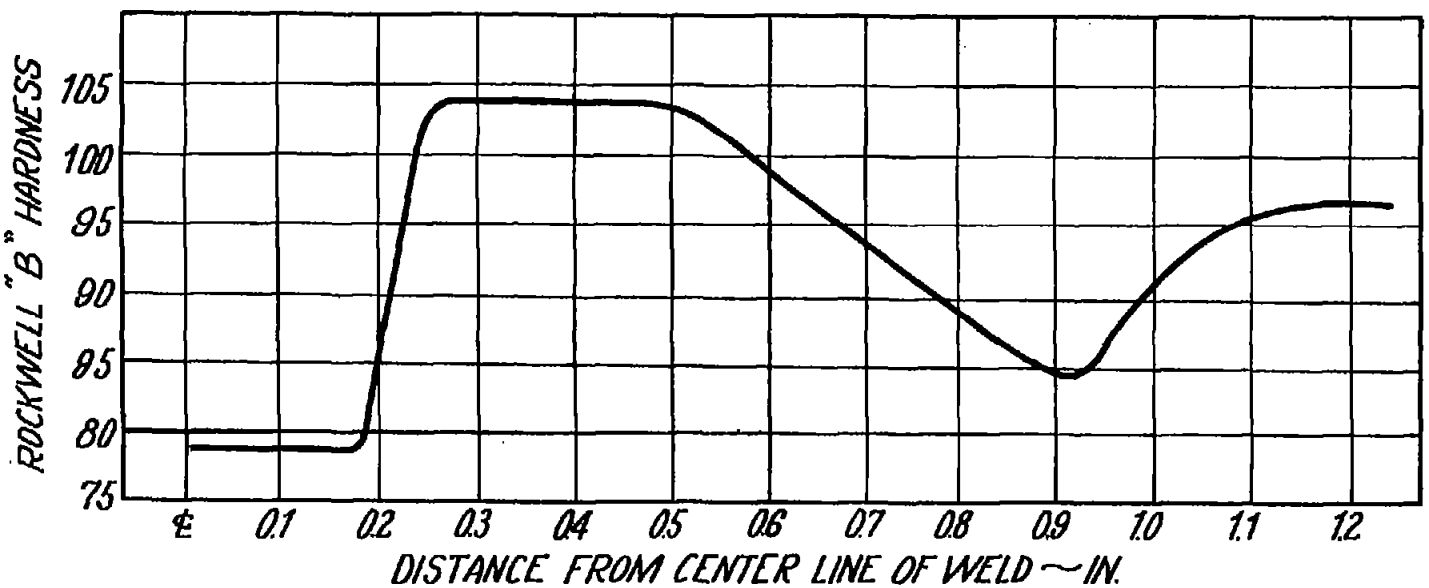


FIGURE 50.—Variation of hardness along an element of the butt-welded tube.

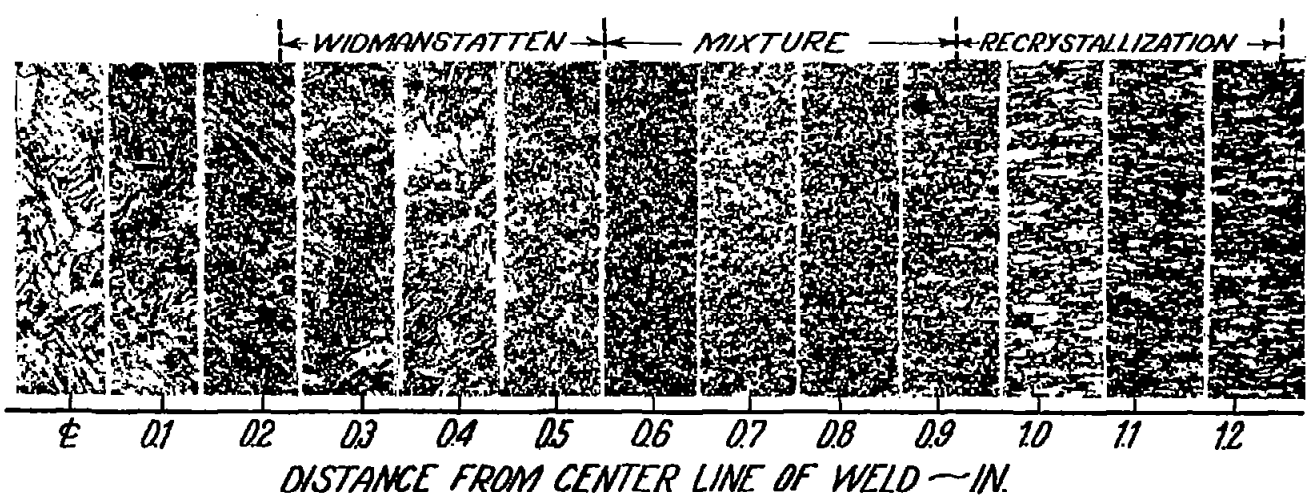


FIGURE 51.—Variation of microstructure along an element of the butt-welded tube.

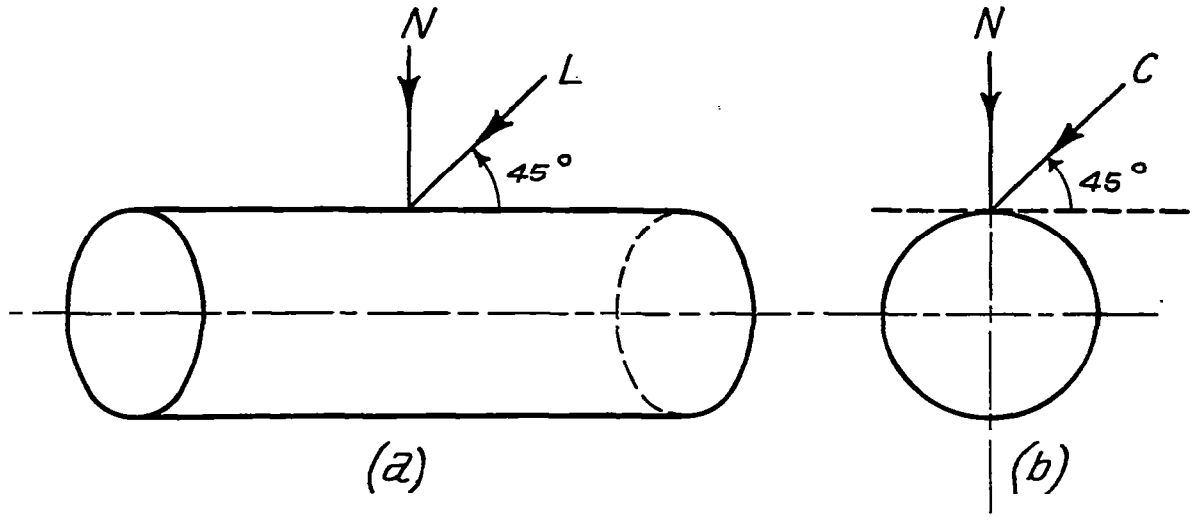


FIGURE 52.—Direction of the incident beam for various types of exposures.

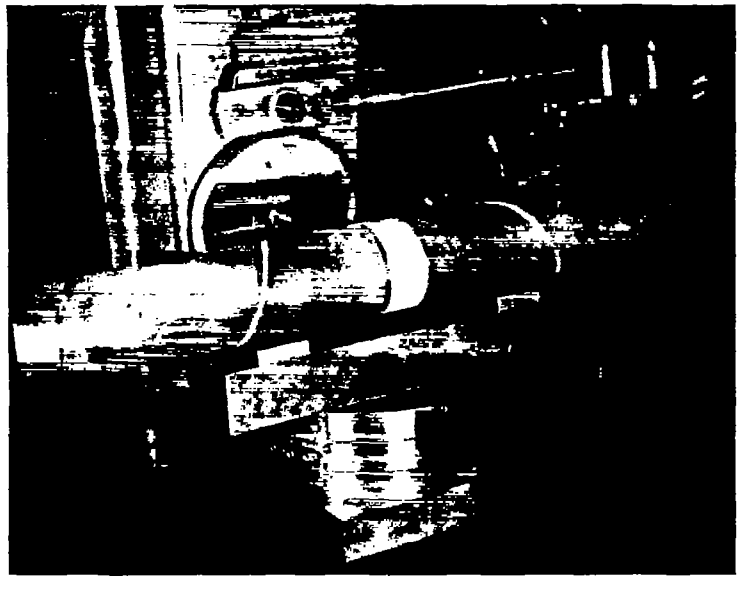

FIGURE 53.—The goniometer used to hold the welded tube in the proper position relative to the X-ray beam.

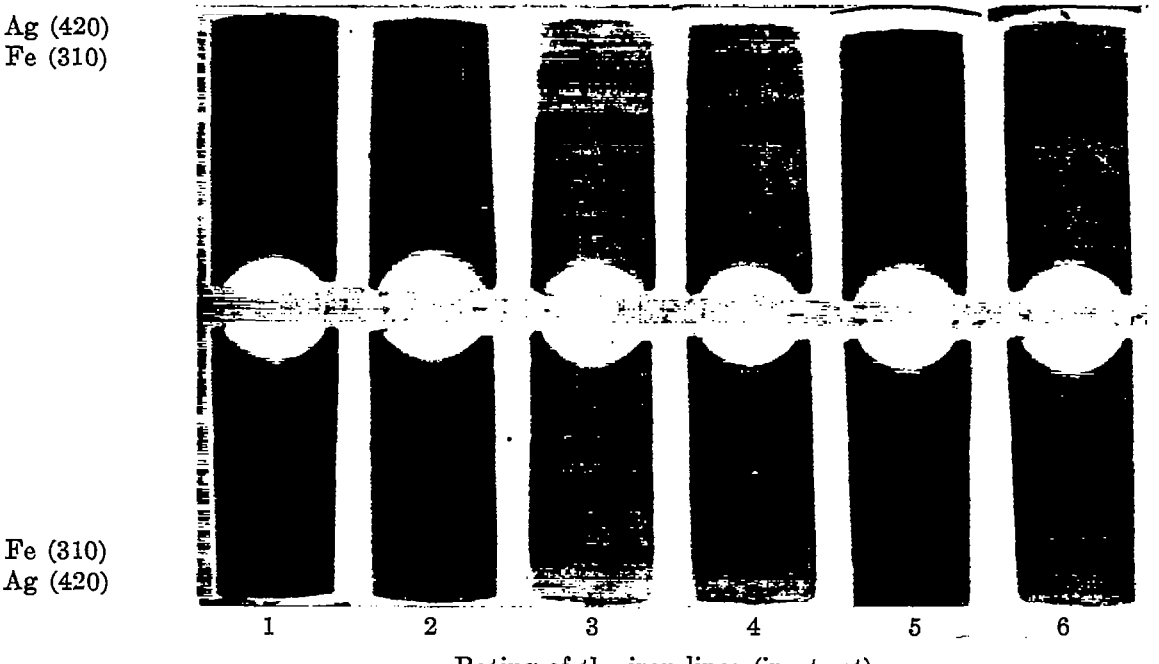


FIGURE 54.—Illustration of the qualitative rating system used to indicate the measurability of X-ray films.

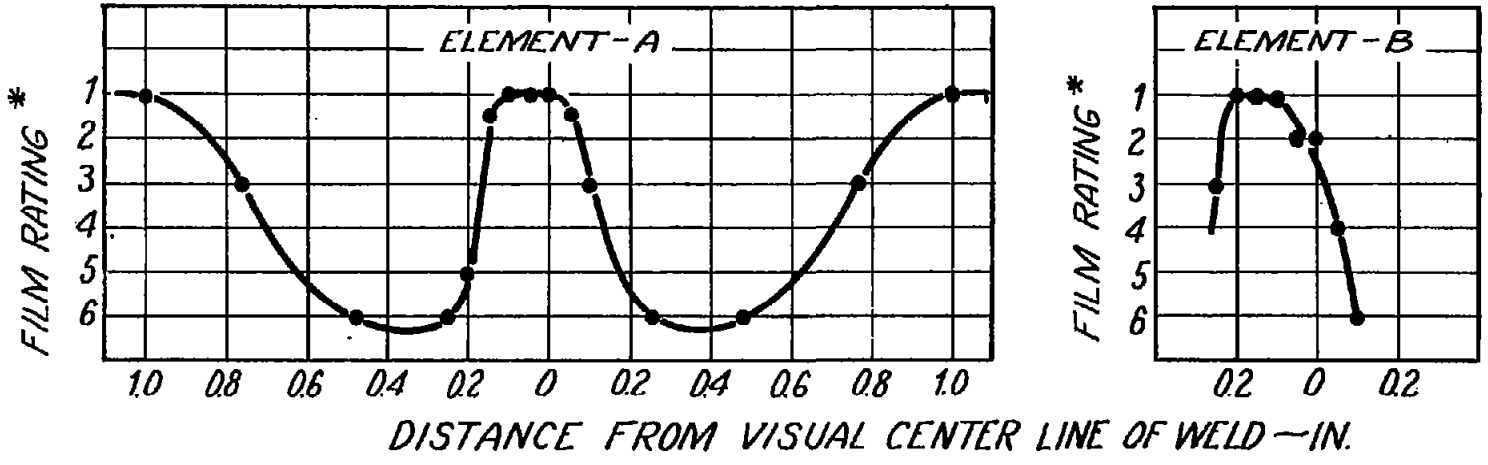


Figure 55.- Variation across the weld of the condition of the metal as it affects the measurability of the X-ray films.

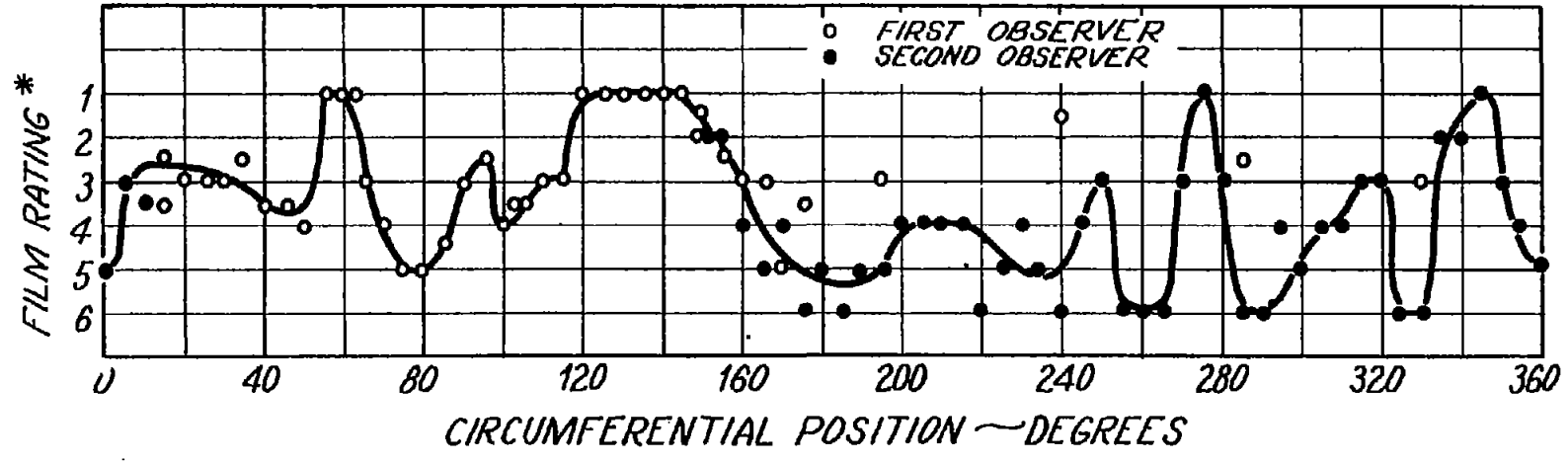


Figure 57.- Variation around the weld of the condition of the metal as it affects the measurability of the X-ray films.

* ARBITRARY, QUALITATIVE MEASURE OF THE SUITABILITY OF THE FILM FOR MEASUREMENT. RATING 1 INDICATES A SHARP, WELL-DEFINED ALPHA DOUBLET.

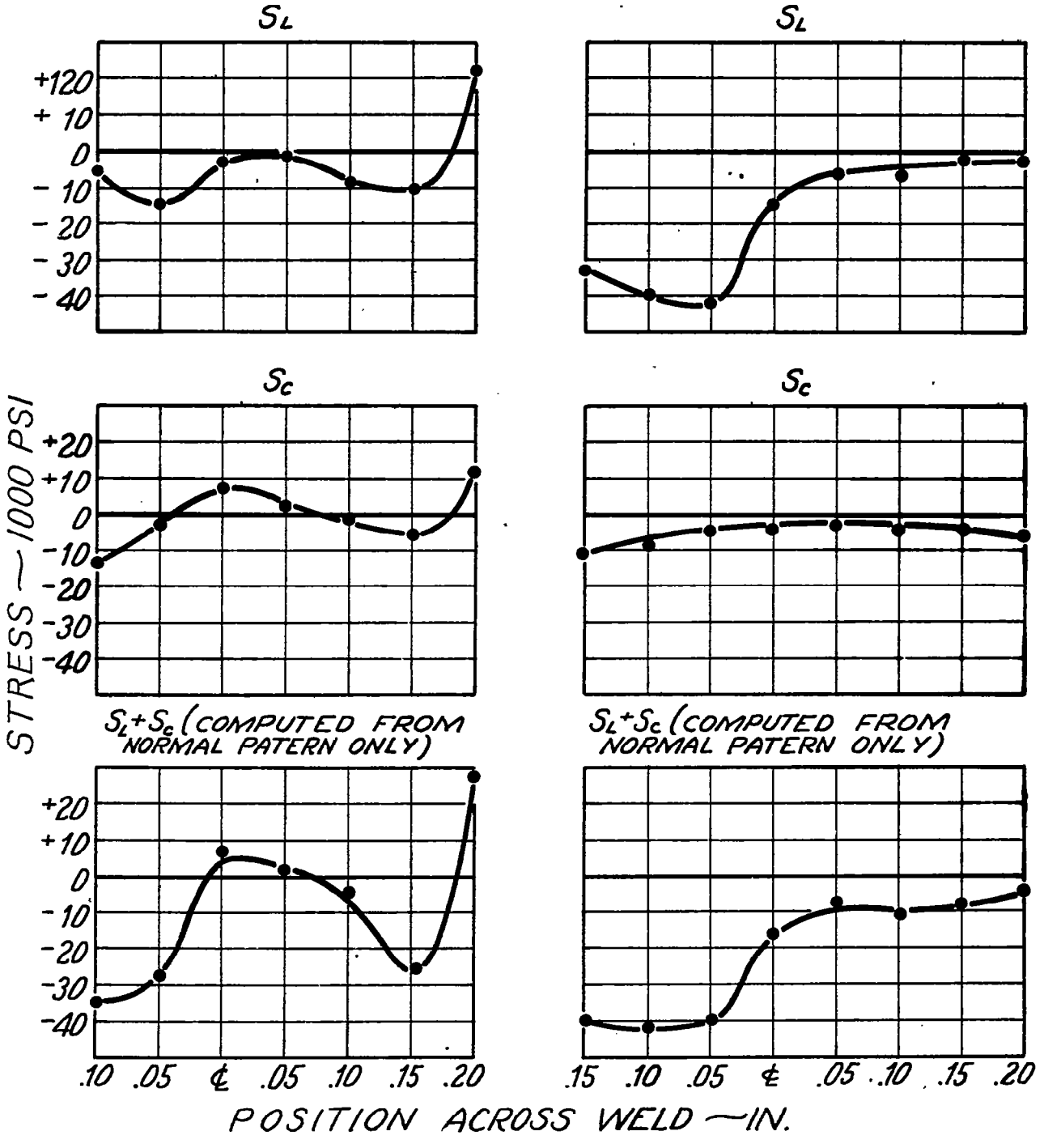


Figure 56.- Longitudinal and circumferential stresses at various points across the weld.

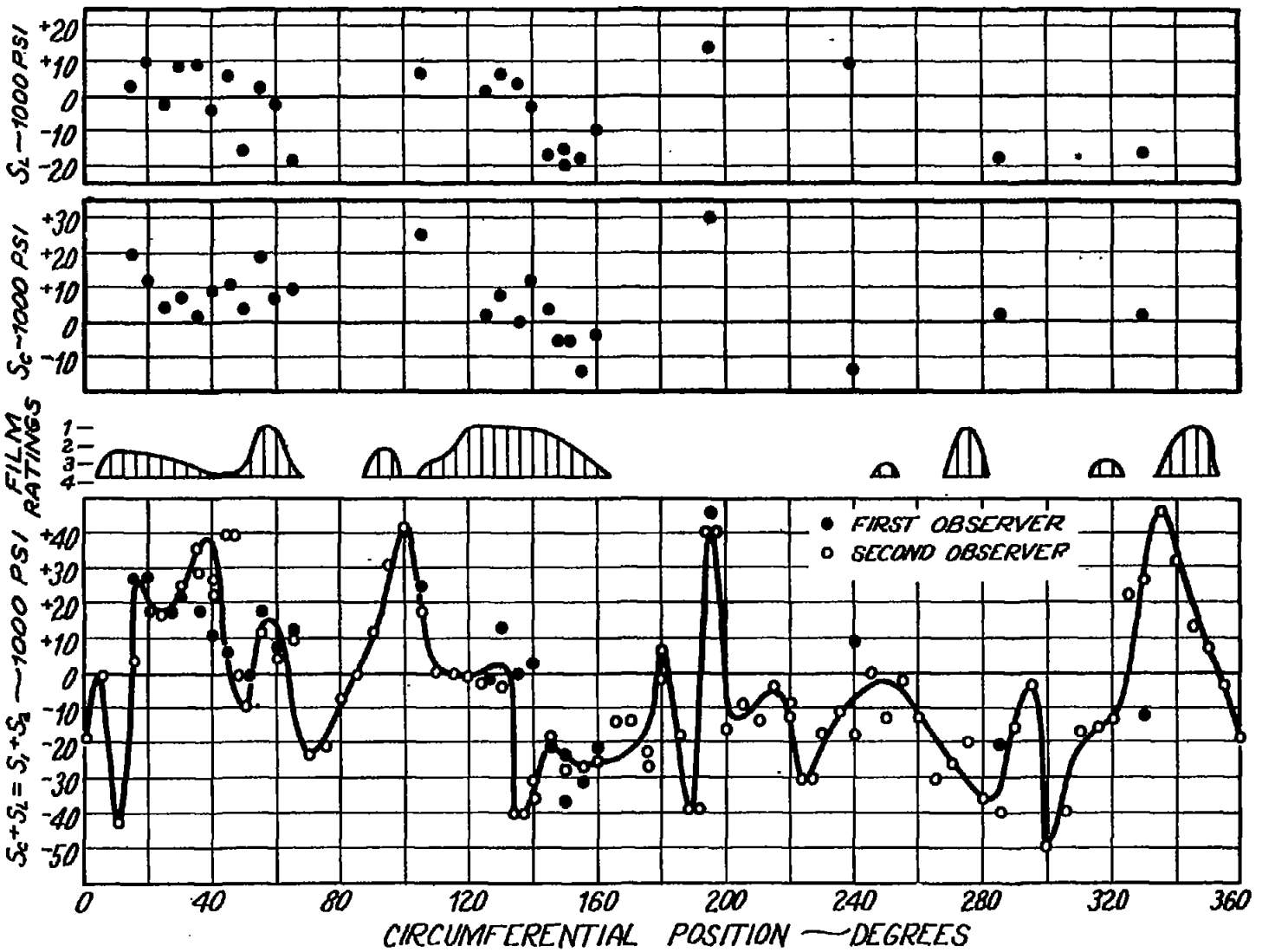


Figure 58.- Longitudinal and circumferential stresses, film measuribility and principal stress sums for various positions around the weld at the visual center line.

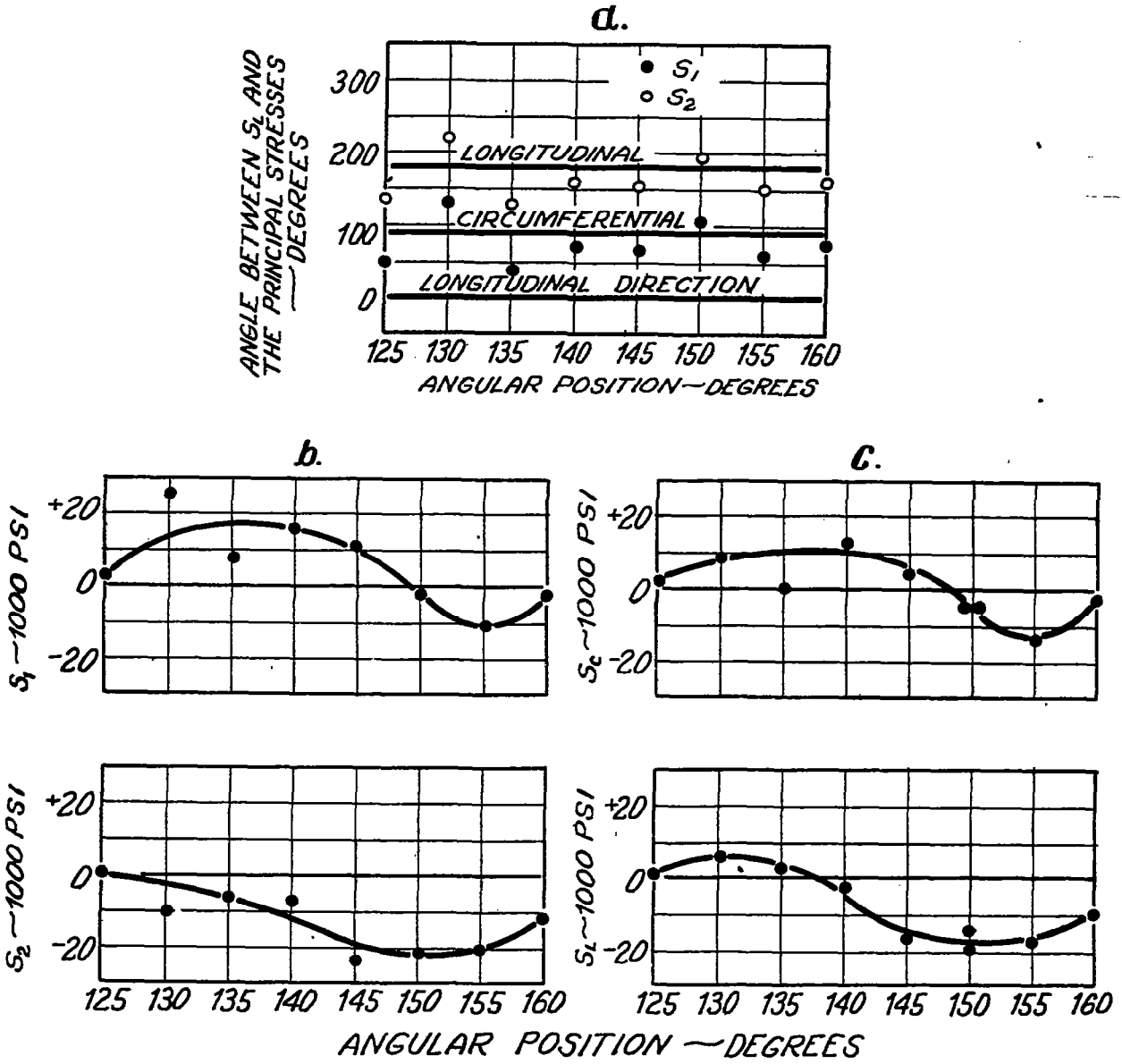


Figure 59.- Magnitude and direction of the principal stresses at various points along one portion of the center line of the weld.